Coherent control and manipulation of atoms using femtosecond pulses

Parvendra Kumar

A thesis

Submitted for the degree of

Doctor of Philosophy

Department of Physics
Indian Institute of Technology Guwahati
Guwahati - 781039, India

May 2013

Coherent control and manipulation of atoms using femtosecond pulses

Parvendra Kumar

A thesis

Submitted for the degree of

Doctor of Philosophy

Supervisor

Dr. Amarendra Kumar Sarma

Department of Physics

Indian Institute of Technology Guwahati

Guwahati - 781039, India

May 2013

Certificate

It is certified that the work contained in the thesis entitled "***Coherent control and manipulation of atoms using femtosecond pulses***" by Mr. Parvendra Kumar, a student of the Department of Physics, Indian Institute of Technology Guwahati was carried out under my supervision and has not been submitted elsewhere for award of any degree.

Dr. Amarendra Kumar Sarma

Dedicated to my late Grandparents, *Smt. Murti Devi* and *Shri Sukhe Singh*

Acknowledgements

It is indeed a pleasure to express my gratitude to all, who have contributed to this thesis in a way of their own.

First and foremost, I wish to convey my deep regards and gratitude to Dr. Amarendra Kumar Sarma. I am fortunate to receive his excellent guidance, encouragement and support at all the stages of my stay at IIT Guwahati. His untiring work ethic and strive for perfection is an example that I hope to emulate. More than a guide, he is a wonderful human being from whom I have learned a lot of things about research as well as life. The freedom he has given in my PhD work helped me a lot to improve my self-confidence and to develop many qualities/skills. I extend my sincere thanks to him for his motivational inputs and friendly behaviour.

I am immensely grateful to my thesis doctoral committee members, Dr. Subhradip Ghosh, Dr. Bosanta R Boruah and Dr. Aditya N. Panda for their support, valuable comments and suggestions during my review seminars and presentations. I also thank Dr. Ashwini K. Sarma and Dr. Manabendra Sarma for their encouragement and support.

I express my sincere gratitude to the present and past Physics Department Heads for supplying the full support and facilities at their best. I extend my whole hearted thanks to all the faculty members in the Physics Department who supported me in several ways during my research period. I am thankful to Ministry of Human Resource Development, Government of India for providing me financial support during the research period.

I would like to thank my senior, Ms. Manirupa Saha for her support and encouragement. I also thank Mr. Samit Gupta, my junior, for his help and support. I extend my thanks towards my lab-mates for the great time we have shared, the small jokes, complaints and healthy arguments.

I extend my gratitude to my friends Indrajit, Akhilesh, Suresh, Mukesh, Munendhar, Lalhriatzuala, Abhijit, Hassan, and other friends for their moral support and company.

I express my wholehearted gratitude to my parents, Smt. Daya Wati Devi and Shri Hariom Singh for their unconditional support of my pursuit of a scientific carrier. I wish to thank my wife, Ms. Yogita for her love and support. I also thank my younger sister and brother, Km. Sonam and Mr. Monu Singh.

Finally, I thank God for his showers of blessings in my life.

Abstract

Coherent control and manipulation of atoms is one of the central themes of research in atomic and optical physics owing to many potential applications including laser cooling, optical lattices, Bose-Einstein condensate, quantum information processing, high precession spectroscopy, and quantum computing. For many of these applications, it is highly desirable to produce samples of cold atoms whose population resides almost entirely in a particular quantum state. Primarily, two methods of coherent control are used to transfer the complete population to a particular state of atoms. These are stimulated Raman adiabatic passage (STIRAP) and adiabatic rapid passage (ARP). On the other hand, since the seventies of the last century, the laser induced forces, the so-called optical dipole force and the dissipative force, have been used routinely for the manipulation of atoms. The optical dipole force and the dissipative force have been used for the trapping of particles and cooling of atoms respectively. This particular area of research, i.e. coherent control and manipulation, is getting tremendous boost due to the recent technological developments in the generation of femtosecond pulses. In the context of coherent control, femtosecond lasers may be advantageous to realize ultrafast population transfer that is decoherence-free and robust. On the other hand, concerning manipulation of atoms or molecules using lasers, the magnitude of the dissipative force induced by commonly used CW lasers is limited due to spontaneous decay process. This limitation may be surmounted by using picosecond or femtosecond pulses, thereby realizing a very strong optical force. In this thesis, a detailed theoretical study is carried out on the manipulation and coherent control of atoms beyond the so-called rotating wave approximation (RWA). In the context of coherent control, we have studied the coherent population transfer (CPT) in two-, Λ-like three- and Y-like four-level atoms. This thesis also reports a study on the femtosecond pulse induced optical force on two- and three-level atoms in an atomic beam.

Contents

List of Figures

Chapter 1

Introduction

1.1 Background

Moshe Shapiro and Paul Brumer, two of the world's leading researchers in the field of quantum coherent control, writes in the preface of their famous book [1]:"*Despite its maturity, quantum mechanics remains one the most intriguing of subjects. Since its emergence over 75 years ago, each generation has discovered, investigated, and utilized different attributes of quantum phenomena. In this book we introduce results from research over the past 15 years that demonstrate that quantum attributes of light and matter afford the possibility of unprecedented control over the dynamics of atomic and molecular systems. This subject is the result of extensive investigations in chemistry and physics since 1985 and has seen enormous growth and interest over the past years. This growth reflects a confluence of developments-—the maturation of quantum mechanics as a tool for chemistry and physics, the development of new laser devices that afford extraordinary facility in manipulating light, and the recognition that coherent laser light can be used to imprint information on atoms and molecules in a manner such that their subsequent dynamics leads to desirable goals. As such, an appreciation of coherent control requires input from optical physics, physical chemistry, atomic and molecular physics, and quantum mechanics.....".* Shapiro's and Brumer's book was published in 2003. Since then, in the last decade the pace of coherent control (CC) research is not getting slowed down, rather it has seen explosive growth of theoretical and experimental studies owing to many new technological developments in the generation of femtosecond and attosecond laser pulses. Coherent control is a method to guide a quantum system to arrive at a given final state via a number of different quantum pathways. The guiding is done by tuning the phases and other parameters of the external laser fields [2]. One starts from an initial pure quantum state, and then uses laser fields to control multiple quantum pathways to place the populations in the final states of interest. The desired target state may be enhanced and undesired one may be suppressed by inducing constructive and destructive interference respectively, between such quantum pathways. Many experimental techniques have been discovered in recent years to control the interferences between different

quantum pathways [3]. The development of many efficient schemes, specifically adiabatic passage which enables the complete transfer of populations between a pair of quantum states, for controlling the population transfer between the quantum states of atoms and molecules has opened new routes for controlling the various atomic and molecular processes [4-13]. For example, coherent control is now conceived as a very useful method to actively influence the outcome of a chemical reaction [14-16]. Moreover, today coherent control techniques are widely used in the fields of robust quantum dot excitation generation [17], controllable coherent population transfer in superconducting qubits [18], collision dynamics [14, 16], atomic interferometry [19, 20], high precession spectroscopy [21, 22], quantum computing [18, 23, 24], quantum information processing [25 ,26], and ultrafast optical switching [27-29].

In order to have an understanding of coherent population transfer (CPT) techniques, in the following we briefly discuss one of the most popular and widely used technique called stimulated Raman adiabatic passage or simply STIRAP [3]. For a basic theoretical description of STIRAP, in Fig. 1.1, we consider a Λ-like three-level excitation scheme. Initially all the population is in the state $|1\rangle$. The state $|1\rangle$ and the final state $|2\rangle$ are coupled by the Stokes laser field E_S and the pump laser field E_P via the intermediate state $|3\rangle$.

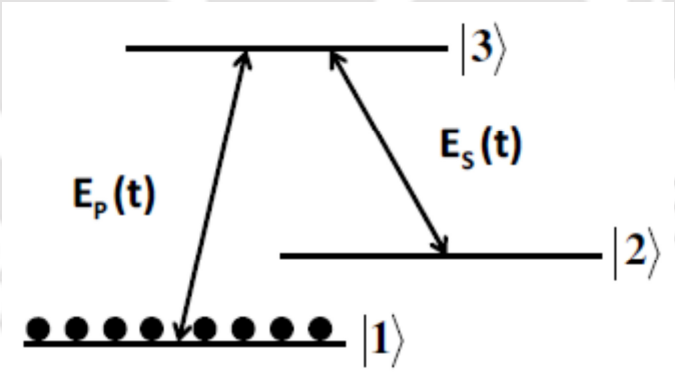

Fig. 1.1 Schematic of Λ-like three-level atom coupled with the pump and Stoke pulse

The single-photon detunings of the pump Δ_P and Stokes pulse Δ_S from their respective transitions are given by $\Delta_P = (\omega_3 - \omega_1 - \omega_P)$ and $\Delta_S = (\omega_3 - \omega_2 - \omega_S)$. Here, ω_1, ω_2 and ω_3, are the frequencies of the states $|1\rangle$, $|2\rangle$ and $|3\rangle$ respectively while ω_P and ω_S are the frequencies of the pump and the Stokes pulse respectively. If the pulses are tuned to two-

photon resonance ($\Delta_P = \Delta_S$) between the states $|1\rangle$ and $|2\rangle$, the dark eigen-state of the system is given by:

$$|d\rangle = \cos\theta|1\rangle - \sin\theta|2\rangle, \tag{1.1.1}$$

where the so-called time dependent mixing angle θ is given by

$$\theta(t) = \arctan\left[\Omega_P(t)/\Omega_S(t)\right]. \tag{1.1.2}$$

Here $\Omega_P(t) = \mu_{13}E_P(t)/\hbar$ and $\Omega_S(t) = \mu_{23}E_S(t)/\hbar$ are the Rabi frequencies. μ_{13} is the dipole moment between the states $|1\rangle$ and $|3\rangle$, and μ_{23} denotes the dipole moment between the states $|2\rangle$ and $|3\rangle$. Let us see the consequences of applying the laser pulse in a counterintuitive sequence, i.e., the Stokes pulse precedes the pump pulse: Initially, i.e., at $t \to -\infty$, the mixing angle is $\theta = 0$ and in the end of the interaction, i.e., at $t \to +\infty$, the mixing angle is $\theta = \pi/2$. Consequently the dark state evolves from the bare state $|1\rangle$ to the target state $|2\rangle$. Hence with the counterintuitive sequence of the pulses, complete population transfer to the target state could be obtained. A robust and complete population transfer with STIRAP scheme can be obtained provided the adiabatic condition $\Omega\tau_p >> 20\pi$ is satisfied. Here, $\Omega = \Omega_P = \Omega_S$ is the peak Rabi frequency. U. Gaubatz et al. [30] first demonstrated the experimental realization of population transfer with STIRAP scheme in the Sodium dimers. Afterwards, many researchers exploited the STIRAP scheme to obtain the complete population transfer between quantum states of atoms and molecules [31-40]. Recently, E. A. Shapiro et al. [41-43] proposed a new and robust method, the so called piecewise rapid adiabatic passage (PAP), for achieving complete population transfer between quantum states in a piecewise manner using a series of femtosecond laser pulses. They used a series of properly shaped pulses to achieve a counterintuitive interaction similar to the STIRAP scheme. More recently, X. H. Yang [44] exploited the STIRAP method to demonstrate sufficiently robust and complete population transfer between the quantum states in a $\Lambda-$like three state atomic systems driven by few-cycle femtosecond laser pulses. However, the STIRAP scheme can not be used for climbing the vibrational ladder because exact tuning to the two-photon resonance is required. This cannot be maintained along the ladder with a single pair of laser frequencies due to the potential anharmonicity. In this regard, S. Chelkowski and G. N. Gibson [45] proposed a new scheme called Raman chirped adiabatic passage (RCAP). Researchers demonstrated that chirping of a pump laser with a simultaneously applied Stokes laser inverts the Λ-like three-

level atomic system efficiently in the regime where both lasers are far from the one-photon resonance but are swept through the two-photon resonance for the transition between lower levels. In addition, they have shown vibrational ladder climbing using this scheme. Later on, J. C. Davis and W. S. Warren [46] have demonstrated the selective excitation of high vibrational states using RCAP the scheme.

The simplest model describing the atomic system is an isolated two-level atom. The excitation of a two-level atom, exactly on resonance, creates a complete population inversion if the so-called pulse area (time integral of the Rabi frequency) is equal to π. Generally, this approach is known as the "π-pulse" technique. In general this scheme, while effective in certain cases [46], is not a robust method for complete population transfer. It is sensitive to variation in the pulse area and to inhomogeneities in the sample [47, 48]. However there is a robust scheme that makes use of the frequency swept (linearly chirped) laser pulses. This scheme is usually known as the adiabatic rapid passage (ARP). This requires the sweeping of the laser pulse frequency through the resonance of atomic or molecular transition. At the beginning of the interaction (leading edge of the laser pulse), the frequency of the laser pulse is far from resonance while at the center of laser pulse it is swept through resonance with the atomic transition, then goes out of resonance at the end of the interaction (trailing edge of laser pulse). If the frequency sweep is sufficiently slow, the transitions it induces in an atomic system are said to be "adiabatic". The adiabatic condition [4, 49] can be written as:

$$\sqrt{\Omega^2(t)+\Delta\omega^2(t)} >> \left|d\theta(t)/dt\right| \qquad (1.1.3)$$

In Eq. (1.1.3), $\Omega(t)$ is the Rabi frequency, $\Omega(t)=\mu E(t)/\hbar$, where μ is the dipole moment, E(t) is the electric field and $\Delta\omega(t)=\omega(t)-\omega_{12}(t)$ is the frequency detuning. Here $\omega(t)$ is the pulse frequency and $\omega_{12}(t)$ is the transition frequency. The phase angle, $\theta(t)$, is given by $\theta(t)=\tan^{-1}\left[\Delta\omega(t)/\Omega(t)\right]$. The ARP scheme was first exploited in nuclear magnetic resonance [50]. Avrillier et al. [51] and Adam et al. [52] observed the signature of ARP in the infrared regime. In the optical regime, the implementation of ARP was first suggested by E. B. Treacy [53] and subsequently demonstrated by several other researchers [54-60]. A comprehensive literature review on the STIRAP and ARP schemes is also presented in chapter three and four of this thesis.

Another exciting area of research developing in parallel with the coherent control research is the manipulation of atoms and molecules using laser pulses [61]. Particularly, manipulation of atoms using optical forces is of tremendous importance to many fields of physics [62-64], chemistry [65, 66] and biology [67-69]. Generally, there are two kinds of optical force that arise from the laser-atom interaction: the reactive or optical dipole force and the dissipative or spontaneous force [70-73]. Optical dipole forces arise from the interaction between the induced dipole moment and the gradient of the electric field amplitude. The magnitude of the field gradient could be controlled by judicious focusing of the laser. The sign of the optical dipole force could be controlled via detuning of the laser from the atomic resonance. Tuning of the laser below the atomic resonance attracts the atom to the centre of laser, while tuning above resonance repels it. The dipole force is a conservative force because there is no net exchange of energy taking place between the atoms and the laser fields. The dissipative force arises from the impulse experienced by an atom when it absorbs or emits a quantum of photon momentum. The dipole force is often used to trap the atoms, while the dissipative one is used to cool them. A systematic derivation of the optical force on two and three-level atom within the rotating wave approximation (RWA) may be found elsewhere [71-73]. The RWA and its limitations are discussed in the next section. The optical force calculation beyond the RWA is presented in the fifth chapter of this thesis and may be found elsewhere as well [74]. Moreover, a comprehensive literature review on optical force is presented in the fifth and sixth chapters of this thesis.

Our study on the coherent control and manipulation of atoms using femtosecond pulses is based the density matrix formalism of quantum mechanics. The density matrix formalism is a useful tool to describe the system in statistical manner under the physical situations where the exact state of the system is not known [75]. An example is a collection of atoms in an atomic vapour, where atoms can interact with each other via collisions. The density matrix equations may be written as follows:

$$\frac{d\rho_{nm}}{dt} = -\omega_{nm}\rho_{nm} - \frac{i}{\hbar}\sum_{\nu}\left(V_{n\nu}\rho_{\nu m} - \rho_{n\nu}V_{\nu m}\right) - \gamma_{nm}\rho_{nm}, \quad n \neq m \tag{1.1.4}$$

$$\frac{d\rho_{nn}}{dt} = -\frac{i}{\hbar}\sum_{\nu}\left(V_{n\nu}\rho_{\nu n} - \rho_{n\nu}V_{\nu n}\right) + \sum_{E_m > E_n}\Gamma_{nm}\rho_{mm} - \sum_{E_m < E_n}\Gamma_{mn}\rho_{nn}, \tag{1.1.5}$$

where ρ_{nm} is the related to the coherence between the n^{th} and the m^{th} states of the atom, ρ_{nn} is related to the population of the n^{th} level and $\omega_{nm} = (E_n - E_m)/\hbar$ is the transition frequency. Here, E_n and E_m are the energies of the n^{th} and the m^{th} state. V is the interaction energy and may be defined as $V_{kl} = -\mu_{kl} \cdot E(t)$. Here μ_{kl} is the electric dipole moment between the arbitrary atomic states 'k' and 'l', and $E(t)$ is the electric field. In Eq. (1.1.4), γ_{nm} is the damping rate of the coherence between the n^{th} and the m^{th} states. In Eq. (1.1.5), Γ_{nm} gives the rate of population decay from the m^{th} state to the n^{th} and similarly Γ_{mn} gives the rate of population decay from the n^{th} state to m^{th} one. Here, we have given the model equations of the density matrix for an n-level atomic system. The complete derivation of the density matrix equations could be found in Ref. [76].

1.2 The relevance and the aim of the topic of research

In this thesis we would focus on studying coherent control and manipulation of atoms using femtosecond pulses. Since the birth of the laser, nearly 53 years ago, researchers have been continuously interested in the generation of shorter laser pulses in the femtosecond (1 fs = 10^{-15} s) and attosecond (1 as = 10^{-18} s) time domain owing to their potential applications in the various branches of science and engineering [77-81]. One of the motivations for generating shorter pulses is the high peak powers offered by these pulses. The peak power of a pulse is linearly proportional to the pulse energy and inversely proportional to the pulse width. Thus for a given pulse energy, high peak power could be achieved by reducing the pulse duration. It is often cheaper to reduce the pulse width than to increase the pulse energy [80]. Now, we review some of the concepts of femtosecond laser pulses which are directly related to our research. A detailed description of the generation and characterization of femtosecond and attosecond pulses could be found in the references [77-79].

Femtosecond laser pulses may be divided into two sub categories: few-cycle-femtosecond and many-cycle-femtosecond pulses. A few-cycle-femtosecond pulse encompasses only a few carrier wave oscillations within the pulse width τ_p. The pulse width τ_p is defined as the temporal full width at the half-maximum of the intensity profile. On the other hand, many-cycle-pulse contains many carrier wave oscillations within τ_p. Based on the wavelength of the carrier wave (central wavelength), a femtosecond pulse with a fixed

temporal length may be considered as a few- or a many-cycle pulse. For example, a pulse with temporal length, $\tau_p = 40$ fs and central wavelength, $\lambda = 6\,\mu m$, contains nearly two carrier wave oscillations, and hence it could be considered as a few-cycle pulse. However, with the same temporal length, $\tau_p = 40$ fs but with a different central wavelength, say, $\lambda = 0.4\,\mu m$, the pulse contains nearly thirty carrier wave oscillations, and hence it may be considered as a many-cycle pulse.

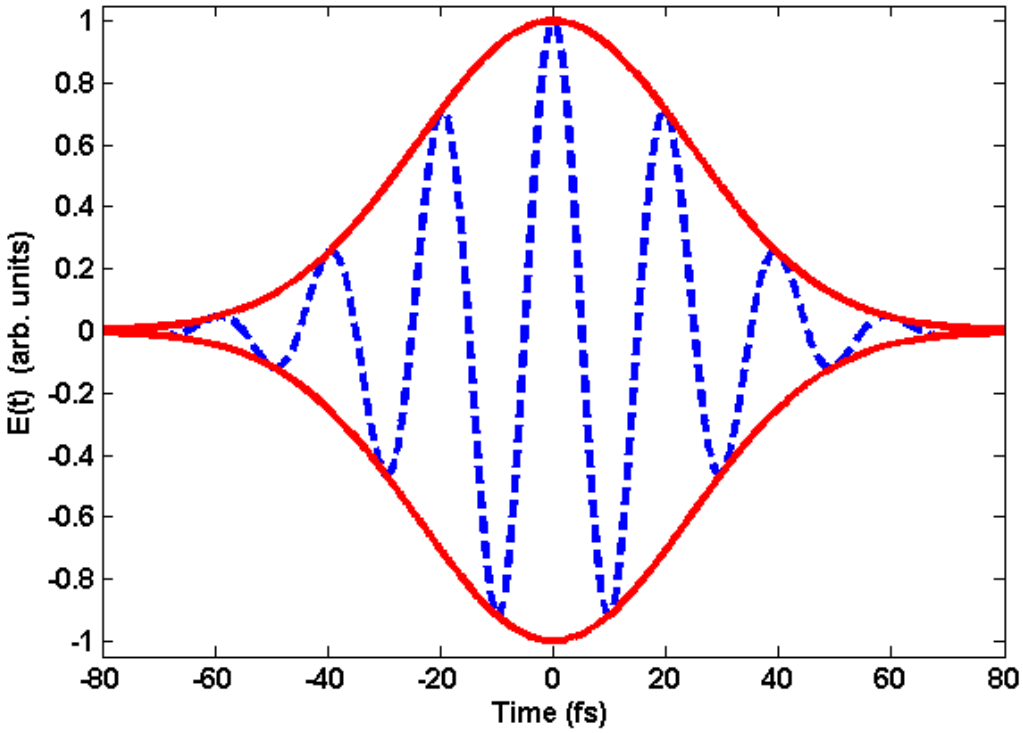

Fig. 1.2 Temporal profile of the electric field of a Gaussian-shaped-few-cycle-femtosecond laser pulse

In Fig. 1.2, we depict the temporal profile of the electric field, $E(t) = f(t)\cos(\omega t)$, of a Gaussian-shaped-few-cycle-femtosecond laser pulse. Here, $f(t) = E_0 \exp\left(-(t/\tau)^2\right)$ is the Gaussian-shaped pulse envelope, ω is the central frequency and E_0 is the peak amplitude of the pulse envelope. The pulse width is $\tau_p = 1.177\tau$ for the chosen pulse envelope. It can be observed from Fig. 1.2 that there are two carrier oscillations within the pulse width. In the regime of few-cycle femtosecond pulses, the so-called carrier-envelope phase (CEP) becomes important and has great impact on the outcome of an experiment. The CEP may be defined as the phase delay between the tallest half-cycle of the electric field under the pulse envelope and the peak of the envelope itself [82]. Recently, Xinhua Xie et al. [83] demonstrated the

selective photo-fragmentation of polyatomic molecules using femtosecond pulses with a well-defined CEP. There are several other studies in which the role of CEP has been found very crucial [84-90]. In the context of few-cycle pulses, it is now widely accepted that the rules of the so- called nonlinear optics or even quantum optics have to be re-examined, modified or corrected. The extremely useful slowly varying envelope approximation (SVEA) in nonlinear optics or the so-called rotating wave approximation (RWA) in quantum optics can no longer be used in this new regime [91-95]. Owing to the SVEA the partial differential equation, which governs the evolution of the complex pulse envelope, contains only the first order derivative with respect to the spatial coordinate along the direction of propagation. S. Hughes [96] reported that the SVEA may not be applicable even in the regime of intense many-cycle-femtosecond pulses. On the other hand, the RWA does not hold when the peak Rabi frequency becomes comparable or even larger than the transition frequency [97]. The electric field time-derivative-driven nonlinearities, which may lead to strong oscillation features during the evolution of the populations, could be explained only if non-RWA physics is included [98]. Femtosecond laser pulses have opened new doors and many fascinating possibilities in atomic and molecular physics and quantum optics research. For example, these pulses have made it possible to visualize and control the many fundamental processes in real time such as formation and breaking of chemical bond [99-101] and electron dynamics in Rydberg atoms [102, 103], which usually occur on a fs time scales. Moreover, femtosecond laser pulses have enabled the generation of attosecond XUV pulses [79, 104-108] by high-order harmonic generation (HHG), which are being used to visualize and control the even shorter time (attosecond) scale phenomena such as motion of electrons in the inner shell of an atom [109, 110]**.** Along with the aforementioned fundamental applications, femtosecond pulses have been found useful in many other diverse areas such as, metrology [111, 112], medical diagnostics and imaging [111], and material processing [113-115], coherent control and manipulation of atoms and molecules [41-44, 116-121].

In the recent past, coherent control and manipulation of atoms have been studied mainly within the RWA. The commonly used RWA does not hold in the physical situations considered in this thesis. For coherent control, we investigate shaped (nonlinearly and linearly chirped) femtosecond pulses. Due to the recent technological advancement in the pulse shaping techniques, it has been possible to generate nearly arbitrarily shaped femtosecond pulses [122].These pulses may be advantageous to realize ultrafast and selective population transfer which completes on a time scale much shorter than the decoherence

processes. Decoherence free population transfer is highly desirable in certain applications such as quantum computation and quantum information processing [41, 123]. Our aim in this thesis to propose some new and sufficiently robust schemes for ultrafast and selective population transfer in a variety of atomic systems such as two-, Λ-like three- and Y-like four-level atomic system. The optical force on atoms, moving in a diverging atomic beam, induced by femtosecond pulses has rarely been explored. So, one of the objectives of the present thesis is to study the effect of femtosecond pulse-induced optical force on the motion of two and three-level atoms. We also carry out a study on the optical dipole force in a ladder- like three-level atomic system induced by the trains of few-cycle-pulse laser fields. It is to be noted that the magnitude of the dissipative force induced by commonly used CW lasers is limited due to spontaneous decay process. This limitation may be surmounted by using picosecond-to-femtosecond pulses, thereby realizing a very strong optical force [124-127]. Moreover, high peak powers of femtosecond pulses offer the possibility to exploit extremely useful nonlinear processes in the context of trapping of particles [116, 118].

1.3 Organization of the Thesis

The contents of the chapters in the remaining part of the present thesis are described briefly as follows:

Chapter 2: Many novel phenomena of quantum optics have been observed in the context of two-level atoms. Examples include oscillations of population between the quantum states of two- level atoms or the so-called Rabi oscillations and the self-induced transparency (SIT). This chapter is devoted to the study of coherent population transfer in dense as well as dilute two- level atomic systems using a train of femtosecond pulses. Many possible applications of this work are briefly sketched.

Chapter 3: This chapter is devoted to a detailed study on coherent population transfer in Λ-like three-level atoms using few-cycle pulses. Here, we have considered the population transfer in three-level atoms with degenerate as well as nondegenerate states.

Chapter 4: We report a scheme for ultrafast and selective population transfer in Y-like four-level atoms using a single nonlinearly chirped femtosecond pulse. The selectivity and robustness of the scheme with respect to various pulse parameters is also discussed.

Chapter 5: This chapter is devoted to our study of the optical force on two-level atoms. We

also give a review of the relevant literature in the area and suggest some possible applications of the work.

Chapter 6: In this chapter, we present a literature review on the optical force on three-level atoms and reported our work on the optical dipole force on two-level atoms.

Chapter 7: We conclude by giving a brief summary and analysis of the work reported in the previous chapters. We also discuss the possible future directions of our research.

Chapter 2

Ultrafast Coherent Population Oscillations in Two-Level Atomic Systems*

2.1 Introduction

Coherent population oscillations (CPOs) have been studied, recently, by many authors in Λ-like three-level atoms, in the context of electromagnetically induced transparency (EIT) [128], spatial optical memory [129], superluminal light [130] and ultraslow light [131]. M. Scalora et al. [132] and M. E. Crenshaw et al. [133] also investigated the coherent population oscillations (CPOs) in two-level dense atomic medium. An atomic medium may be considered as a dense medium if there are many atoms within a cubic resonance wavelength. In a dense medium, the near dipole-dipole (NDD) interactions among the atoms, which lead to the so-called Lorentz local-field (LFC) correction, must be considered [134]. However, in the case of a dilute medium, it is valid to assume that atoms interact with the light field independently. In the context of CPOs, M. E. Crenshaw et al. [133] have considered optical pulses with pulse duration much less than an induced-dipole dephasing time, incident upon a thin film of homogeneously broadened material composed of two-level atoms with NDD interaction. Researchers have found that the final inversion (when the pulse has passed through the medium), w, has a nearly step-function response to the peak Rabi frequency. The medium initially in the ground state, $w = -1$, is always returned to the ground state when the peak Rabi frequency is less than the strength of NDD parameter. However, the final state of the inversion is the fully excited state, $w=1$, when the peak Rabi frequency is nearly equal to the NDD parameter. Researchers have suggested that these step-like transition characteristics could be used for ultrafast optical switching. Furthermore, under the rotating wave approximation (RWA) and the slowly varying envelope approximation (SVEA), some other fascinating phenomena have been observed in dense two-level medium such as intrinsic

*Part of the results presented in this chapter have been published in a paper, P. Kumar and A. K. Sarma, "Frequency-modulated few-cycle optical-pulse-train-induced controllable ultrafast coherent population oscillations in two-level atomic systems", Phys. Rev. A 87, 025401 (2013).

optical bistability [135] and invariant pulse propagation [136] etc. On the other hand, beyond the RWA and the SVEA approximations, Song et al. [137] reported that the so-called area theorem becomes invalid for attosecond pulse propagation in dense two-level medium. In an another study on the femtosecond pulse propagation in dense two-level medium, Kalosha et al. have reported the intra-pulse third-order four-wave mixing (FWM) and the formation of optical subcycle pulses [138]. In the context of dilute two-level atoms, Rabi flopping, self-induced transparency, and photon echoes [139] are some of the well-known phenomena that have been observed within the framework of SVEA and/or RWA.

In this chapter, we discuss the phenomenon of CPOs in dense and dilute two-level atoms induced by the train of femtosecond pulses. We term these new kinds of CPOs as ultrafast coherent population oscillations (UCPOs) owing to the ultrafast nature of the oscillations. The model atomic system for this work is chosen to be a two-level Na atom. However, the proposed scheme may also be applicable to all other atoms, which could be modelled as two-level atoms for judiciously chosen pulse parameters.

2.2 UCPOs in dense two-level atomic systems

The sketch of our scheme is depicted in Fig.1, where a train of femtosecond pulses is incident on a system of two-level atoms. In Fig.1 (b), the states $|1\rangle$ and $|2\rangle$ refers to $3s$ and the $3p$ quantum states of neutral sodium atoms respectively.

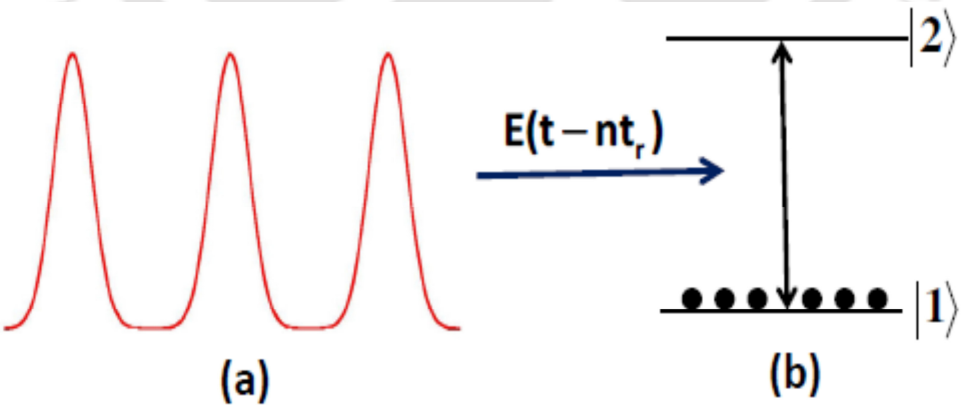

Fig. 2.1 (a) Train of pulses, (b) Sketch of two-level atoms

The total electric field for the train of pulses can be written as $\vec{E}(t-nt_r)=\sum_{n=0}^{N-1}\hat{\varepsilon}\,E_0 f(t-nt_r)\cos(\omega(t-nt_r))$. Here, $f(t-nt_r)=exp\left(-\left((t-nt_r)/\tau\right)^2\right)$ is the Gaussian shaped pulse envelope, $\tau=1.177\tau_p$, where τ_p is the temporal pulse width at full width at half

maximum (FWHM), N is the number of pulses, and t_r and $\hat{\varepsilon}$ are the pulse repetition time and electric field polarization direction, respectively. In this work, the states $|1\rangle$ and $|2\rangle$ refer to the down and the up state respectively. The optical Bloch equations describing the temporal evolution of the density matrix elements for a dense two-level medium, without invoking the so called rotating wave approximation, , is [134]:

$$\begin{aligned}
\frac{du}{dt} &= \Omega v - \frac{u}{T_2} \\
\frac{dv}{dt} &= -\Omega u - 2(\Omega_R(t) + \varepsilon u)w - \frac{v}{T_2} \\
\frac{dw}{dt} &= 2(\Omega_R(t) + \varepsilon u)v - \frac{(w+1)}{T_1}
\end{aligned} \tag{2.2.1}$$

Here u, v and w are the three components of the Bloch vector [135]. T_2 and T_1 are respectively the dipole-dephasing and spontaneous decay times, Ω is the transition frequency of the two-level atoms, ε is the NDD parameter and $\Omega_R(t)$ is the Rabi frequency, defined as $\Omega_R(t) = \vec{\mu}.\vec{E}(t)/\hbar$. The NDD parameter $\varepsilon = N\mu^2/3\varepsilon_0\hbar$ has units of frequency. Here, N, μ, and ε_0 are the density of the two-level atoms, the dipole moment, and the permittivity of free space respectively, and $\hbar = h/2\pi$, where h is Planck's constant. Equation (2.2.1) will represent the optical Bloch equations of dilute two-level medium if $\varepsilon = 0$. In the present study, we have neglected the terms associated with T_2 and T_1. This may be attributed to the fact that the atom-field interaction time, owing to the extremely short duration of the femtosecond laser field, is negligibly small compared to T_2 and T_1. We solve Eq. (2.2.1) numerically using a standard fourth-order Runge-Kutta method. We assume that initially all the atoms are in the ground state $|1\rangle$. We use the following typical parameters: $\Omega = \omega = 3.19$ rad/fs, $\tau = 25$ fs, $\mu = 1.85\times10^{-29}$ C·m [25], the peak Rabi frequency, $\Omega_R(0) = \mu E_0/\hbar = 0.50$ rad/fs, and $\varepsilon = 0.50$ rad/fs. Fig. 2.2 depicts the temporal evolution of the population inversion with respect to the pulse repetition time.

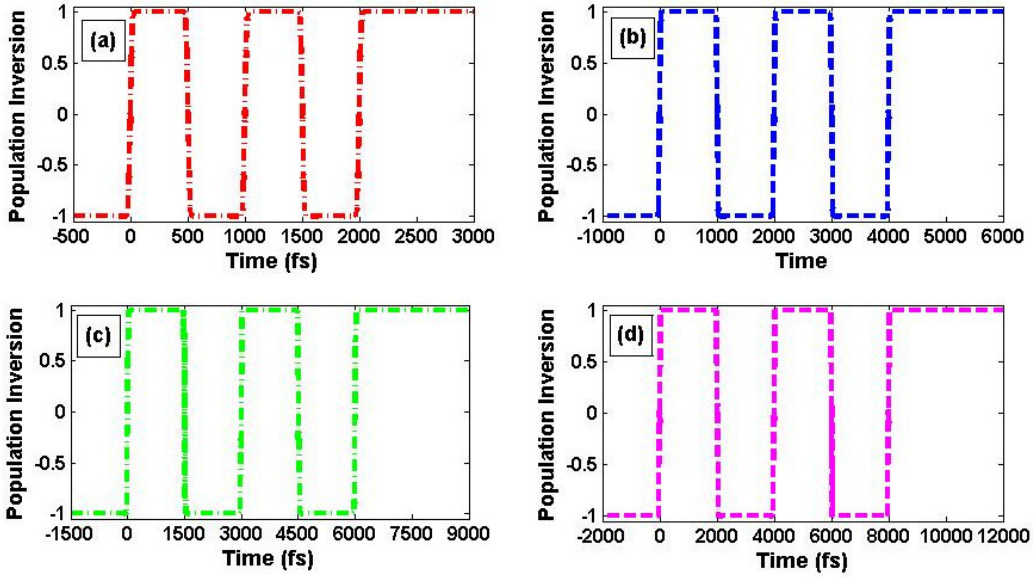

Fig. 2.2 Temporal evolution of population inversion for N=5, with pulse repetition time, (a) t_r=500 fs (b) t_r=1000 fs (c) t_r=1500 fs and (d) t_r=2000 fs.

It can be observed from Fig. 2.2 (a) that all the atoms are transferred to the up-state during the interaction with the initial the pulse (n=0) in the pulse train, with the peak Rabi frequency at t=0. On the other hand, all the atoms are transferred to the down-state, when the next pulse (n=1) in the pulse train interact with the up-state atoms. The holding time of atoms in the up-state is nearly equal to the pulse repetition time (t_r), chosen to be 500 fs in Fig. 2(a). Moreover, it can be seen from Fig. 2.2 that every odd number of pulses act as a pump pulse that leads to the atoms in the up-state while every even number of pulses act as a dump pulse, leads to the atoms in the down-state. Therefore, the final state of atoms may be controlled by manipulating the number of pulses in the pulse train. A careful inspection of Fig. 2.2 reveals that the holding time of atoms (τ_a) in up and down-states follows the relation, $\tau_a \approx t_r$ and the frequency of ultrafast coherent population oscillations (f_{ucpo}) between up and down state is $f_{ucpo} \approx 1/2t_r$. Hence the hold on time of atoms in down and up-states and the frequency of population oscillations may be controlled with judicious choice of the pulse repetition time. Physically speaking, pumping and dumping of atoms to up and down-states occur via the so-called stimulated absorption and stimulated emission respectively. The spontaneous decay is negligible at such a short interaction time scale. In section 2.3, we will discuss the possible applications of the reported UCPOs in the context of ultrafast optical switching. It is worthwhile to mention that the materials in which these effects might be observed include

oxygen ions in KCl: O_2^{-2} and bound I_2 excitons at the doner sites in CdS single crystals [133]. Fig. 2.3 depicts the robustness of the UCPOs against the slight variation in the peak Rabi frequency and the resonant condition.

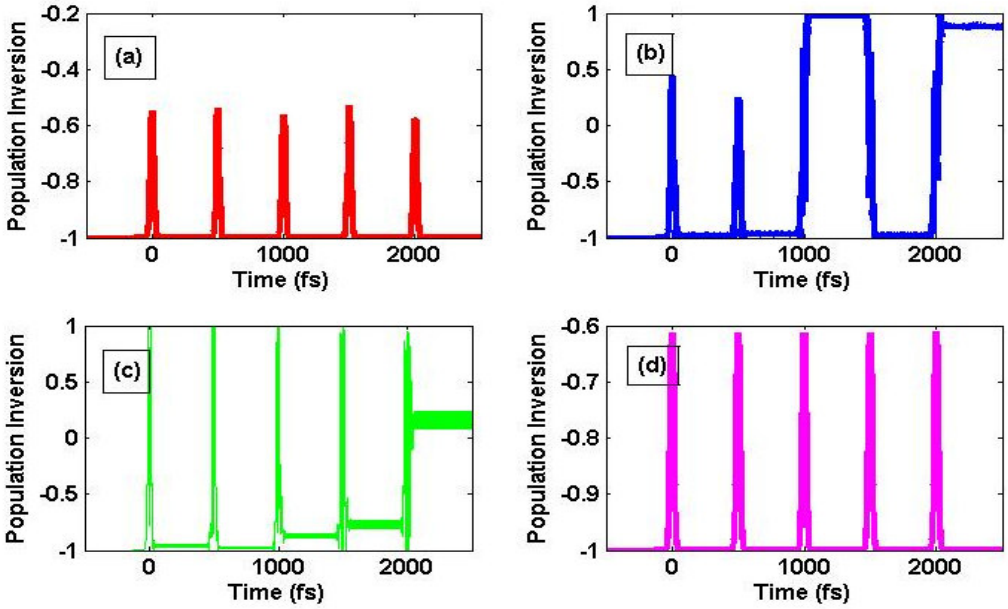

Fig. 2.3 Temporal evolution of population inversion for N=5, with pulse repetition time, t_r =500 fs (a) Ω_{21}=0.40 rad/fs and Δ= 0 rad/fs (b) Ω_{21}=0.60 rad/fs, and Δ= 0 rad/fs (c) Δ=0.10rad/fs and Ω_{21}= 0.50 rad/fs, (d) Δ= -10 rad/fs and Ω_{21}= 0.50 rad/fs. Here other parameters are same as in Fig. 2.2.

It can be observed from Fig. 2.3 (a) and Fig. 2.3 (b) and that the features of UCPOs, $\tau_a \approx t_r$ and $f_{ucpo} \approx 1/2t_r$, do not persist if the peak Rabi frequency is not equal to the NDD parameter. As could be seen from Fig. 2.3(c) and (d), these features of UCPOs also do not persist for slight positive or negative detuning from the exact resonance. Here, $\Delta = \Omega - \omega$ denotes the detuning from the exact resonance. In the next section, we report our studies on UCPOs induced by a train of linearly chirped femtosecond pulses in a dilute two-level medium.

2.3 UCPOs in dilute two-level atomic systems

Now, we consider a dilute two-level atomic system on which a linearly chirped train of femtosecond pulse is incident. The total electric field of the train of linearly chirped pulses can be written as $\vec{E}(t-nt_r) = \sum_{n=0}^{N-1} \hat{\varepsilon} E_0 f(t-nt_r)\cos(\omega(t-nt_r)+\alpha(t-nt_r)^2)$. Here, α is the linear chirp rate. We solve Eq. (2.2.1), with ε=0, numerically using a standard fourth-order Runge-Kutta

method. We assume that initially all the atoms are in the ground state $|1\rangle$. We use the following typical parameters: $\Omega = \omega = 3.19$ rad/fs, $\tau = 25$ fs, $\mu = 1.85\times10^{-29}$ C.m [140], peak Rabi frequency $\Omega_{21} = \mu E_0 / \hbar = 0.50$ rad/fs, and α=0.015 fs^{-2}. The laser pulse parameters such as linear chirp rate, pulse duration, and peak Rabi frequency have been investigated numerically in order to achieve the maximum population inversion. It should be noted that a laser pulse with parameters similar to the ones chosen here could be generated experimentally [141, 142]. Fig. 2.4 depicts the temporal evolution of the population inversion with respect to the pulse repetition time.

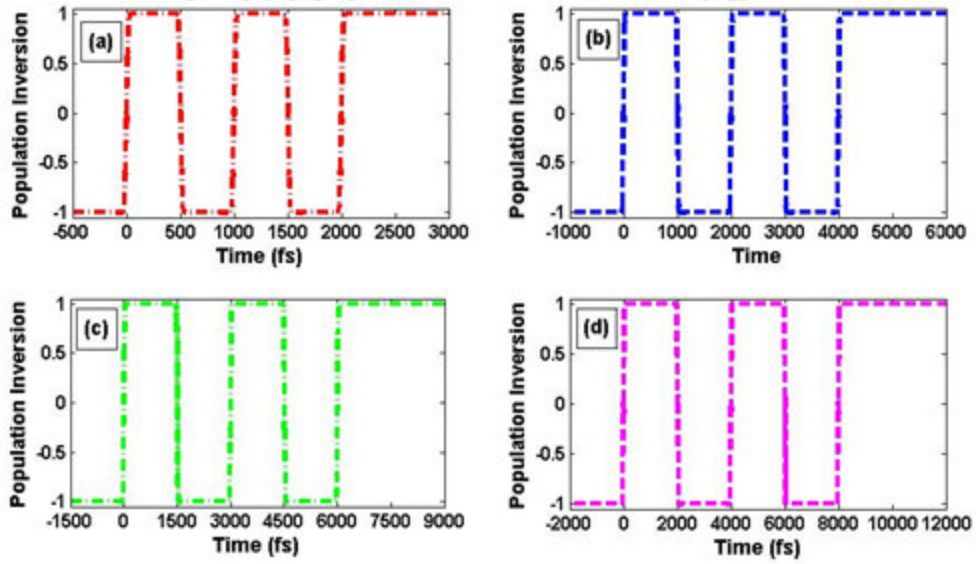

Fig. 2.4 Temporal evolution of population inversion for N=5, with pulse repetition time, (a) t_r=500 fs (b) t_r=1000 fs (c) t_r=1500 fs and (d) t_r=2000 fs.

In Fig. 2.4, we recovered exactly the same features of UCPOs which were obtained in dense medium. For example, it can be observed from Fig. 2.4 that the hold on time of atoms (τ_a) in up and down-states follows the relation, $\tau_a \approx t_r$ and the frequency of ultrafast coherent population oscillations (f_{ucpo}) between up and down state follows the relation, $f_{ucpo} \approx 1/2t_r$. Here, we used a train of linearly chirped pulses to obtain the UCPOs. On the other hand, we used a train of unchirped pulses to obtain the UCPOs in a self-chirped medium as discussed in section 2.2. Hence, with the chosen simulation parameters, a train of linearly chirped pulses interacting with dilute medium produce the same UCPOs as produced by a train of unchirped pulses in dense medium. A careful inspection of Fig.2.4 reveals that the atoms exhibits a step like transition, from absorbing (w<0) to amplifying (w>0) and amplifying

(w>0) to absorbing (w<0) as a function of the number of the pulses in the pulse train. The atomic medium, for odd number of pulses in the pulse train may be interpreted as an 'on' state and for the even number of pulses in the pulse train may be interpreted as an 'off' state. Therefore the present scheme may serve as a unique ultrafast optical switch, in which switching time may be controlled as follows: when a switching signal enters into the absorbing medium (w<0), the interaction may take place between the switching signal and the absorbing medium; thereby the switching signal may get absorbed in the medium due to the absorptive character of the medium. This corresponds to the 'off' state of the optical switch for a switching signal. On the other hand, when a switching signal enters into the amplifying medium (w>0), the interaction may take place between the switching signal and amplifying medium; thereby the switching signal may not get absorbed in the medium due to the amplifying character of the medium. This corresponds to the 'on' state of optical switch for a switching signal. It is worthwhile to mention that the reported UCPOs are similar to those reported by Scalora *et al.* [21, 22] for ultrafast optical switching. Therefore the present scheme may also find similar applications. In order to verify the robustness of the scheme, in Fig. 2.5 we depict the evolution of $w(\infty)$ against the variation of chirp rate for t_r=1000 fs and N=5.

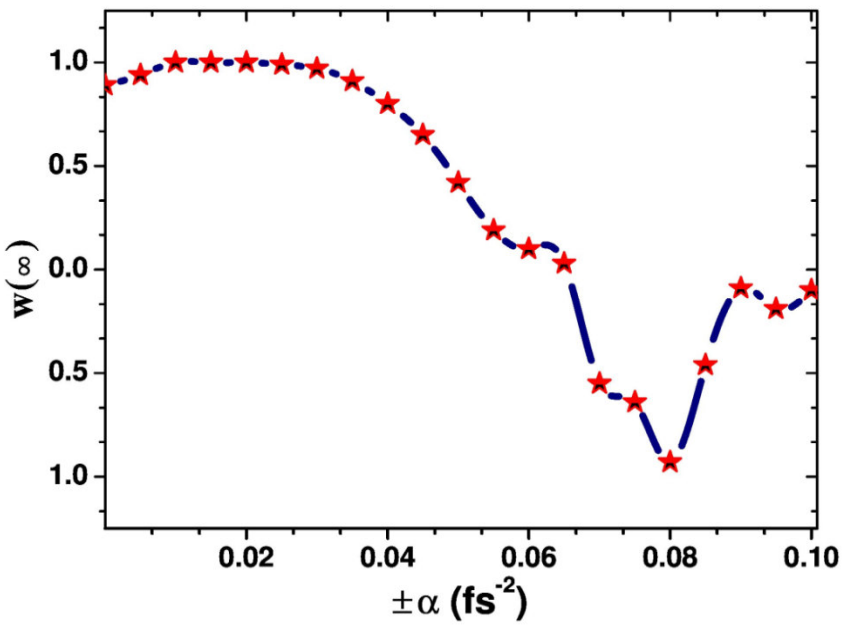

Fig. 2.5 Evolution of the final population inversion, $w(\infty)$ against the variation of chirp rate (α).

It is clear from Fig. 2.5 that the final population inversion is robust against the variation in chirp rate to a sufficiently large range e.g. $\alpha \approx \pm 0.01 - \pm 0.03\,\text{fs}^{-2}$ for the chosen t_r and N. From our numerical study, we found that the phenomenon of UCPOs is robust against the variation in pulse duration, Rabi frequency and detuning to a sufficiently large range e.g. $\tau_p \approx 19 - 110$ fs, $\Omega_{12} \approx 0.35 - 1.50$ rad/fs and $\Delta = 0 - \pm 0.35$ rad/fs respectively. For the variation in pulse parameters ($\tau_p \approx 19 - 110$ fs, $\Omega_{12} \approx 0.35 - 1.50$ rad/fs and $\Delta = 0 - \pm 0.35$ rad/fs), we observed the same kind of UCPOs as reported in Fig. 2.4. The remarkable features, namely, $\tau_a \approx t_r$ and $f_{ucpo} \approx 1/2t_r$, of UCPOs remain invariant to the pulse envelopes of various shapes such as: Sech, Sinc and Lorentz shaped pulse envelope. Since the final population inversion and UCPOs are sufficiently robust against the variation of the laser pulse parameters, the proposed scheme may enable efficient generation of complete population inversion in atoms of an ensemble located in different spatial points covered by the laser pulse. Hence the proposed scheme may be explored experimentally as well.

2.4 Chapter Summary

We observed the phenomenon of controllable UCPOs in the dense and dilute two-level atoms by utilizing the train of femtosecond pulses. We found that the holding time for atoms in the up and the down-states may be controlled by controlling the pulse repetition time. It is shown that a train of linearly chirped pulses interacting with dilute medium produce the same UCPOs as produced by a train of unchirped pulses in dense medium. However, in dense medium the phenomenon of controllable UCPOs is found to be unstable against slight variations in the peak Rabi frequency and the resonance condition. On the other hand, in dilute medium the phenomenon of controllable UCPOs is found to be robust against the sufficiently large variations in the peak Rabi frequency and resonance condition. Possible applications of the proposed scheme in ultrafast optical switching are also suggested. The proposed scheme may find new applications in the area of ultrafast optical switching.

Chapter 3

Coherent Population Transfer in Λ-Like Three-level Atomic Systems*

3.1 Introduction

Stimulated Raman adiabatic passage (STIRAP) and adiabatic rapid passage (ARP) are the two main techniques that have been used for controlling the population transfer in $\Lambda-$like three-level atomic systems [4]. Many researchers have utilized continuous or narrow-band laser (nanosecond time duration) pulses for implementing the STIRAP scheme. For complete and robust population transfer with the STIRAP scheme, the adiabatic condition, $\Omega\tau_p > 20\pi$ or $\Omega^2\tau_p > (20\pi)^2/\tau_p$, should be fulfilled, where Ω and τ_p are the peak Rabi frequency and the pulse width respectively. U. Gaubatz et al. and other researchers [30, 143] found that to implement the STIRAP technique with CW lasers, one has to achieve a Rabi frequency Ω large enough to satisfy the adiabatic condition. On the other hand, nanosecond pulses with transform limited bandwidth are required to reduce the phase fluctuations, which are detrimental to the adiabatic evolution [144, 145]. The essential requirement of adiabatic evolution of the system for complete and robust population transfer may also be an issue of concern with the use of femtosecond pulses, because the pulse energy ($E \sim \Omega^2\tau_p$) required to achieve the adiabatic condition increases with decrease in the pulse width. Researchers have found that for pulses in the picosecond or the femtosecond regime, use of linearly chirped laser pulses may be an alternative to the counterintuitive sequence of (fixed carrier frequency) pulses usually used for STIRAP [146]. Moreover, the counterintuitive sequence of pulses may also be realized with frequency chirped laser pulses [147, 148]. In this regard, B. Broers et al. [147] have shown coherent population transfer (CPT) in a three-level rubidium ladder system by utilizing a single linearly chirped pulse. They demonstrated that a single

* Part of the results presented in this chapter have been published in a paper, P. Kumar and A. K. Sarma, "Gaussian and sinc-shaped few-cycle-pulse-driven ultrafast coherent population transfer in Λ -like atomic systems", Phys. Rev. A 85, 043417 (2012).

linearly chirped pulse may interact with the transition levels of system in a counter intuitive manner similar to that of the STIRAP scheme. The same researchers have shown that the population of the intermediate level, at intermediate times of interaction, is highly reduced when a single chirped pulse interacts with the system in counter intuitive manner in contrast to the intuitive interaction. For the complete population transfer between the quantum states, the STIRAP and the rapid adiabatic passage are generally energetically expensive, for example, relative to a $\pi-$pulse technique [140, 149]. On the other hand, sometimes the $\pi-$pulse technique is not robust against variation of the laser pulse parameters.

In this chapter, we are presenting a relatively simple scheme using nonlinearly chirped and unchirped laser pulses, in which no time delay is required between the two pulses in contrast to the STIRAP scheme. It is worthwhile to mention that nonlinearly chirped femtosecond pulses have been found suitable for many applications [150-153] and can be generated experimentally [154]. We study coherent population transfer in $\Lambda-$like three-level atomic systems with non-degenerate or nearly degenerate lower states. We have presented a scheme to obtain nearly complete CPT in the nondegenerate atomic systems either by utilizing two nonlinearly chirped Gaussian shaped or two unchirped sinc-shaped few-cycle laser pulses. In addition, we have shown CPT in the nearly degenerate atomic systems by utilizing a single nonlinearly chirped Gaussian shaped few-cycle pulse.

3.2 Few-cycle-femtosecond pulse driven coherent population transfer

We consider a Λ-like atomic system interacting with two few-cycle laser pulses as shown in Fig. 3.1. The electric field of the linearly polarized laser interacting between $|3\rangle$ and $|1\rangle$ is given by $\vec{E}_1(t)=\vec{E}_{10}f(t)\cos\left(\omega_{10}t+\delta_1(t)\right)$, where $\vec{E}_{10}, f(t)$ and ω_{10} are respectively, the amplitude, the field envelope and the carrier frequency of the pulse. Exactly analogous expression for the linearly polarized laser pulse interacting between $|3\rangle$ and $|2\rangle$ is given by $\vec{E}_2(t)=\vec{E}_{20}f(t)\cos\left(\omega_{20}t+\delta_2(t)\right)$. For the Gaussian shaped few-cycle laser fields, $f(t)=\exp\left[-(t/\tau)^2\right], \delta_1(t)=\chi_1 t^3$ and $\delta_2(t)=\chi_2 t^3$. Here χ_1 and χ_2 are the respective chirp rate of the Gaussian pulses. On the other hand, for the sinc-shaped few-cycle pulses, $f(t)=\sin(t/\tau)/(t/\tau)$, $\delta_1=\phi_1$ and $\delta_2=\phi_2$, where ϕ_1 and ϕ_2 are the respective carrier-envelope phases. Here, τ_p is the temporal width of the laser pulses. For Gaussian and sinc-

shaped pulses, temporal pulse duration is given by $\tau_p = 1.177\,\tau$ and $\tau_p = 2.783\,\tau$ respectively. In the given scheme, we assume that only $|3\rangle \rightarrow |1\rangle$ and $|3\rangle \rightarrow |2\rangle$ transitions are dipole allowed while $|2\rangle \rightarrow |1\rangle$ transitions are forbidden.

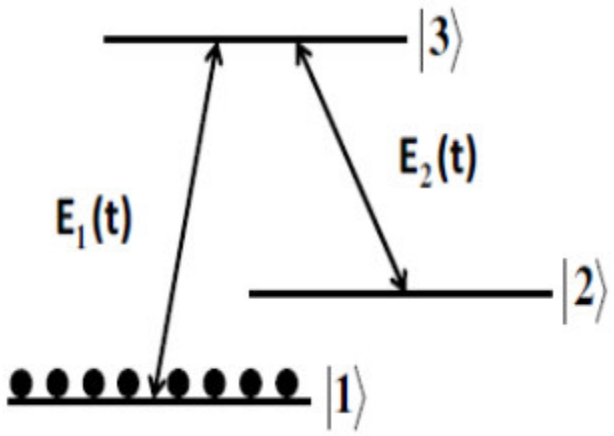

Fig. 3.1 Schematic of the Λ-like three-level atom with two acting few-cycle laser pulse

The Hamiltonian of the system is given by $\hat{H} = \hat{H}_0 + \hat{H}_{int}$ where $\hat{H}_0 = \hbar\left(\omega_1|1\rangle\langle 1| + \omega_2|2\rangle\langle 2| + \omega_3|3\rangle\langle 3|\right)$ and $\hat{H}_{int} = -\vec{\mu}.\vec{E} = -\hbar\Omega_{31}(t)|3\rangle\langle 1| - \hbar\Omega_{32}(t)|3\rangle\langle 2| + \text{h.c.}$

Here $\Omega_{31}(t) = \mu_{31}\vec{E}_1(t)/\hbar$ and $\Omega_{32}(t) = \mu_{32}\vec{E}_2(t)/\hbar$ are the time dependent Rabi frequencies for the transitions with electric dipole moments μ_{31} and μ_{32} respectively. The Bloch equations, without invoking the rotating wave approximation, describing the temporal evolution of the density matrix elements are:

$$\begin{aligned}
\dot{\rho}_{31} &= -i\,\omega_{31}\,\rho_{31} + i\,\Omega_{32}(t)\,\rho_{21} - i\,\Omega_{31}(t)(\rho_{33} - \rho_{11}) \\
\dot{\rho}_{32} &= -i\,\omega_{32}\,\rho_{32} + i\,\Omega_{31}(t)\,\rho_{12} - i\,\Omega_{32}(t)(\rho_{22} - \rho_{33}) \\
\dot{\rho}_{21} &= -i\,\omega_{21}\,\rho_{21} + i\,\Omega_{32}(t)\,\rho_{31} - i\,\Omega_{31}(t)\,\rho_{23} \\
\dot{\rho}_{11} &= i\,\Omega_{31}(t)(\rho_{31} - \rho_{13}) \\
\dot{\rho}_{22} &= i\,\Omega_{32}(t)(\rho_{32} - \rho_{23}) \\
\dot{\rho}_{33} &= i\,\Omega_{31}(t)(\rho_{13} - \rho_{31}) + i\,\Omega_{32}(t)(\rho_{23} - \rho_{32})
\end{aligned} \qquad (3.2.1)$$

Here, $\omega_{ij} = \omega_i - \omega_j$. It may be noted that $\rho_{ij} = \rho_{ji}^*$. We solve Eq. (1) numerically using a standard fourth-order Runge-Kutta method. We assume that initially all the atoms are in the ground state $|1\rangle$. We use the following typical parameters: $\omega_{31} = \omega_{10} = 3.0$ rad/fs, $\omega_{21} = 0.4$ rad/fs, $\omega_{32} = \omega_{20} = 2.6$ rad/fs, $\Omega_{31} = 0.76$ rad/fs, $\Omega_{32} = 0.79$ rad/fs, $\chi_1 = \chi_2 = 0.016\,\text{fs}^{-3}$,

$\phi_1 = \phi_2 = 0$. The temporal pulse width is taken to be, τ_p = 4.70 fs and 5.06 fs respectively for the Gaussian and the sinc pulses. For our chosen parameters, the pulse areas are too small for the adiabatic condition to be fulfilled. It is worthwhile to note that in the usual adiabatic passage scheme for population transfer between the initial state and the final one, the adiabatic condition can be written as: $\Omega \tau_p >> 2\pi$, where $\Omega = \Omega_{31}(0) = \Omega_{32}(0)$ is the maximal Rabi frequency [4]. In practical applications the pulse area should exceed 20π, i.e. $\Omega \tau_p > 20\pi$ to provide efficient population transfer via the adiabatic passage scheme [4]. We find that for complete population transfer with our proposed scheme, the total temporal area of the Gaussian pulses is calculated to be 3.49π, while it is 13.53π for the STIRAP scheme with same laser pulse parameters. Fig. 3.2 and Fig. 3.3 depict the respective temporal evolution of the populations ρ_{11}, ρ_{22} and ρ_{33} when Gaussian chirped and unchirped sinc-pulses are used.

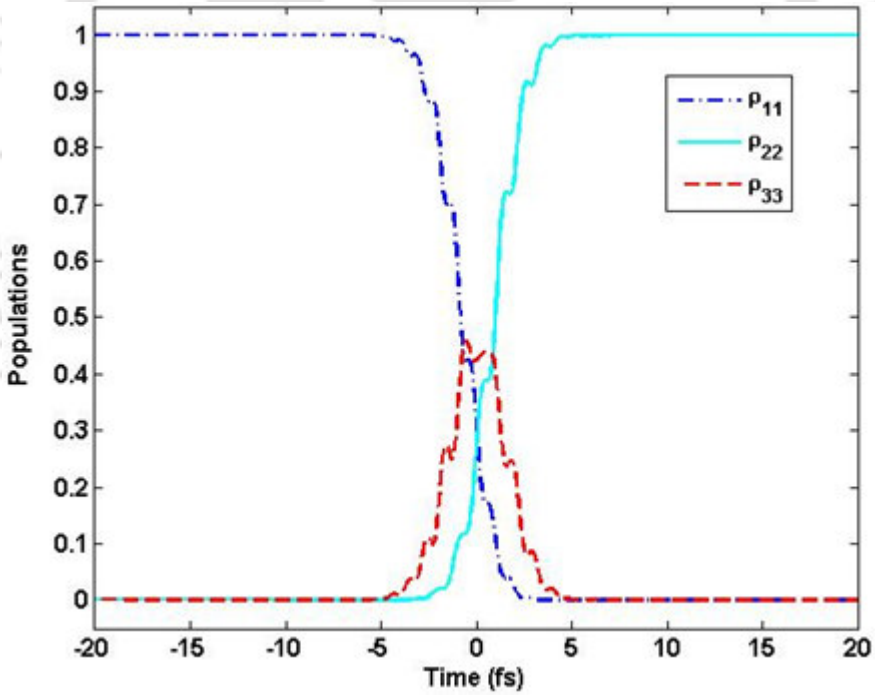

Fig. 3.2 Temporal evolution of populations with the nonlinearly-chirped Gaussian shaped few-cycle pulse

It is clear from Fig. 3.2 that one can obtain complete population transfer (99.94 %) from the ground state $|1\rangle$ to the state $|2\rangle$ using two nonlinearly chirped Gaussian shaped laser pulses. On the other hand, as evident from Fig. 3.3, near complete population transfer (99.05 %)

from $|1\rangle$ to $|2\rangle$ is possible due to the simultaneous interaction of two sinc-shaped pulses with the three-level atomic system.

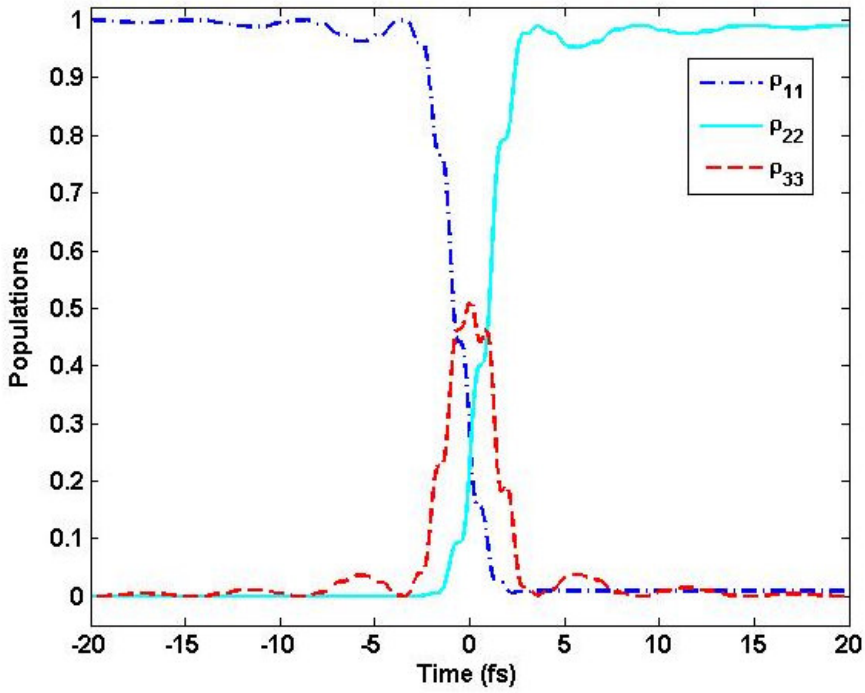

Fig. 3.3 Temporal dynamics of populations with the Sinc-shaped few-cycle pulse

These results could be explained on the basis of the so-called Stimulated Emission Pumping (SEP) [31]. In SEP with continuous laser or short laser pulses, all the relaxation processes in atomic system take place on time scales shorter than the interaction time. Hence the maximum amount of population transfer between the quantum states is restricted by the spontaneous emission. For example, one can achieve a maximum 30 % population transfer in Λ – like three-level atomic systems with the SEP technique [4]. However, in our scheme, we have shown that almost complete population transfer in Λ – like atomic systems is possible owing to the use of few-cycle pulses where interaction takes on a time scale shorter than that of the relaxation processes. Non-adiabatic consequences on the temporal evolution of the populations can be observed from Fig. 3.2 and Fig. 3.3. Unlike the adiabatic passage techniques, population in quantum state $|3\rangle$ during the intermediate time is approaching a large value (ρ_{33}=45 % for Gaussian pulse and ρ_{33} = 46 % for sinc pulse) as the adiabatic criteria is not fulfilled for the chosen laser pulse areas. However, ultimately the quantum state $|2\rangle$ receives almost all the populations in both cases.

The non-RWA effects on the temporal evolution of the populations can also be observed from Fig. 3.2 and Fig. 3.3. Some authors have pointed out that when few-cycle laser pulses are considered, the time-derivative driven nonlinearities will have a significant impact on the interaction of the laser pulses with the atomic medium which may lead to strong oscillation features during the evolution of the populations [98, 155]. These features are not present in the RWA solutions. Now, in order to have some insight or understanding why the use of Gaussian shaped or sinc-shaped few-cycle pulse results in almost similar behaviour with regard to population transfer, in Fig. 3.4 we plot the temporal evolution of both the pulses.

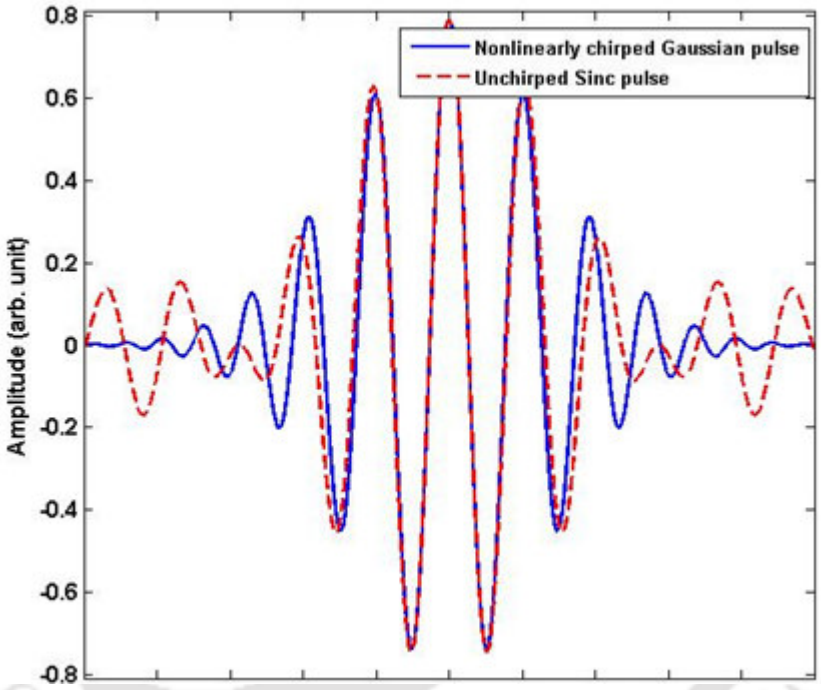

Fig. 3.4 Temporal evolution of nonlinearly-chirped Gaussian and unchirped sinc shaped pulses

Fig. 3.4 reveals that the nonlinearly-chirped Gaussian and the unchirped sinc shaped pulses are equivalent to each other, particularly in the temporal range from -2 to +2 fs. For other temporal range from -6 to -2 fs and +2 to +6 fs, the amplitude of the nonlinearly chirped Gaussian pulse is slightly greater than that of the unchirped sinc shaped pulse. Also, the carrier oscillation frequency of the Gaussian shaped few-cycle pulse is slightly larger, owing to the nonlinear chirp, than that of the unchirped sinc shaped few-cycle pulse in the same temporal range. This might be the reason behind the almost similar nature of interaction of the pulses with the atomic system. Hence, we may conclude that, subject to the chosen parameters, the nonlinearly chirped Gaussian and the unchirped sinc shaped few-cycle pulses

exhibit almost identical behaviour. It may be observed from Fig. 3.4 that one ($\Delta_1 = \omega_{31} - \omega_{10} = \Delta_2 = \omega_{32} - \omega_{20} = 0$) and two-photon ($\Delta = \Delta_1 - \Delta_2 = 0$) resonance conditions are fulfilled for unchirped sinc-shaped laser pulse. However, for the nonlinearly chirped Gaussian laser pulse, the one-photon resonance condition is partially fulfilled during the intermediate time of interaction while the two-photon resonance condition is fulfilled during the whole interaction.

It is important to verify the robustness of the scheme against the variation of the chirp rate and the temporal pulse width of the Gaussian shaped few-cycle pulse. So, in Fig. 3.5 we present the simulation result for the variation of the final population transfer to the state $|2\rangle$, i.e. $\rho_{22}(\infty)$ with τ_p, while in Fig. 3.6 we check the robustness of the scheme against chirp rates for the nonlinearly chirped Gaussian shaped few-cycle pulses.

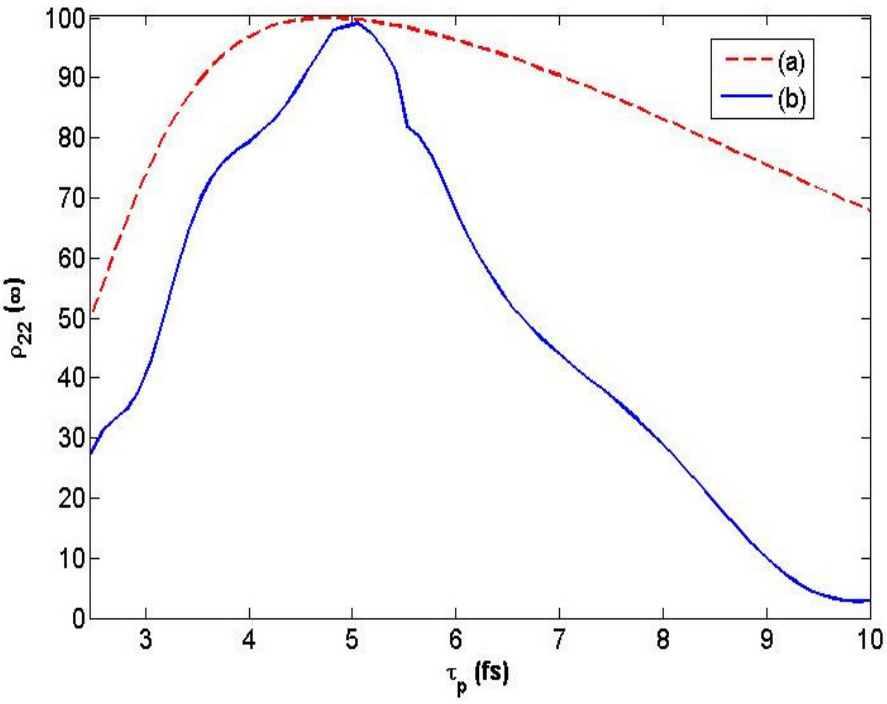

Fig. 3.5 Final population transfer to quantum state $|2\rangle$ as a function of (a) temporal pulse width, τ_p of the nonlinearly chirped Gaussian pulse and (b) temporal pulse width, τ_p of the sinc pulse. Here all the other parameters are kept constant.

It can be seen from Fig. 3.5(a) that the final population transfer $\rho_{22}(\infty)$ to the quantum state $|2\rangle$ is sufficiently robust against the variation (4-6 fs) of the temporal width of a Gaussian

pulse , while Fig. 3.5(b) shows that the final population transfer $\rho_{22}(\infty)$ to quantum state $|2\rangle$ is robust against small variations (4.94-5.17 fs) of the temporal width of a sinc pulse.

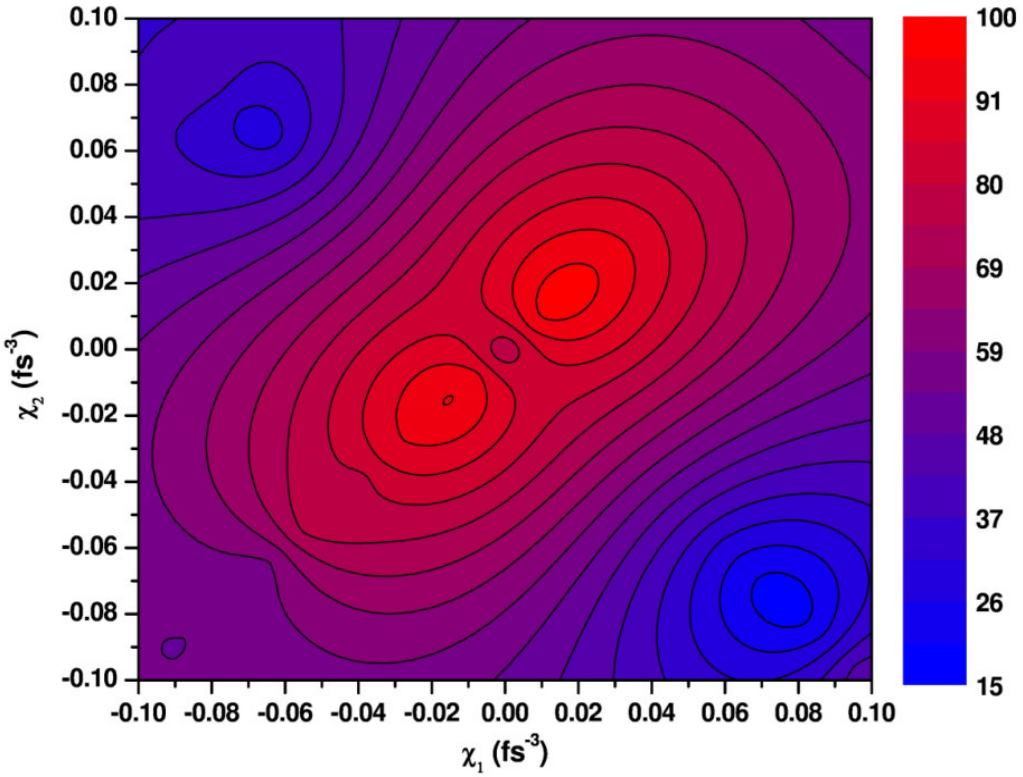

Fig. 3.6 Final population transfer $\rho_{22}(\infty)$ to quantum state $|2\rangle$ as a function of chirp rates, χ_1 and χ_2. Here, the other parameters are same as those in Fig. 3.2.

It can be observed from Fig. 3.6 that the final population transfer $\rho_{22}(\infty)$ is sufficiently robust against the variation of the chirp rates, χ_1 and χ_2. It can be seen that the final population transfer $\rho_{22}(\infty)$ to the quantum state $|2\rangle$ is robust against the small variation (0.012-0.020 fs^{-3}) of the chirp rates χ_1 and χ_2. In Fig. 3.7 we plot the variation of the final population $\rho_{22}(\infty)$ with the carrier envelope phases to check the robustness of the scheme for sinc-shaped few-cycle pulses.

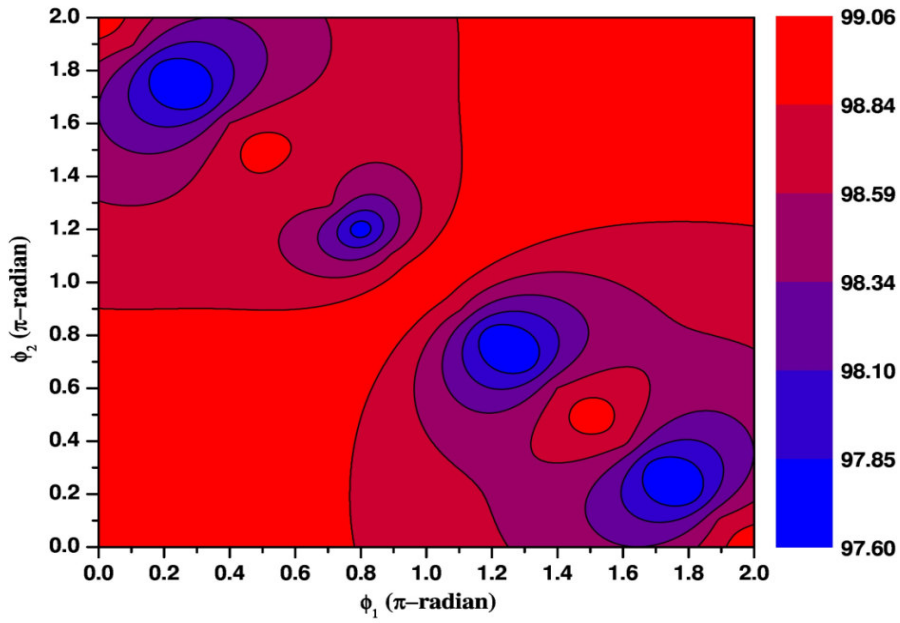

Fig. 3.7 Final population transfer $\rho_{22}(\infty)$ to quantum state $|2\rangle$ as a function of (a) carrier-envelope phases, ϕ_1 and ϕ_2 in unit of π radians. The other parameters are same as those in Fig. 3.3.

We find that, from Fig. 3.7, the final population transfer $\rho_{22}(\infty)$ is highly robust against the variation of the carrier-envelope phases ϕ_1 and ϕ_2 of the sinc-shaped few cycle pulses.

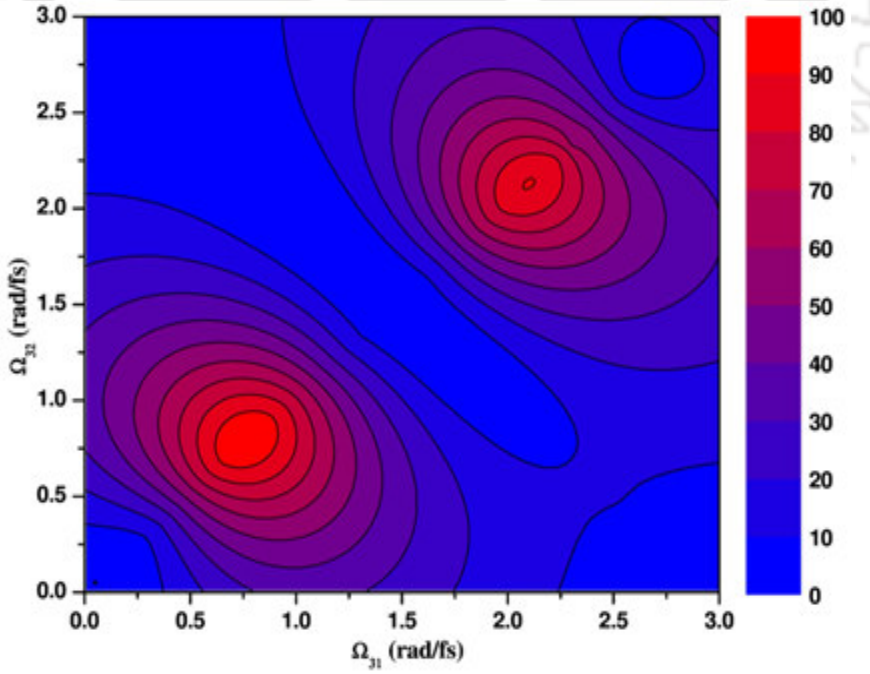

Fig. 3.8 Contour maps of the final population (in %) transfer for varying Rabi frequencies Ω_{31} and Ω_{32} of nonlinearly chirped Gaussian pulse. Here the other parameters are same as those in Fig. 3.2.

We also test the robustness of our proposed scheme against variation of the Rabi frequencies of the few-cycle laser pulses considered in this work. In Fig. 3.8, we depict the contour map of the final population to the quantum state $|2\rangle$, i.e. $\rho_{22}(\infty)$, against Rabi frequencies Ω_{31} and Ω_{32} of the nonlinearly chirped Gaussian shaped few-cycle pulse. A careful inspection of Fig. 3.8 reveals that the final population transfer is fairly robust against the variation of the Rabi frequencies Ω_{31} and Ω_{32} in the range of 0.70-0.92 rad/fs, which amounts to more than 95 % population. Population in the range of 88-90% could be possible for variation of the Rabi frequencies in the range 2.30-2.40 rad/fs.

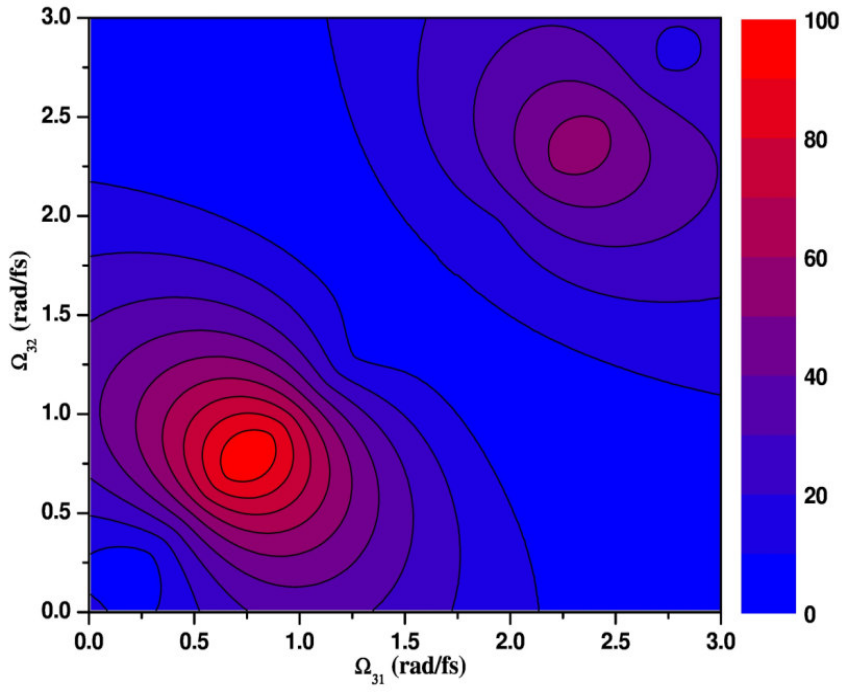

Fig. 3.9 Contour maps of the final population (in %) transfer for varying Rabi frequencies Ω_{31} and Ω_{32} of unchirped sinc pulses. The other parameters are the same as those in Fig. 3.3.

The robustness of the population transfer with sinc shaped few-cycle pulses is depicted in Fig. 3.9. The population transfer to the quantum state $|2\rangle$ exhibits sufficient robustness with the small variation of Rabi frequencies. In fact one can obtain more than 95% population transfer for the variation of Ω_{31} and Ω_{32} in the range of 0.70-0.85 rad/fs. It is worthwhile to mention that we have tested our proposed scheme for atomic systems like indium and thallium. We observe near complete population transfer, with appropriate choice of simulation parameters, in these atomic systems with both Gaussian and sinc-shaped few-

cycle pulses. Hence the model proposed by us may be tested experimentally in atomic systems like indium and thallium and in other atoms which exhibit the same quantum states configuration. In passing, it may be noted that indium, thallium and gallium have been studied extensively both theoretically and experimentally in the context of laser cooling of atoms [156-159].

3.2 Single few-cycle-femtosecond pulse driven coherent population transfer

In section 3.2, we presented a scheme to obtain nearly complete population transfer in a Λ-like three-level atomic systems with nondegenerate lower states (state $|1\rangle$ and state $|2\rangle$). The system was driven by two few-cycle femtosecond pulses. It is to be noted that the reported scheme may not be useful if the frequency bandwidth ($\Delta\omega$) of the pulses is equal or greater than the frequency difference of the lower states (ω_{21}). For example, in the case of Λ-like three-level atomic systems with nearly degenerate lower states, we cannot claim that the pulse $E_1(t)$ interacts only with the $|3\rangle \rightarrow |1\rangle$ transition path and $E_2(t)$ interacts only with $|3\rangle \rightarrow |2\rangle$ transition path. In fact both pulses may interact via both the transition paths, if not restricted by the transition selection rules.

Our analysis is based on the scheme depicted in Fig. 3.10. We consider a Λ-like atomic system interacting with a single few-cycle laser pulse. The electric field of the linearly polarized laser pulse, interacting between $|3\rangle \leftrightarrow |1\rangle$ and $|3\rangle \leftrightarrow |2\rangle$ is given by $\vec{E}(t) = \vec{E} f(t) \cos(\omega t + \delta(t))$, where $\vec{E}, f(t)$ and ω are respectively, the amplitude, the field envelope and the carrier frequency of the pulse. For Gaussian shaped few-cycle laser fields, $f(t) = \exp[-(t/\tau)^2]$, $\delta(t) = \chi t^3$. Here χ is the chirp rate of the Gaussian pulse.

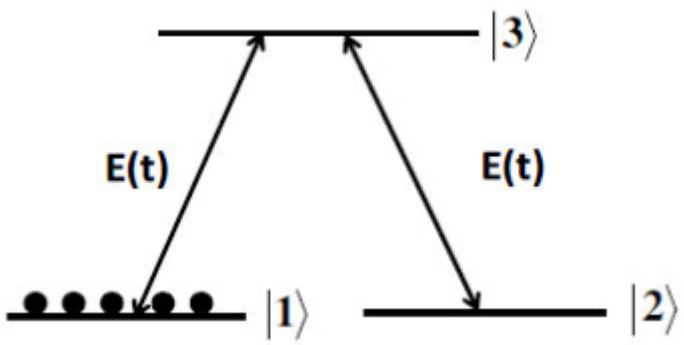

Fig. 3.10 Schematic of Λ-like system with a single acting few-cycle laser pulse

In the given scheme, we assume that only $|3\rangle \rightarrow |1\rangle$ and $|3\rangle \rightarrow |2\rangle$ transitions are dipole allowed while the $|2\rangle \rightarrow |1\rangle$ transition is forbidden. We have chosen a model Λ-like three-level atomic systems with nearly degenerate lower states. This scheme may be realized in some real atomic systems such as aluminium, boron, and gallium and possibly in alkali metals with hyperfine states.

The Hamiltonian of the system is given by $\hat{H} = \hat{H}_0 + \hat{H}_{int}$ where $\hat{H}_0 = \hbar\left(\omega_1|1\rangle\langle 1| + \omega_2|2\rangle\langle 2| + \omega_3|3\rangle\langle 3|\right)$ and $\hat{H}_{int} = -\vec{\mu}.\vec{E} = -\hbar\Omega_{31}(t)\left(|3\rangle\langle 1| + \beta|3\rangle\langle 2|\right) + \text{h.c.}$

Here, h.c. refers to hermitian conjugate, and $\Omega_{31}(t) = \mu_{31}\vec{E}(t)/\hbar$ and $\Omega_{32}(t) = \mu_{32}\vec{E}(t)/\hbar$ are the time dependent Rabi frequency with electric dipole moment μ_{31} and μ_{32} respectively. Also, $\mu_{32} = \beta\mu_{31}$, where β is termed as the dipole moment coefficient. The density matrix equations, without invoking the so called rotating wave approximation, describing the temporal evolution of the density matrix elements are:

$$\begin{aligned}
\dot{\rho}_{31} &= -i\,\omega_{31}\,\rho_{31} - i\,\Omega_{31}(t)(\rho_{33} - \rho_{11} - \beta\rho_{21}) \\
\dot{\rho}_{32} &= -i\,\omega_{32}\,\rho_{32} + i\,\Omega_{31}(t)(\rho_{12} - \beta\rho_{22} + \beta\rho_{33}) \\
\dot{\rho}_{21} &= -i\,\omega_{21}\,\rho_{21} - i\,\Omega_{31}(t)(\rho_{23} - \beta\rho_{31}) \\
\dot{\rho}_{11} &= i\,\Omega_{31}(t)(\rho_{31} - \rho_{13}) \\
\dot{\rho}_{22} &= i\,\beta\,\Omega_{31}(t)(\rho_{32} - \rho_{23}) \\
\dot{\rho}_{33} &= i\,\Omega_{31}(t)(\rho_{13} - \rho_{31}) + i\,\beta\,\Omega_{31}(t)(\rho_{23} - \rho_{32})
\end{aligned} \tag{3.3.1}$$

Here $\omega_{ij} = \omega_i - \omega_j$. It may be noted that $\rho_{ij} = \rho_{ji}^*$. We solve Eq. (3.3.1) numerically using a standard fourth-order Runge-Kutta method. We assume that initially all the atoms are in the ground state $|1\rangle$. We use the following typical parameters: $\omega_{31} = \omega = 3.18$ rad/fs, $\omega_{21} = 0.0001$ rad/fs, $\Omega_{31} = 0.55$ rad/fs, $\chi = 0.0035$ fs^{-3}, and β=0.99. The temporal pulse width is taken to be, τ_p=5.86 fs. In Fig. 3.11, we depict the temporal evolution of the populations ρ_{11}, ρ_{22} and ρ_{33}. It is clear from Fig. 3.11 that one can obtain nearly complete population transfer (99.24 %) from the ground state $|1\rangle$ to the state $|2\rangle$ using a single nonlinearly chirped laser pulse. The non-adiabatic consequences on the temporal evolution of the populations could be observed from Fig. 3.11. Unlike the adiabatic passage techniques, population in quantum state $|3\rangle$

during the intermediate time is approaching a large value (ρ_{33} =45 %) as the adiabatic criteria is not fulfilled for the chosen laser pulse area. However, at the end of interaction, quantum state $|2\rangle$ receives almost all the populations.

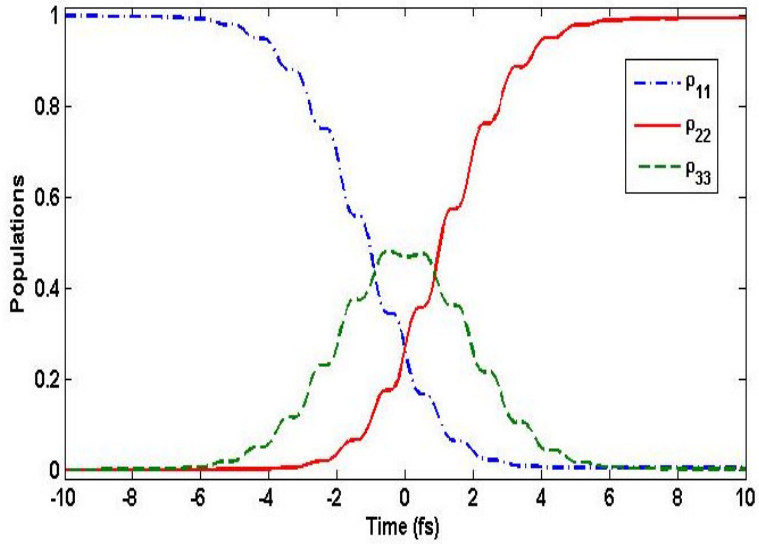

Fig. 3.11 Temporal evolution of populations with a single Gaussian shaped few-cycle pulse

Fig. 3.12 depicts the robustness of the final population transfer to quantum state $|2\rangle$ as a function of the dipole moment coefficient and the peak Rabi frequency.

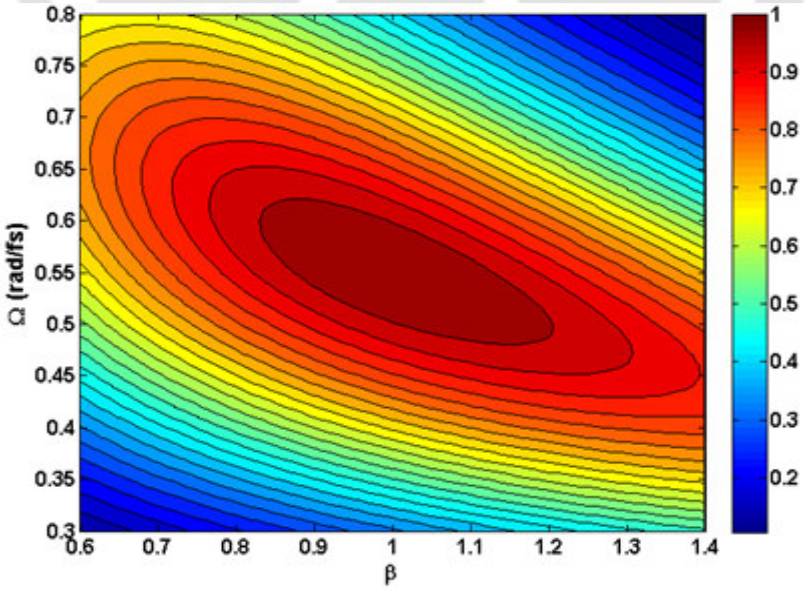

Fig. 3.12 Final population transfer to quantum state $|2\rangle$ as a function of dipole moment coefficient β and peak Rabi frequency Ω. Here other parameters are the same as those in Fig. 3.11.

It can be observed from Fig. 3.12 that the final population transfer to quantum state $|2\rangle$ is robust against the variation in the dipole moment coefficient and the peak Rabi frequency. For example, more than 0.95 (95 %) populations could be obtained inspite of variations in the peak Rabi frequency and the dipole moment coefficient in the range of 0.52 – 0.58 rad/fs and 0.92 – 1.12 respectively. Next, we examine the robustness of the final population transfer to quantum state $|2\rangle$ as a function of the pulse duration and the peak Rabi frequency.

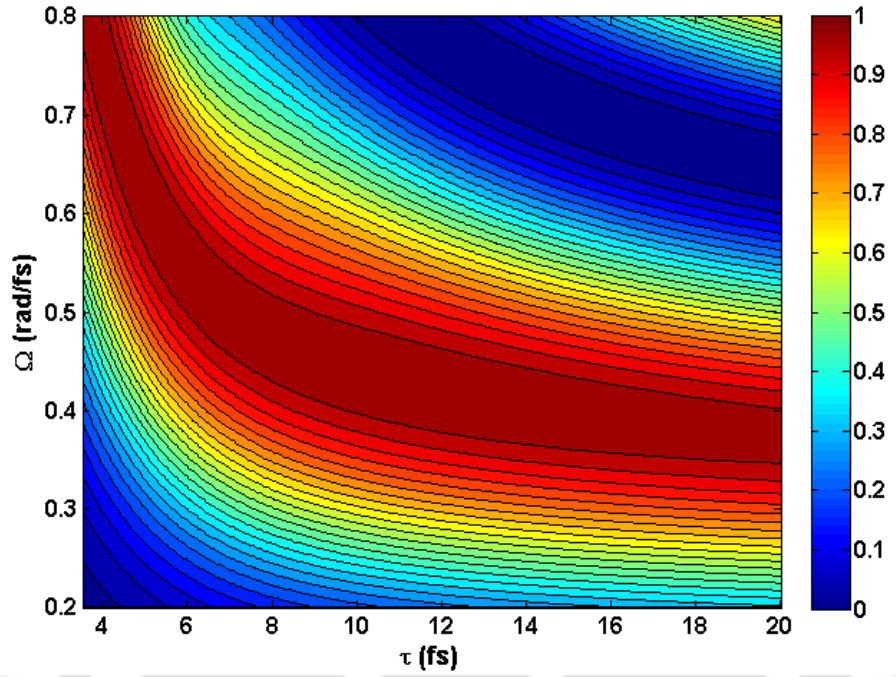

Fig. 3.13 Final population transfer to quantum state $|2\rangle$ as a function of pulse duration τ_p and Rabi frequency Ω. Here other parameters are the same as those in Fig. 3.11.

It can be observed from Fig. 3.13 that the final population transfer to the quantum state $|2\rangle$ is fairly robust against the variation in the pulse duration and the peak Rabi frequency. Fig. 3.13 reveals that with longer pulse duration, one can obtain almost complete population transfer at smaller values of the peak Rabi frequency.

3.4 Chapter Summary

In summary, we have reported almost complete population transfer to the target quantum state in Λ-like three-level atomic systems with non-degenerate and nearly degenerate lower states. In non-degenerate systems, we demonstrated population transfer by utilizing either two nonlinearly chirped Gaussian shaped or two unchirped sinc-shaped few-cycle laser

pulses. Population transfer with two nonlinearly chirped Gaussian pulses is found to be sufficiently robust against the variation of temporal pulse width, Rabi frequencies and the chirp rates. However, the population transfer with two unchirped sinc-shaped pulse is found to be highly robust against the variation of the carrier-envelope phase and fairly robust against the variation of the temporal pulse width and the peak Rabi frequencies. We find that compared to the STIRAP technique, our scheme for complete population transfer with few-cycle Gaussian shaped laser pulses requires less pulse area. Hence, nonlinearly chirped Gaussian shaped few-cycle laser pulses or the sinc-shaped few cycle laser pulses even with highly fluctuating carrier-envelope phase, may be employed for an efficient and ultrafast coherent population transfer with judicious choice of laser pulse parameters. In nearly degenerate systems, we demonstrated the population transfer by utilizing a single nonlinearly chirped few-cycle laser pulse. The population transfer with a single nonlinearly chirped pulse is found to be sufficiently robust against the variation in the peak Rabi frequency, the dipole moment coefficient and the temporal pulse width.

Chapter 4

Coherent Population Transfer in Multi-level Atomic Systems*

4.1 Introduction

In the previous two chapters, we have presented schemes for coherent population transfer (CPT) in two and three-level atoms. However, under certain conditions the modelling of a real atom as a four or higher- level atom is desirable. Many prior researchers have demonstrated CPT in four or higher level atoms. For example, M. Krug et al. [142] considered nine-levels (3s, 3p, 3d, 4s, 5p, 5f, 6p, 6f and 7p) of sodium atom in an experimental study on strong field control of multiple levels by an intense single chirped femtosecond laser pulse. Dipole allowed transitions among these levels, via single or multi-photon absorption, may take place owing to the high intensity of the chirped femtosecond pulse. In addition, Y. B. Band and O. Magnes [160] demonstrated selective CPT in Λ-like or ladder-like four-level atoms by combining STIRAP and Raman chirped adiabatic passage (RCAP) techniques. Moreover, Xihua Yang and Shiyao Zhu [161] investigated the effect of collisions on the control of CPT in inverse Y-type four-level atoms driven by three laser fields with STIRAP scheme. They found that low population transfer efficiency could be enhanced dramatically with the increase of the collision-induced coherence decay rates. In another study, Xihua Yang et al. [162] presented an efficient scheme for selective CPT in the Λ-like four-level atoms by combining STIRAP, temporal coherent control (TCC) and RCAP techniques. Apart from the coherent control of population transfer using two or more pulses, recently, much attention has been paid towards realizing CPT by using a single frequency chirped pulse in Λ-like three and four-level atoms, owing to the easy realization of the complete population transfer. In particular, G. P. Djotyan et al. [163] demonstrated CPT in Λ-like atoms using a single frequency-chirped laser pulse. In this study the researchers found that for the realization of complete population transfer, the width of the frequency spectrum

*This work has been published in a paper, P. Kumar and A. K. Sarma, "Ultrafast and selective coherent population transfer in four-level atoms by a single nonlinearly chirped femtosecond pulse", Phys. Rev. A 88, 033823 (2013).

of the transform-limited laser pulse must be smaller and the peak Rabi frequency of the pulse must be larger than the frequency interval between the two ground-state levels of the Λ atom Very recently, T. A. Collins and S. A. Malinovskaya [22] demonstrated CPT in ultracold Λ-like three level Rubidium atoms with a low intensity chirped-pulse. Again, Z. Zhang et al. [164] have proposed a scheme for CPT and arbitrary superpositions of quantum states by a single-chirped laser pulse in a Λ-like excited-doublet four-level system. They demonstrated efficient and robust CPT via a single-chirped pulse when the pulse bandwidth is smaller than about 1/10 of the energy separation between the excited-doublet levels and between the ground states. In the present chapter, we discuss a scheme for selective and ultrafast CPT in a system of Y-like four-level Na atoms by using a nonlinearly chirped femtosecond laser pulse.

4.2 Selective coherent population transfer in Y-like four-level atoms

Our proposed scheme is depicted in Fig. 4.1. In Fig. 4.1, the levels, $|1\rangle$, $|2\rangle$, $|3\rangle$, and $|4\rangle$ represent the 3s, 3p, 5s, 4d states of sodium atoms respectively.

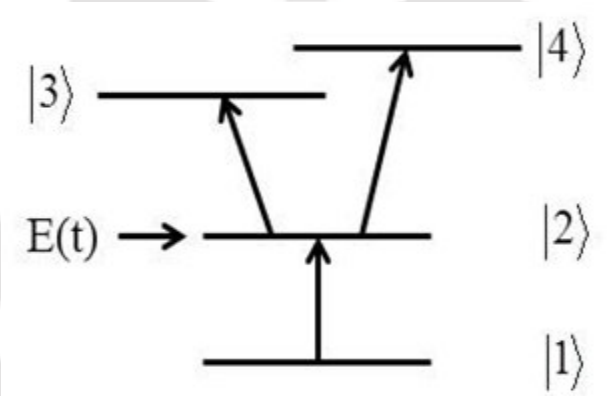

Fig. 4.1 Schematic of the scheme

The complete Hamiltonian without invoking the RWA approximation, which describes the interaction of a single pulse with four-level atoms, is given by:

$$\hat{H} = \hbar \begin{pmatrix} \omega_1 & -\Omega_{12}(t) & 0 & 0 \\ -\Omega_{12}(t) & \omega_2 & -\beta\Omega_{12}(t) & -\gamma\Omega_{12}(t) \\ 0 & -\beta\Omega_{12}(t) & \omega_3 & 0 \\ 0 & -\gamma\Omega_{12}(t) & 0 & \omega_4 \end{pmatrix} \quad (4.2.1)$$

Here, $\Omega_{12}(t) = \mu_{12}E(t)/\hbar$ is the time dependent Rabi frequency, μ_{12} is the transition dipole moment of $|1\rangle \rightarrow |2\rangle$ transition. The transition dipole moments μ_{23} and μ_{24} are chosen as

follows: $\mu_{23} = \beta\mu_{12}$ and $\mu_{24} = \gamma\mu_{12}$. Here, β and γ are the dipole moment coefficients. The electric field part of the pulse is defined as follows: $E(t) = f(t)\cos(\omega t + \delta(t))$, where $f(t)$ is the pulse envelope, given by: $f(t) = E_0 \exp\left(-(t/\tau_p)^2\right)$. Here, E_0 is the peak amplitude of the pulse envelope, $\tau_{FWHM} = 1.177\tau_p$, ω is the central frequency and $\delta(t)$ is the time varying phase. The temporal profile of $\delta(t)$ is defined as $\delta(t) = -\alpha \tanh\left(\frac{t - t_0}{\tau}\right)$. This temporal profile has been considered by other researchers as well in various contexts [151, 153]. The chirped form of the pulse may be controlled by manipulating the three parameters α, t_0 and τ. In this work, these three control parameters are termed as frequency sweeping, frequency offset and frequency steepening parameters respectively. The time-varying frequency of the pulse has the form: $\omega(t) = \omega - \frac{\alpha}{\tau}\text{sech}^2\left(\frac{t - t_0}{\tau}\right)$. The Bloch equations, without invoking the rotating wave approximation, describing the temporal evolution of the density matrix elements are:

$$
\begin{aligned}
\frac{d\rho_{11}}{dt} &= i\Omega_{12}(t)(\rho_{21} - \rho_{12}) \\
\frac{d\rho_{22}}{dt} &= i\Omega_{12}(t)(\rho_{12} - \rho_{21} + \beta(\rho_{32} - \rho_{23}) + \gamma(\rho_{42} - \rho_{24})) \\
\frac{d\rho_{33}}{dt} &= i\Omega_{12}(t)(\beta(\rho_{23} - \rho_{32})) \\
\frac{d\rho_{44}}{dt} &= i\Omega_{12}(t)(\gamma(\rho_{24} - \rho_{42})) \\
\frac{d\rho_{43}}{dt} &= -i\omega_{43}\rho_{43} + i\Omega_{12}(t)(\gamma\rho_{23} - \beta\rho_{42}) \\
\frac{d\rho_{42}}{dt} &= -i\omega_{42}\rho_{42} + i\Omega_{12}(t)(\gamma(\rho_{22} - \rho_{44}) - \rho_{41} - \beta\rho_{43}) \\
\frac{d\rho_{41}}{dt} &= -i\omega_{41}\rho_{41} + i\Omega_{12}(t)(\gamma\rho_{21} - \rho_{42}) \\
\frac{d\rho_{32}}{dt} &= -i\omega_{32}\rho_{32} + i\Omega_{12}(t)(\beta(\rho_{22} - \rho_{33}) - \rho_{31} - \gamma\rho_{34}) \\
\frac{d\rho_{31}}{dt} &= -i\omega_{31}\rho_{31} + i\Omega_{12}(t)(\beta\rho_{21} - \rho_{32}) \\
\frac{d\rho_{21}}{dt} &= -i\omega_{21}\rho_{21} + i\Omega_{12}(t)(\rho_{11} - \rho_{22} + \beta\rho_{31} + \gamma\rho_{41})
\end{aligned}
\qquad (4.2.2)
$$

Here $\omega_{ij} = \omega_i - \omega_j$. It may be noted that $\rho_{ij} = \rho_{ji}^*$. $\rho_{nm}(n,m=1\rightarrow 4)$ is a component of the density matrix, where ρ_{nn} is related to the population of the n^{th} level and ρ_{nm} refers to the coherence between the level 'n' and the level 'm'. The time independent Rabi frequencies are defined as follows: $\Omega_{12} = \mu_{12}E_0/\hbar$, $\Omega_{23} = \mu_{23}E_0/\hbar = \beta\Omega_{21}$ and $\Omega_{24} = \mu_{24}E_0/\hbar = \gamma\Omega_{21}$. We use the following typical parameters: Ω_{12} =0.60 rad/fs, ω_{21} =3.19 rad/fs, $\omega_{32} = 3.06$ rad/fs, ω_{42} =3.30 rad/fs, τ_p=16.5 fs, $t_0 = \mp$ 16.5 fs, τ= 16.5 fs, $\omega = 3.6\,\text{rad/fs}$, β=0.90, γ=1.10 and α = 10.0 rad. It is worth mentioning that the aforementioned pulse parameters are chosen so that selective and maximum population transfer could be achieved. In Fig. 4.2, the effects of the variation of the control parameters on the time varying pulse frequency are depicted.

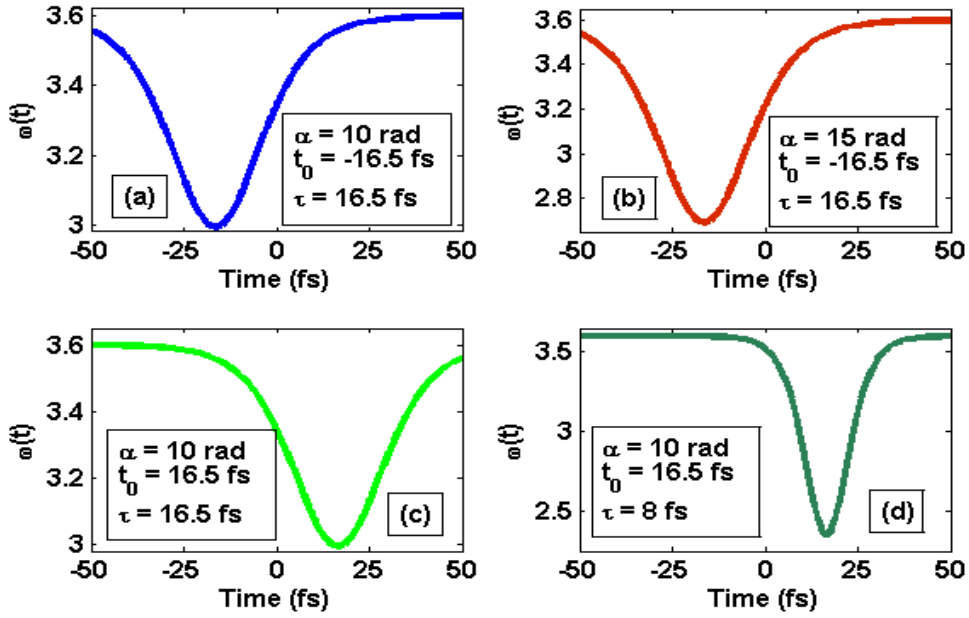

Fig. 4.2 Temporal evolution of pulse frequency

Fig. 4.2(a) depicts the temporal evolution of the pulse frequency for control parameters, α= 10.0 rad, t_0 = -16.5 fs and τ = 16.5 fs. It can be observed from Fig. 4.2(a) that with α= 10.0 rad, the sweeping of pulse frequency occurs from 3.6 rad/fs to 3.0 rad/fs while the dip in time varying frequency occurs at time t = -16.5 fs, which matches to the frequency offset parameter, t_0= -16.5 fs. It should be noted that for the chosen pulse parameters (α= 10.0 rad, τ= 16.5 fs) the frequency spectrum of the nonlinearly chirped pulse overlaps with the transition frequencies of the chosen states of a real sodium atom. On the other hand, transitions between the other states are either off resonant or dipole forbidden. However, the same frequency sweeping range (3.6 rad/fs to 3.0 rad/fs) may be achieved for other

parameters (e.g., α = 14 and τ = 24) also. In Fig. 4.2(b), the result is plotted for a different frequency sweeping parameter α, while keeping the other parameters unchanged. It can be seen from Fig. 4.2(b) that with α = 15 rad, the sweeping of pulse frequency occurs from 3.6 rad/fs to 2.5 rad/fs. It can be seen from Fig. 4.2(c) that the dip in the time varying frequency occurs at time t= 16.5 fs, which is equal to the frequency offset parameters, t_0 = 16.5 fs. Hence, the frequency offset parameter is responsible for shifting the temporal position of dip in time varying frequency. In Fig. 4.2(d), we have changed the frequency steepening parameter, τ, while keeping the other parameters same as in Fig 4.2(c), to examine its effect on the time varying frequency. It can be observed from Fig 4.2(d) that for frequency steepening parameter τ = 8 fs, along with the sweeping, steepening of temporal profile of the pulse frequency also occurs. The chosen temporal profile of the phase offers the possibility to select a particular transition path by choosing the control parameters judiciously. Next, in Fig. 4.3, we depict the temporal evolution of the pulse frequency, the pulse envelope and the populations in different states.

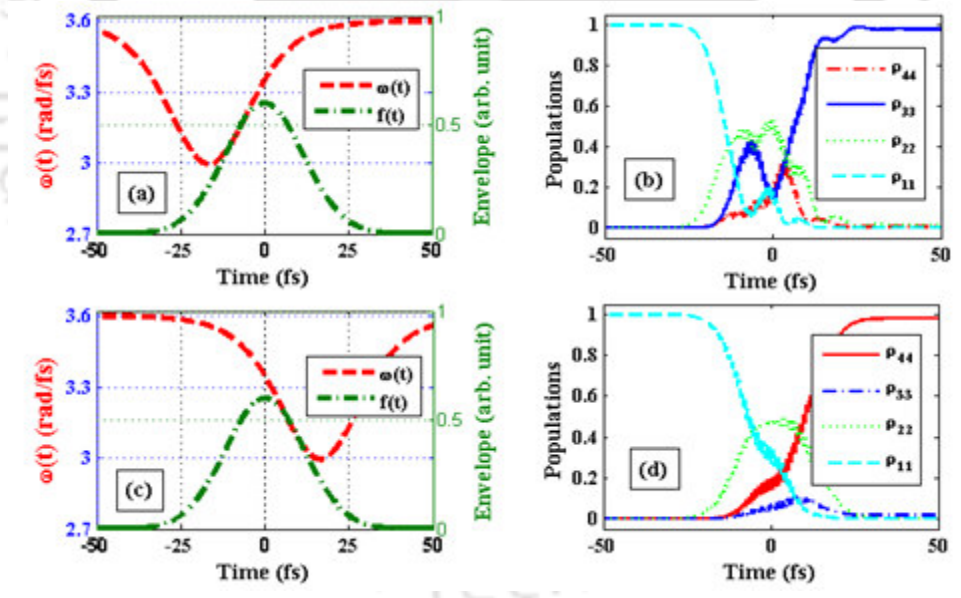

Fig. 4.3 Temporal evolution of pulse frequency (a, c), pulse envelope (a, c) and populations (b, d).

It can be understood from Fig. 4.3(a) that the pulse is interacting with $|1\rangle \rightarrow |2\rangle$ and $|2\rangle \rightarrow |3\rangle$ transitions in a counterintuitive manner because with the chosen frequency offset parameter, t_0 = -16.5 fs, initially the time varying frequency is resonant with the $|2\rangle \rightarrow |3\rangle$ transition

frequency at time t ≈ -18 fs and at a later time t ≈ -8 fs, it is resonant with the $|1\rangle \rightarrow |2\rangle$ transition frequency. This counterintuitive sequence makes the $|2\rangle \rightarrow |4\rangle$ transition nearly forbidden and leads to almost complete (98.40 %) population transfer to the state $|3\rangle$, as could be observed from Fig. 4.3(b). On the other hand, it might be clear from Fig. 4.3(c) that the pulse is interacting with $|1\rangle \rightarrow |2\rangle$ and $|2\rangle \rightarrow |4\rangle$ transitions in a counterintuitive manner, and also because with the chosen frequency offset parameter, t_0 = 16.5 fs, initially the time varying frequency is resonant with the $|2\rangle \rightarrow |4\rangle$ transition frequency at t ≈ 2 fs and at a later time t ≈ 6 fs, it is resonant with the $|1\rangle \rightarrow |2\rangle$ transition frequency. This counterintuitive sequence makes the $|2\rangle \rightarrow |3\rangle$ transition nearly forbidden and leads to the almost complete (98.50 %) population transfer to state $|4\rangle$ as could be observed from Fig. 4.3(d). Hence the selective population transfer could be achieved just by manipulating the chirp offset parameter. It is important to verify the robustness of the scheme against the variation of the pulse parameters for practical realization of the scheme. So, in Fig. 4.4 and Fig. 4.5, we present the simulation result for the variation of the final population transfer to the state $|3\rangle$, i.e., $\rho_{33}(\infty)$ and state $|4\rangle$, i.e., $\rho_{44}(\infty)$ with frequency sweeping and frequency steeping parameters.

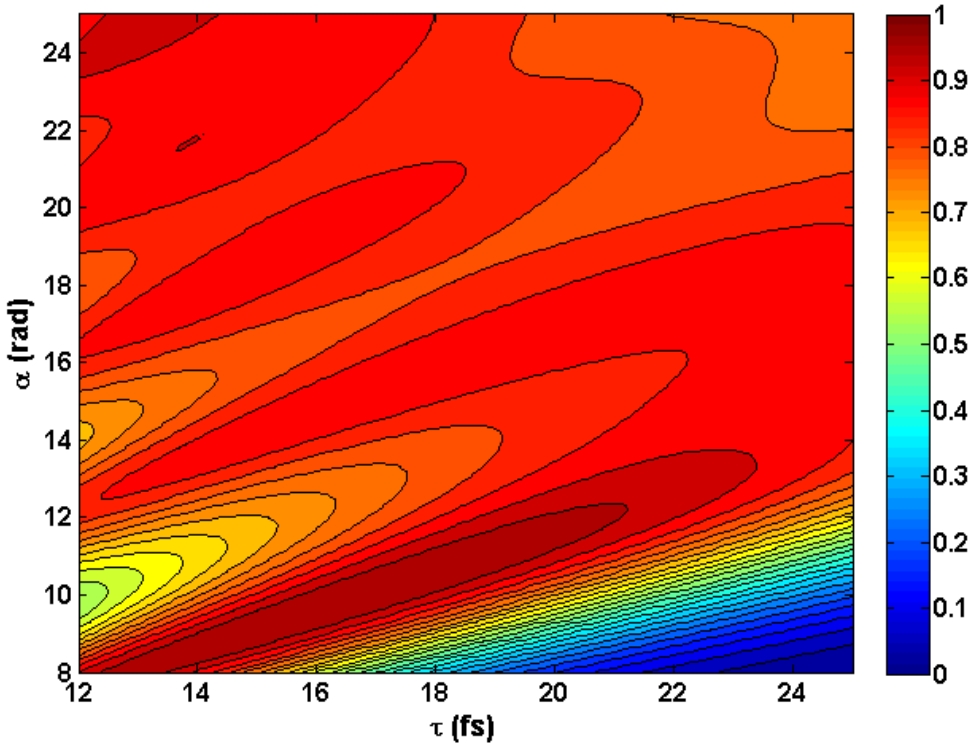

Fig. 4.4 Contour plots of the final population, $\rho_{33}(\infty)$ for varying frequency sweeping parameter, α, and frequency steepening parameter, τ. Other parameters are the same in Fig. 4.3(a).

A careful inspection of Fig. 4.4 reveals that the final population in state $|3\rangle$, $\rho_{33}(\infty)$, is fairly robust against the small variation in the frequency sweeping parameter, α, and frequency steepening parameter, τ. One can obtain more than 95% population transfer against the variation in these parameters in the range; say $\alpha \approx$ 8-11 rad and $\tau \approx$ 12.5 - 21 fs. However, more than 85 % population transfer is possible in a sufficiently large range of variation in α and τ.

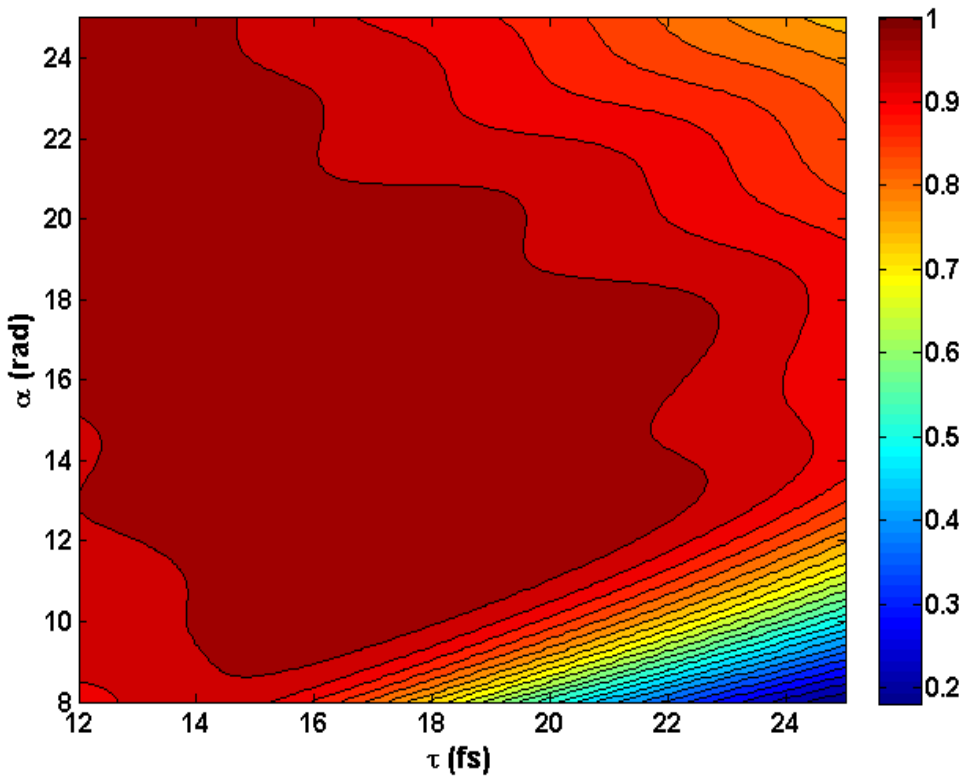

Fig. 4.5 Contour plots of the final population $\rho_{44}(\infty)$ for varying frequency sweeping parameter, α and frequency sweeping-steepening parameter, τ. Other parameters are the same as in Fig. 4.3(c).

Fig. 4.5 reveals that the final population in the state $|4\rangle$, $\rho_{44}(\infty)$, is sufficiently robust against the variation in the frequency sweeping parameter, α and frequency steepening parameter, τ, over a large range, $\alpha \approx$ 9-25 rad and $\tau \approx$ 12-22 fs respectively, yielding more than 95 % population. Thus the final population transfer to the state $|4\rangle$ is more robust compared to that of the final population transfer to the state $|3\rangle$. For example, one can obtain nearly 67 %

population transfer to state $|3\rangle$ with $\alpha = 11$ rad and $\tau = 14$ fs as could be observed from Fig. 4.4 while with the same set of control parameters, one can obtain nearly 97 % population transfer to state the $|4\rangle$ as could be observed from Fig. 4.5. In order to investigate the reason behind this difference more clearly, we depict the temporal evolution of the time varying pulse frequency in Fig. 4.6.

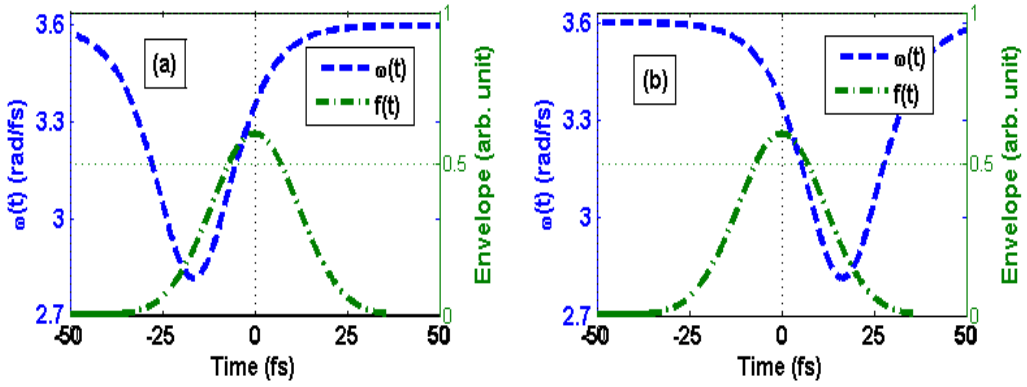

Fig. 4.6 Temporal evolution of pulse frequency and pulse envelope (a) $\omega(t)$ with $\alpha = 11$ rad, $t_0 = -16.5$ fs and $\tau = 14$ fs (b) $\omega(t)$ with $\alpha = 11$ rad, $t_0 = 16.5$ fs and $\tau = 14$ fs

It can be observed from Fig. 4.6(a) that the time varying frequency $\omega(t)$ with $\alpha = 11$ rad, $t_0 = -16.5$ fs and $\tau = 14$ fs is resonant with the frequency of the $|2\rangle \rightarrow |3\rangle$ transition at time $t \approx -24.4$ fs. At a later time $t \approx -4.7$ fs, it is resonant with the frequency of the $|1\rangle \rightarrow |2\rangle$ transition. It can be seen that at time t= -24.4 fs, the corresponding value of the pulse envelope is too low (0.04) to transfer population to the state $|3\rangle$ completely, while the pulse envelope has a value (0.25) at time t = -18 fs (please see Fig. 4.3(a)). However, the time varying frequency $\omega(t)$ with $\alpha = 11$ rad, $t_0 = 16.5$ fs and $\tau = 14$ fs is resonant with the frequency of $|2\rangle \rightarrow |4\rangle$ transition at time $t \approx 1.65$ fs and at later time $t \approx 25.7$ fs is resonant with the frequency of the $|1\rangle \rightarrow |2\rangle$ transition. At time t= 1.65 fs the corresponding value of the pulse envelope is sufficient (0.59) to transfer nearly complete population to the state $|4\rangle$ which is nearly equal to the pulse envelope value (0.58) at time t = 2 fs, as can be seen from Fig. 4.3(c). In Fig. 4.7, we depict the robustness of the final population transfer to the state $|3\rangle$ with respect to the pulse duration and time independent Rabi frequency. In this case $\rho_{33}(\infty)$ is fairly robust against the

variation in the pulse duration and the time independent Rabi frequency in the range τ_{FWHM} = 21- 26 fs and Ω_{12} = 0.35 – 0.55 rad/fs.

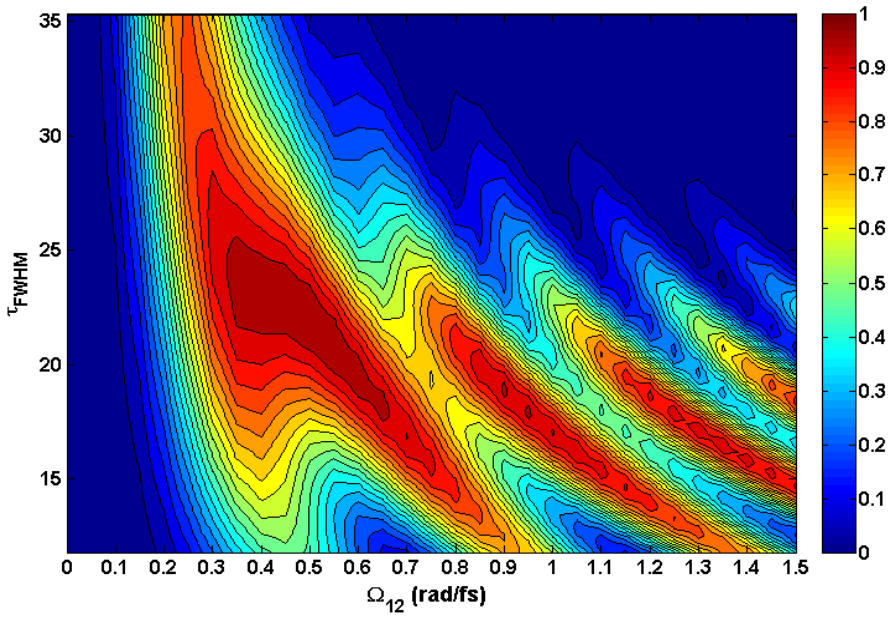

Fig. 4.7 Contour plots of the final population, $\rho_{33}(\infty)$ for varying Rabi frequency Ω_{12} and pulse width τ_{FWHM}. Other parameters are the same as in Fig. 4.3(a).

In Fig. 4.8, we depict the robustness of final population transfer to the state $|4\rangle$ with respect to the pulse duration τ_{FWHM} and the time independent Rabi frequency Ω_{12}.

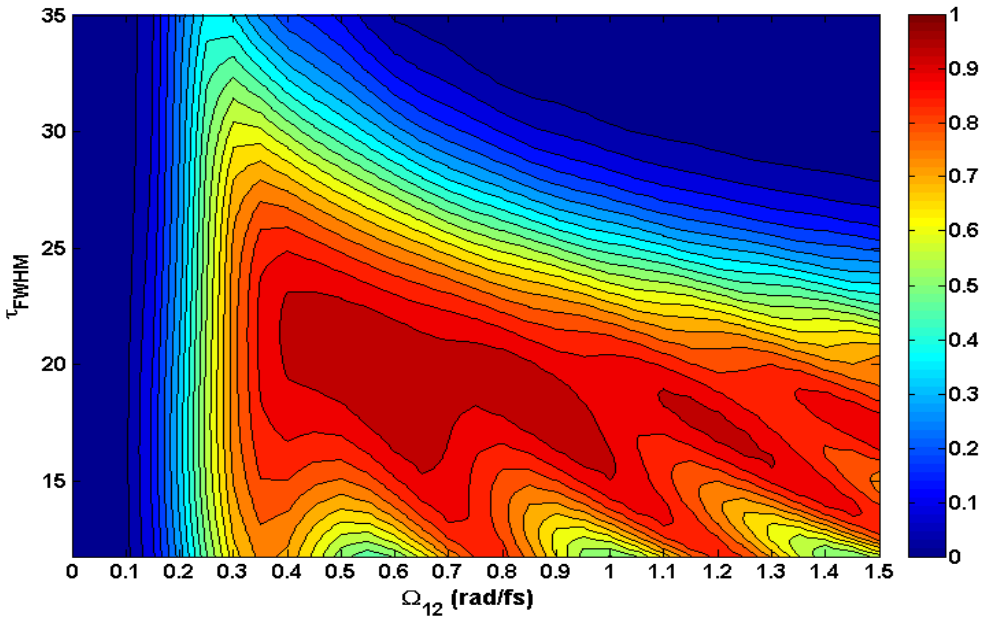

Fig. 4.8 Contour plots of the final population, $\rho_{44}(\infty)$ for varying Rabi frequency Ω_{12} and pulse width τ_{FWHM}. Other parameters are the same as in Fig. 4.3(c).

It can be observed from Fig. 4.8 that $\rho_{44}(\infty)$ is fairly robust against variations in the pulse duration and the time independent Rabi frequency in the range τ_{FWHM} = 16- 22 fs and Ω_{12} = 0.4 – 1.0 rad/fs respectively. In addition, $\rho_{33}(\infty)$ and $\rho_{44}(\infty)$ are found to be nearly 96 % and 97 % respectively for $\beta=\gamma=1$ and nearly 92 % each for $\beta=1.1$ and $\gamma=0.9$. However, one can achieve more than 92 % population with $\beta=1.1$ and $\gamma=0.9$ by judiciously choosing the pulse parameters such as Ω_{12}, α and τ. For example, nearly 97 % population transfers to the state $|3\rangle$ could be achieved with Ω_{12} =0.55 rad/fs, α =11.50 rad and τ = 18 fs.

4.3 Chapter Summary

We have reviewed some of the work on CPT in multilevel atoms driven by a single or multiple laser pulses. In our study on CPT, we modelled the neutral sodium atom as a Y-like four-state atom and demonstrated ultrafast and selective population transfer using a single nonlinearly chirped femtosecond pulse. Effects of control parameters on the temporal phase have been investigated. We suggested that by judicious choice of the control parameters, one can select the specific final states populated in an atom. We demonstrated selective CPT either to the third or the fourth state by manipulating the frequency offset parameter. The selective population transfer is found to be robust against variations of the simulation parameters such as the time- independent Rabi frequency, frequency sweeping parameter, frequency steepening parameter, and dipole moment coefficients. This scheme may be explored in the other atoms as well which can be modelled as Y-like four-level atoms. The scheme may also be explored in molecules owing to the selectivity offered by the frequency offset parameter.

Chapter 5

Optical forces on two-level atoms*

5.1 Introduction

Manipulation of atoms or molecules using laser light has both fundamental significance and relevance to applications in quantum optics, atomic physics and chemistry [62-66]. In this context, the appearance of the classic paper by Ashkin [165] on atomic beam deflection by resonance-radiation pressure force owing to laser light gave rise to many theoretical and experimental studies on resonance-radiation force in various contexts [70-73, 166-171]. After successful trapping of atoms by the resonance radiation pressure force due to continuous-wave (cw) light, followed by experimental demonstration of focusing of neutral atoms [167], the field of atom trapping virtually exploded and it still remains an interesting area of research [116-118]. It may be noted that the mechanical effects of light, particularly laser beam, on particles such as atoms, molecules, ions, etc. have been successfully exploited in as diverse areas as optical tweezers [116, 118], atom optics [169], Bose–Einstein condensation [170], laser cooling and trapping [168], and quantum information [171]. Many researchers have studied the radiation forces exerted on neutral atoms [172-176]. In this context, the two-level atomic system may be the most studied one [168]. The forces on two-level atoms are generally calculated by using the steady-state solutions of the so-called optical Bloch equations within the rotating wave approximation (RWA) [70]. It may be worthwhile to mention that the recent experiments on semiconductors have shown that in the regime of extreme nonlinear optics, where $\Omega_R / \omega \approx 1$ or $\Omega_R / \omega >> 1$, the description of atomic system in terms of two-level systems has been able to reproduce the experimental results amazingly well [78]. Here, Ω_R is the peak Rabi frequency and ω is the carrier frequency of the laser pulse. It may be quite interesting to relook or re-examine the so-called light or optical force on a two-level atomic system in a few-cycle pulsed laser field. In fact, recently Lembessis and Ellinas [74] have carried out a theoretical analysis in the context of optical dipole

*The results presented in this chapter have been published in a paper, P. Kumar and A. K. Sarma, "Optical Force on Two-level Atoms by Few-cycle Pulsed Gaussian Laser field beyond the Rotating Wave Approximation", Phys. Rev. A 84, 043402 (2011).

trapping beyond the RWA. Their analysis is based on Heisenberg operator perturbation techniques, rather than the optical Bloch equations. In 2013, Xunming Cai et al. [177] calculated the optical force on two-level atoms induced by sub-cycle-pulsed focused vector fields beyond the RWA. These researchers demonstrated that the optical force can change from a focusing force to a defocusing force depending on the initial state of the atom. Our study on optical forces, presented in this chapter, is largely motivated by the work of Bjorkholm *et al.* [167] who carried out experimental studies of focusing of sodium atoms by using a cw beam tuned near an atomic resonance. Our analysis is loosely based on the treatment by R. J. Cook [73]. It may be noted that the theory of atomic motion in resonant electromagnetic wave proposed by R. J. Cook [73, 172] within the RWA successfully explains the nature of the resonant radiation forces. This theory, however, may fail in the regime of extreme nonlinear optics due to the limitations of RWA.

In this chapter, we report our study on optical force on a beam of neutral two-level atoms superimposed upon a few-cycle-pulsed Gaussian laser fields. Manipulation of the neutral atoms in the laser field is analyzed by solving the optical Bloch equation, beyond the rotating wave approximation, and the force equation self-consistently.

5.2 Theoretical Model

The schematic of our scheme for the calculation of optical forces acting on a beam of neutral two-level atomic beam superimposed upon a few-cycle-pulsed Gaussian laser fields is shown in Fig. 5.1.

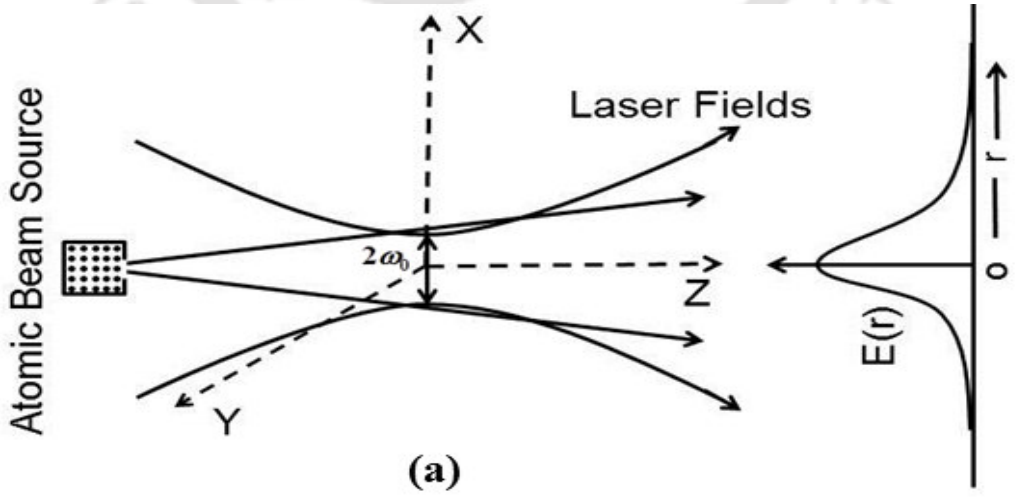

Fig. 5.1 Sketch of an atomic beam superimposed upon a pulsed Gaussian laser fields

The interaction between a system of two-level atoms, within the electric dipole and two-level approximations [178-180], with a superimposed and co-propagating collimated classical laser field is described by the following Hamiltonian [181]:

$$H = \frac{\vec{P}^2}{2M} + H_0 - \vec{\mu}\cdot\vec{E}\left(\vec{R},t\right). \tag{5.2.1}$$

Here $\vec{P}$ is the centre-of-mass momentum operator of the atoms, $\vec{\mu}$ is the atomic dipole moment operator and $\vec{E}\left(\vec{R},t\right)$ is the electric field of the laser field evaluated at the centre-of-mass (CM) position $\vec{R}$ of the atoms. M is the centre of mass. On the right hand side of Eq. (5.21), the first term is the CM kinetic energy of the moving atoms; the second one refers to the internal energy Hamiltonian of the unperturbed atoms while the last term describes the interaction energy between the atoms and light field within the electric dipole approximation. In the so called Raman-Nath approximation [181], the approximate Hamiltonian is given by the following equation:

$$H = H_0 - \vec{\mu}\cdot\vec{E}\left(\vec{R},t\right) \tag{5.2.2}$$

The Raman Nath approximation is valid in the present study due to our assumption that the interaction energy is very large compared to the centre of mass kinetic energy and the interaction time involved is of the order of a few femtosecond. The change in momentum of the atoms is given by the following Heisenberg equation of motion:

$$\frac{d\vec{P}}{dt} = \frac{i}{\hbar}\left[H,\vec{P}\right] = \vec{\nabla}_R\left(\vec{\mu}.\vec{E}\right) \tag{5.2.3}$$

The light force acting on the atomic centre of mass can be thought as the expectation value of Eq. (5.2.3). Setting $\vec{r} = \left\langle \vec{R} \right\rangle$, we obtain the average force on the atoms as follows:

$$\vec{F} = M\,\ddot{\vec{r}} = \left\langle \frac{d\vec{P}}{dt} \right\rangle = \left\langle \vec{\nabla}\left(\vec{\mu}.\vec{E}\right) \right\rangle. \tag{5.2.4}$$

We consider the laser field in the following form:

$$\vec{E}\left(\vec{r},t\right) = \hat{\eta}A\left(\vec{r},t\right)\cos\left(\phi(z) - \omega t\right), \tag{5.2.5}$$

where, $A(\vec{r},t)$ denotes the envelope, $\hat{\eta}$ represents the polarization direction, $\phi(z)$ is the phase and ω is the operating frequency of the laser field. Then from Eq. (5.2.4) and Eq. (5.2.5), assuming $\vec{\nabla}\left|\vec{E}(\vec{r},t)\right|$ to be uniform across the atomic wave packet, we obtain:

$$\vec{F} = \langle \vec{\mu}.\hat{\eta} \rangle \left[\left\{ \vec{\nabla} A(\vec{r},t) \right\} \cos(\phi(z) - \omega t) - \vec{\nabla}\phi(z) A(\vec{r},t) \sin(\phi(z) - \omega t) \right] \tag{5.2.6}$$

The expectation value in Eq. (5.2.6) can be written in terms of a density matrix as $\langle \vec{\mu}.\hat{\eta} \rangle = \mu(\rho_{12} + \rho_{21}) = \mu u$, where u, one of the three Bloch vector components, accounts for the dispersive effects of the two-level atomic medium. Here, ρ_{12} and ρ_{21} are the off-diagonal elements of the density matrix with $|1\rangle$ and $|2\rangle$ referring to the ground and the excited state of the two-level atom respectively. The Bloch vector component u is described by the following optical Bloch equations [78]:

$$\begin{aligned} \frac{du}{dt} &= \Omega v - \frac{u}{T_2} \\ \frac{dv}{dt} &= -\Omega u - 2\Omega_R(\vec{r},t) w - \frac{v}{T_2} \\ \frac{dw}{dt} &= 2\Omega_R(\vec{r},t) v - \frac{(w+1)}{T_1}, \end{aligned} \tag{5.2.7}$$

where v and w are the other two components of the Bloch vector [139]. Here, T_2 and T_1 are respectively the dipole-dephasing and spontaneous decay time. As the atom-field interaction time is negligibly small compared to T_1 due to extremely short duration of the few-cycle laser field, the terms associated with it could be neglected [178, 182]. Here, Ω is the transition frequency of the two-level atoms and $\Omega_R(\vec{r},t)$ is the Rabi frequency which is defined as $\Omega_R(\vec{r},t) = \vec{\mu}.\vec{E}(\vec{r},t)/\hbar$. The so-called detuning parameter, to be used later in this work, is defined as $\Delta = \Omega - \omega$. It may be noted that the optical Bloch equations are written without invoking the RWA. So, in terms of Bloch vector we can write the expression for light force as follows:

$$\vec{F} = \mu u \left[\left\{ \vec{\nabla} A(\vec{r},t) \right\} \cos(\phi(z) - \omega t) - \vec{\nabla}\phi(z) A(\vec{r},t) \sin(\phi(z) - \omega t) \right]. \tag{5.2.8}$$

We find that the light force is explicitly dependent on the u -component of the Bloch vector unlike previous expressions for the light force, derived under the RWA, where the force was found to depend both on u and v component of the Bloch vector [73]. We may interpret this difference in results physically as follows: In the RWA approximation, the light force is generally expressed as the sum of two forces, namely, the reactive force and the dissipative force [70]. The reactive force, being proportional to the u -component of Bloch vector, does not involve absorption of energy from the laser field. Rather, it is solely due to the exchange and redistribution of momentum between the atoms and various plane waves composing the laser field. On the other hand, the dissipative force, proportional to the v-component of the Bloch vector, is related to the absorption and emission of energy. The dissipative force arises from the impulse experienced by an atom when it absorbs or emits a quantum of photon momentum. The light force expression that we have derived does not depend on the v-component of Bloch vector explicitly owing to the fast laser-atom interaction compared to the slow spontaneous process and the non-RWA treatment of forces in the regime of extreme nonlinear optics. So the light force that we obtain is conservative and solely due to the interaction of the two-level atoms with the gradient of the electric field envelope and of the phase. Now we consider a few-cycle pulsed Gaussian laser field propagating along the z-direction as described by the following equation:

$$\vec{E}(r,z,t) = \hat{\eta} E_0 \exp\left[-\left\{\left(\frac{r^2}{\omega_0^2}\right)+\left(\frac{t^2}{\tau^2}\right)\right\}\right]\cos(k\,z-\omega t), \tag{5.2.9}$$

where E_0 is the peak amplitude, ω_0 is the beam waist, $\mathrm{r} = \sqrt{\mathrm{x}^2+\mathrm{y}^2}$ and k is the wave-vector of the Gaussian laser field. Here, τ is the temporal pulse width, related to the full-width at half maximum (FWHM) of the laser field by $\tau_p = 1.177\,\tau$. From Eq. (5.2.8) and Eq. (5.2.9) we obtain the transverse and longitudinal component of the light force as follows:

$$\begin{aligned} F_T &= -\frac{2\mu E_0\, r\, u}{\omega_0^2}\exp\left[-\left\{\left(\frac{r^2}{\omega_0^2}\right)+\left(\frac{t^2}{\tau^2}\right)\right\}\right]\cos(k\,z-\omega t) \\ F_z &= -\mu k\, E_0\, u \exp\left[-\left\{\left(\frac{r^2}{\omega_0^2}\right)+\left(\frac{t^2}{\tau^2}\right)\right\}\right]\sin(k\,z-\omega t) \end{aligned} \tag{5.2.10}$$

The so-called optical potential [74], defined by $\vec{F} = -\vec{\nabla} U$, associated with the light force can be easily expressed by the following equation:

$$U = -\mu E_0 u \exp\left[-\left\{r^2/\omega_0^2 + (t/\tau)^2\right\}\right]\cos(k z - \omega t) \tag{5.2.11}$$

In order to derive the above expression for the optical potential we have assumed that the spatial variation of u is negligible.

5.2 Numerical results and Discussions

Eq. (5.2.7) and (5.2.10) are numerically solved in a self-consistent manner, in order to understand the temporal evolution of the optical force on the two-level atoms in a few-cycle pulsed Gaussian laser field described by Eq. (5.2.9). We assume the atoms to be in the ground state initially and the beam to be focussed at $z = 0$. We compare both the RWA and non-RWA cases. We find that the phenomena of focusing, defocusing and steering of the atomic beam may occur depending on the detuning parameter and the peak Rabi frequency. The peak Rabi frequency is defined as the Rabi frequency at $r = 0$ and $t = 0$. In the rest of the work, the Rabi frequency used refers to the peak Rabi frequency. We choose the following parameters for our numerical calculations: τ_p =13.8 fs, Ω =2.2758 rad/fs, T_2 =200 fs, $\mu = 4.24\times10^{-29}\,\mathrm{C\cdot m}$, M= 6.94 amu and ω_0 =1 μm . The numerical parameters chosen for the atom, particularly the transition frequency and dipole moment are similar to those of the rubidium and lithium atom. The r- component of the light force is termed as the transverse force, F_T , while the z-component is termed as the longitudinal force, F_L . Both these forces are calculated at $r = 0.7071\,\mu\mathrm{m}$. Fig. 5.2 depicts the temporal evolution of the light force on the two-level atoms in an atomic beam at different Rabi frequencies for $\Delta = 1.7758$ rad/fs.

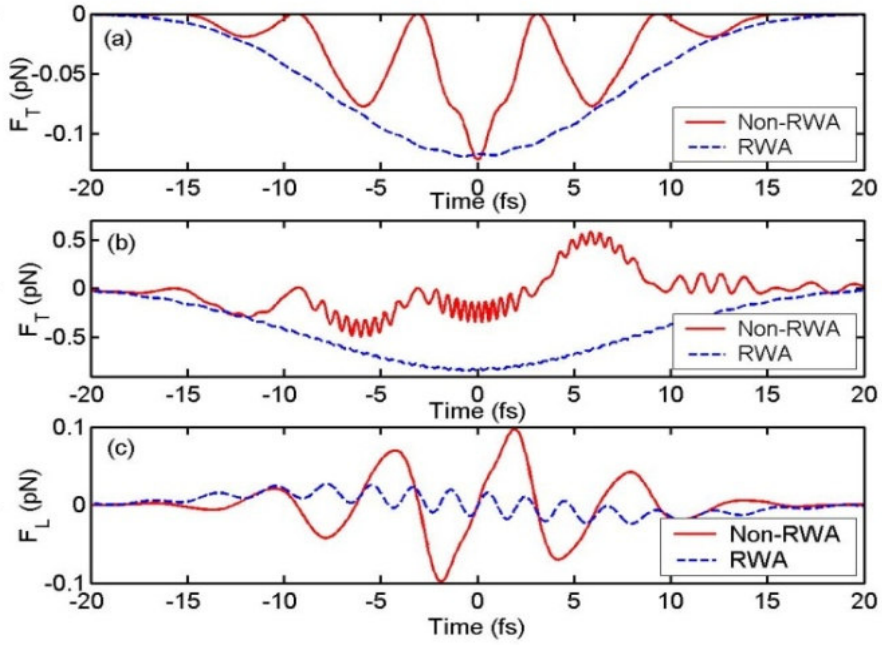

Fig. 5.2 Temporal evolution of light force: (a) Transverse force vs. Time for Ω_R=2.2758 rad/fs, (b) Transverse force vs. Time for $\Omega_R = 14.2758$ rad/fs, (c) Longitudinal force vs. Time for $\Omega_R = 2.2758$ rad/fs

Fig. 5.2 (a) shows that, the transverse force being negative, the two-level atoms in the atomic beam experiences a net attractive force which may result in focusing of the atoms around $z = 0$. Both the RWA and non-RWA treatments qualitatively predict the same result in the limit $\Omega \approx \Omega_R$ and large detuning. However, as the Rabi frequency is increased further, for $\Omega_R > \Omega$, the non-RWA treatment of the transverse force deviates from that of RWA. As could be observed from Fig. 5.2(b), the non-RWA transverse force may become positive or negative with time. The time averaged longitudinal force is found to be nearly zero, as can be seen from Fig. 5.2(c). To analyze the trajectory of atoms under the influence of the focusing force, in Fig. 5.3, we depict in Fig. 5.3 the focusing of atoms due to the transverse force calculated at $r = 0.7071\,\mu\text{m}$ for $\Omega_R = 2.2758$ rad/fs and $\Delta = 1.7758$ rad/fs for various initial values of the transverse velocity v_T. It can be observed from Fig. 5.3 that atoms moving with transverse velocities up to $v_T = 50$ m/s may be focused. It should be noted that the atoms are focused on the picosecond time scale. A train of few-cycle pulses may be used to enhance the effective focusing of the atoms. This issue will be discussed in the next chapter in the context of a three-level atomic system.

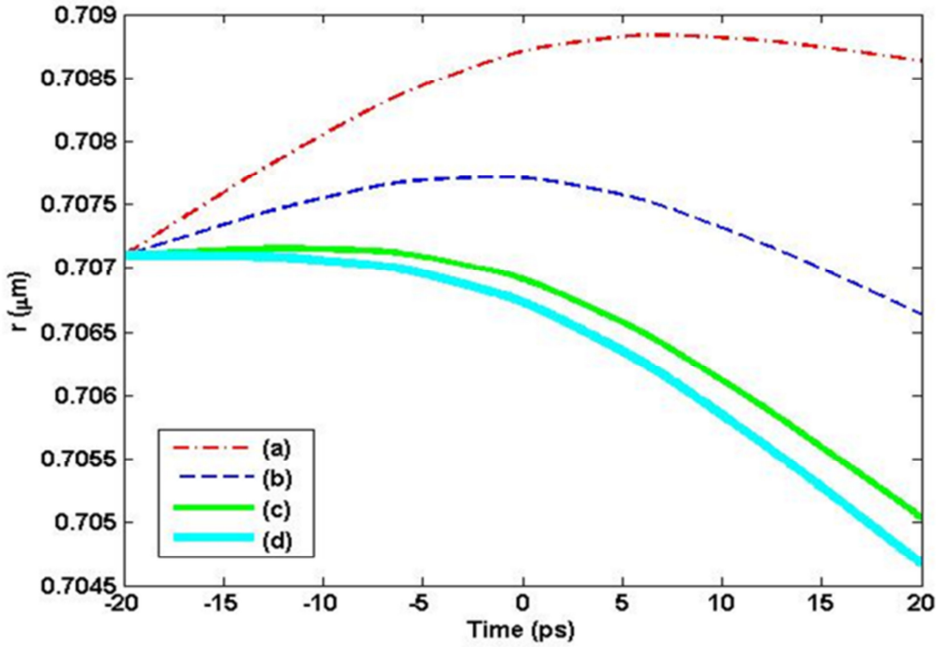

Fig. 5.3 Focusing of atoms due to transverse force (a) v_T = 100 m/s; (b) v_T = 50 m/s; (c) v_T = 10 m/s; and (d) v_T = 1 m/s.

Next, we consider the case of negative detuning with, say Δ = -1.7758 rad/fs. Fig. 5.4 exhibits the temporal evolution of the transverse light force for different Rabi frequencies. It should be noted that in Fig. 5.4, in order to get proper scaling, we have reduced the RWA force by a factor of three.

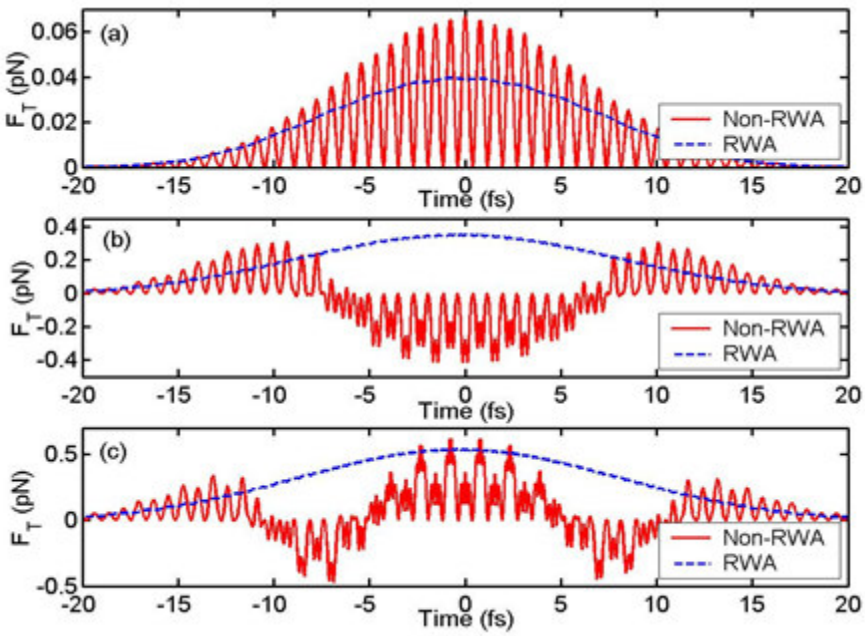

Fig. 5.4 Temporal evolution of transverse light force: (a) Ω_R =2.2758 rad/fs, (b) Ω_R = 18.2758 rad/fs, (c) Ω_R = 28.2758 rad/fs.

The RWA treatment of the transverse force shows that its temporal evolution is independent of the Rabi frequency and is always positive. So the atomic beam would experience a net repulsive force leading to defocusing. On the other hand, the non-RWA treatment shows significant deviation in results. As could be seen from Fig. 5.4(b) and Fig. 5.4(c), with an increase in the Rabi frequency beyond $\Omega_R > \Omega$, the transverse force exhibits both attractive and repulsive features. We may conclude that time-controlled focusing and defocusing of atoms may be achieved with large negative detuning. This might enable us to deposit atoms onto a substrate in a controllable way with judicious choices of the Rabi frequency and the detuning parameter. The resonant case, which seems to be the most studied in literature [70], is discussed next. Fig. 5.5 depicts the temporal evolution of the transverse force at different Rabi frequencies under resonance conditions, i.e. $\Delta = 0$, while Fig. 5.6 depicts the temporal evolution of the longitudinal force. It is clear from Fig. 5.5 that under resonant condition the transverse component of the light force vanishes for the RWA. The non-RWA transverse force shows oscillatory behaviour and the time-average vanishes. The fact that the transverse component of the light force vanishes within the RWA under the resonant condition is supported by the analytical calculations reported in Ref. [176].

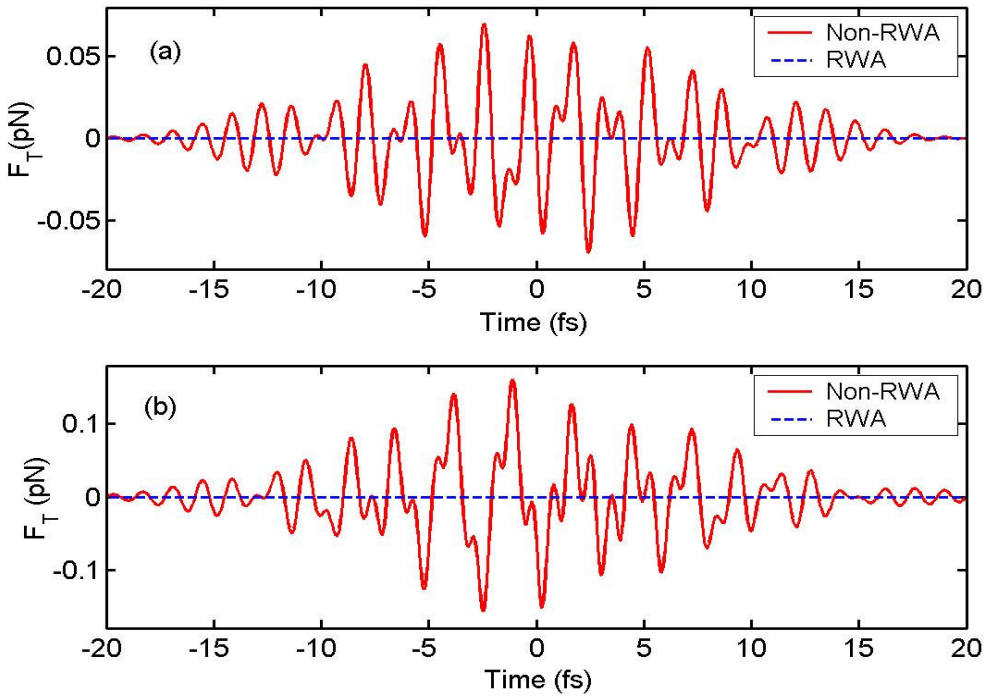

Fig. 5.5 Temporal evolution of transverse light force: (a) Ω_R =2.2758 rad/fs, (b) Ω_R = 4.2758 Rad/fs.

Fig. 5.6(a) shows that the longitudinal component of the light force is non-zero when $\Omega_R < \Omega$, a regime where the RWA may be valid. So steering of atoms may be possible in this regime. However, as the Rabi frequency is increased, the time-averaged longitudinal force vanishes and steering of atoms may no longer be possible for $\Omega_R \geq \Omega$. It is worthwhile to note that the peak amplitude of the electric field cannot be increased arbitrarily, thereby increasing the

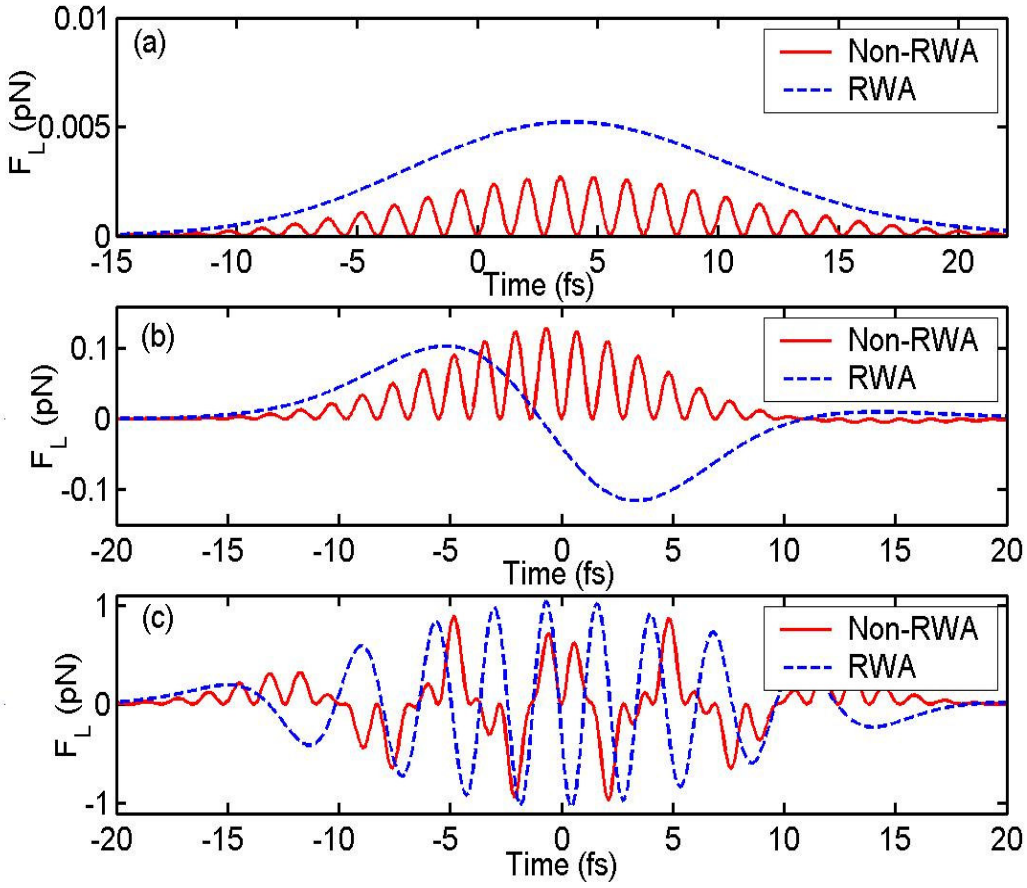

Fig. 5.6 Temporal evolution of longitudinal light force: (a) Ω_R =0.02758 rad/fs, (b) Ω_R = 0.2758 rad/fs, and (c) Ω_R = 2.2758 rad/fs.

Rabi frequency, because if the peak amplitude of the electric field becomes comparable to the electric field strength of the atom, it may be ionized and the description as a two-level atom governed by the optical Bloch equations would no longer be valid. Finally, in Fig. 5.7 (a) and Fig. 5.7(b), we plot the spatio-temporal profile of the optical potential for $\Omega_R < \Omega$ and $\Omega_R = \Omega$ with Δ =1.7758 rad/fs, while Fig. 5.7(c) depicts the case for $\Omega_R > \Omega$ with Δ =1.9578 rad/fs.

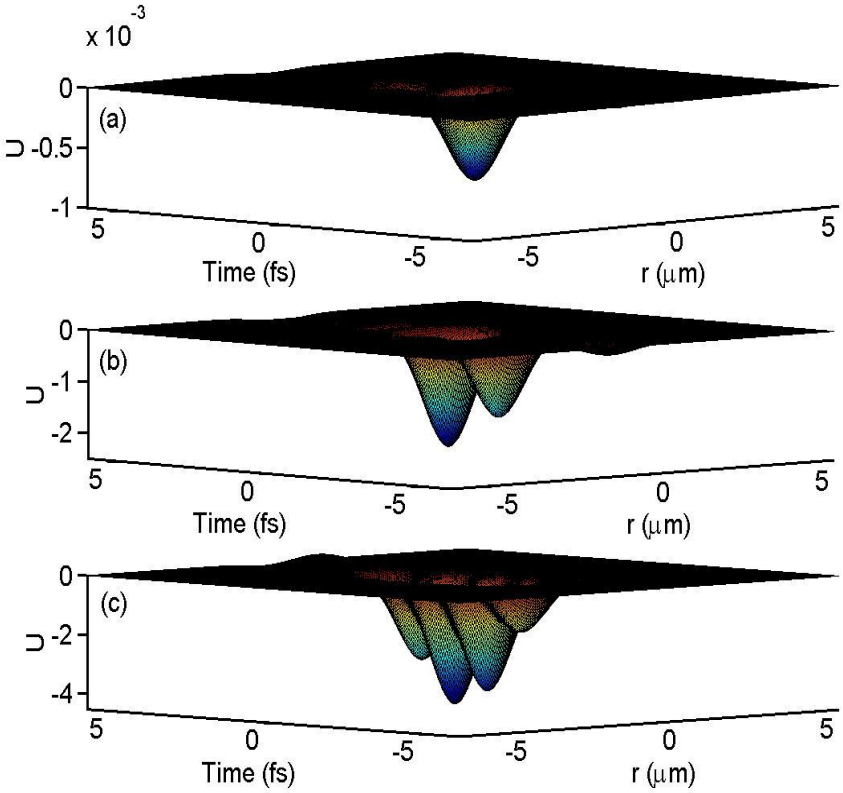

Fig. 5.7 Spatio-temporal profile of the optical potential (a) Ω_R=0.02758 rad/fs; (b) Ω_R =2.2758 rad/fs; (c) Ω_R =4.2758 rad/fs.

A careful look at Fig. 5.7(a) and Fig. 5.7(b) reveals that the optical potential is negative, mainly around $r, t = 0$ and its magnitude increases with an increase in the Rabi frequency. Thus, two-level atoms in an atomic beam may be trapped by the time dependent optical potential even in the regime of extreme nonlinear optics. However, if we increase Ω_R further, keeping Δ fixed, the optical potentials oscillate between positive and negative values, a feature that could be understood from Fig. 5.2 intuitively. We find that the optical potential can be kept negative by enhancing the Δ-parameter, as indicated by Fig. 5.7(c). One may note that for $\Omega_R > \Omega$, as could be seen from Fig. 5.7(c), the optical potential becomes negative in other temporal regimes as well. This may give us a tool to manipulate the optical trap in the regime of extreme nonlinear optics. Fig. 5.8 depicts the spatial variation of the optical potential for various Rabi frequencies with $\Delta = 1.7758$ rad/fs. It may be worthwhile to mention that the nature of the optical potential reported in this work matches quite well with that of recent experimental work, in the context of trapping of nanoparticles with femtosecond pulses, reported in Ref. [116]. The optical potential is getting split with the increase of the Rabi frequency. One may note the absence of splitting of the optical potential

in Fig. 5.7 as against the one in Fig. 5.8. This difference is occurring owing to the fact that in Fig. 5.7, the u -component of the Bloch vector is taken to be spatially independent while spatial dependency is taken into account while plotting Fig. 5.8. As u is related to the polarization of the atoms, our argument may be justified by one similar to that provided in Ref. [116].

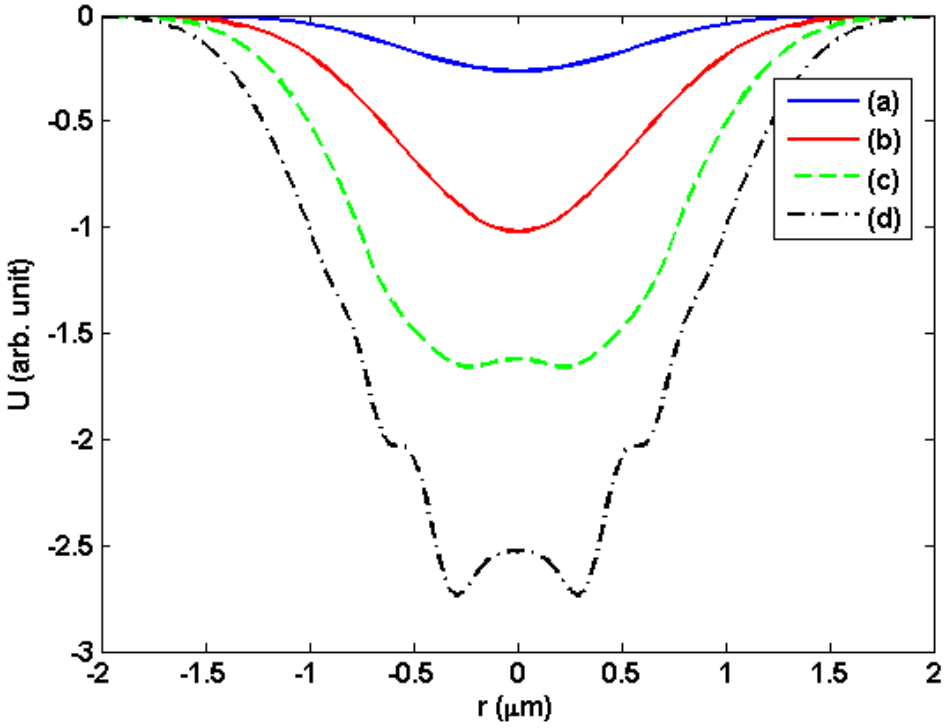

Fig. 5.8 Spatial profile of the optical potential with (a) Ω_R=0.6379 rad/fs, (b) Ω_R=1.2758 rad/fs, (c) Ω_R=2.2758 rad/fs, and (d) Ω_R=4.2758 rad/fs.

5.3 Chapter Summary

We have studied the optical force on a beam of neutral two-level atoms in a few-cycle pulsed Gaussian laser field under both resonant and off-resonant condition. A rigorous numerical study is carried out to analyse focusing, defocusing and steering of the neutral atoms in the laser field. We find that two-level atoms in an atomic beam could be focused and defocused for large, positively and negatively detuned interactions in the regime of extreme nonlinear optics. The so-called optical potential may be used for stable trapping of the neutral two-level atoms for large positively detuned interaction. We find that the light force beyond the RWA has turned out to be conservative for the particular problem considered in this work and so it cannot be used to cool a sample of two-level atoms. The treatment based on Ehrenfest's theorem [11] describes only the mean light force and is silent about the fluctuations of the

light force about its mean value. This, however should not reduce the effectiveness of our work as our main objective was to get a comprehensive idea about the light force on an atomic beam of two-level atoms beyond RWA the in a few-cycle pulsed Gaussian laser field. Moreover this work successfully reproduces some of the features reported in other recent experimental and theoretical works [74, 116]. This work is extended to the case of three-level atomic systems in the next chapter.

Chapter 6

Optical Dipole Force on Three-level Atoms*

6.1 Introduction

In the 1990s, considerable attention was paid to the study of optical forces in three-level system. It has been suggested by some researchers [183] that these studies of three-level forces may explain some of the discrepancies between real trapped atoms and the theoretical predictions offered by a two-level atomic model system. For example, in the cooling of two-level atoms by the radiative force, the minimum value of attainable temperature is given by the single-photon classical limit, $T_\gamma = \hbar\gamma/K_B$, where γ is the FWHM of the natural line width of the atomic transition, K_B is the Boltzmann constant and $\hbar$ is Planck's constant. However, V. G. Minogin et al. [184] demonstrated that Λ-like three-level atoms, under the condition of coherent atomic population trapping, could be cooled below the single-photon classical limit to a temperature corresponding to the recoil energy, $T_R = \hbar^2K^2/2MK_B$, where $\hbar K$ is the photon momentum and M is the mass of an atom. In Λ-like three-level atoms, J. Javanainen [185] has reported that the nonlinear mixing of wave vectors result in the generation of long wavelength optical force. He found that the magnitude of the optical force exceeds considerably as compared to the one predicted via a two-level model. In an another study, P. R. Hemmer et al. [186] carried out the first experimental observation of forces on Λ-like three-level atoms in a standing wave optical field and demonstrated the deflection of a sodium atomic beam. W. Rooijakkers et al. [187] calculated the optical forces, friction, and diffusion for ladder-like three-level atoms. Researchers have also demonstrated that atoms can be decelerated within a much shorter distance using cascaded excitation by overlapping traveling waves. In 2000, P. V. Pant and S. V. Lawande [188] derived the analytical expressions for optical forces on three-level atoms. In this study, they considered all three configurations, Λ-like, V-like and ladder-like, of a three-level atom. In 2013, T. Vanderbruggen and M. W. Mitchell [189] studied near resonant optical forces beyond

*The results presented in this chapter have been published in a paper, P. Kumar and A. K. Sarma, "Optical dipole force on ladder-like three-level atomic systems induced by few-cycle-pulse laser fields", Phys. Rev. A 86, 053414 (2012).

the two-level approximation for a continuous source of spin-polarized cold atoms.

All the aforementioned study on optical forces have been done using CW laser fields. In the present chapter, we report a study of the optical dipole force on three-level atoms under three different excitation schemes. First, we consider the non-resonant interaction of atoms with trains of few-cycle pulses; second, time-dependent detuned interaction of atoms with trains of chirped-few-cycle pulses is considered and finally, time-dependent detuned interaction of atoms with chirped-nanosecond pulses instead of pulse trains is considered. It is worth noting that many researchers have utilized optical forces, from the linearly chirped laser pulses for slowing, acceleration [190] and forced rotation [191] of molecules. The creation of an optical lens for atomic and molecular beam by optical dipole force has also been demonstrated by several authors [192-194].

6.2 The Model

The sketch of our scheme for the calculation of optical dipole forces on sodium atoms is depicted in Fig. 6.1.We consider a ladder-like atomic system interacting with two few-cycle pulsed laser fields. In this work the states $|1\rangle$, $|2\rangle$ and $|3\rangle$, respectively refers to the $3s, 3p$ and $4s$ quantum states of neutral sodium atoms.

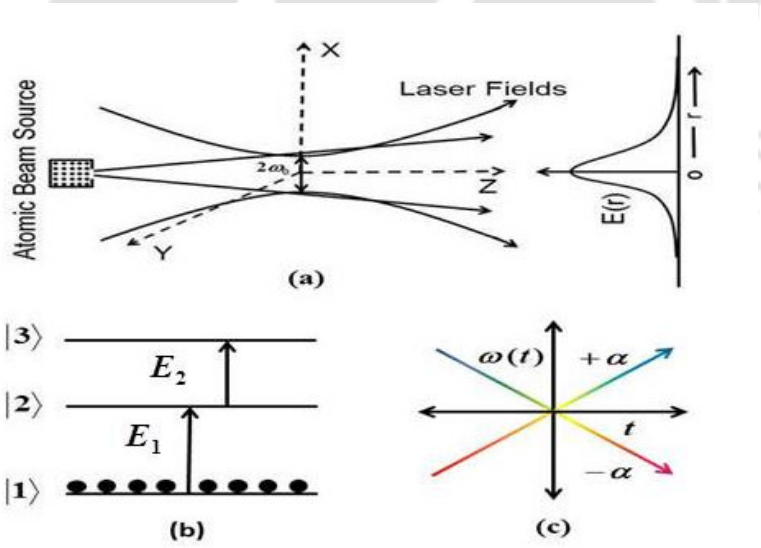

Fig. 6.1 (a) Sketch of the proposed scheme for the calculation of optical dipole force on an atomic beam co-propagating with pulsed laser fields. (b) Three-level atomic system. (c) Time-dependent frequency of up-chirped ($+\alpha$) and down-chirped ($-\alpha$) pulses.

The total electric field of each of the two pulse laser radiation can be written as

$$\vec{E}_{i(\,i=1,2\,)}(\,t-nt_r\,)=\sum_{n=0}^{N-1}\hat{\varepsilon}_i\,A_i(\,t-nt_r\,)cos(\,\omega_i(\,t-nt_r\,)+\alpha_i(\,t-nt_r\,)^2+\omega_{Di}+\phi_i(\,z\,)). \tag{6.2.0}$$

Here, $A_i(\,t-nt_r\,)=E_{oi}\,exp(-(((\,t-nt_r\,)/\tau\,)^2+(r/\omega_0)^2\,))$. We assume that the pulse train with electric field E_1 and the pulse train with electric field E_2 connect the states $|1\rangle\leftrightarrow|2\rangle$ and $|2\rangle\leftrightarrow|3\rangle$, respectively. In Eq. (6.2.0), $\omega_{Di}=\vec{k}_i.\vec{v}$ refers to the detuning of the transition lines of the atom moving with velocity $\vec{v}$ due to the Doppler shift, $\tau=1.177\tau_{\mathrm{p}}$, where τ_{p} is the temporal pulse width at full width at half maximum (FWHM), N is the number of pulses, t_r is the pulse repetition time, α_i is the chirp rate, ω_0 is the beam waist, ω_i is the laser frequency and $\phi_i(\,z\,)=k_iz$ is the longitudinal phases. Also, $k_i(\,i=1,2\,)$ is the wave vector of the corresponding electric fields. The density matrix equations, without invoking the so called rotating wave approximation, describing the temporal evolution of the density matrix elements, are:

$$\begin{aligned}
\frac{\mathrm{d}\rho_{11}}{\mathrm{dt}}&=\mathrm{i}(\Omega_{12}\rho_{21}-\Omega_{21}\rho_{12})\\
\frac{\mathrm{d}\rho_{22}}{\mathrm{dt}}&=\mathrm{i}(\Omega_{12}(\rho_{12}-\rho_{21})+\Omega_{23}(\rho_{32}-\rho_{23}))\\
\frac{\mathrm{d}\rho_{33}}{\mathrm{dt}}&=\mathrm{i}(\Omega_{32}\rho_{23}-\Omega_{23}\rho_{32})\\
\frac{\mathrm{d}\rho_{21}}{\mathrm{dt}}&=-\mathrm{i}\omega_{21}\rho_{21}+\mathrm{i}(\Omega_{12}(\rho_{11}-\rho_{22})+\Omega_{23}\rho_{31})\\
\frac{\mathrm{d}\rho_{32}}{\mathrm{dt}}&=-\mathrm{i}\omega_{32}\rho_{32}+\mathrm{i}(\Omega_{32}(\rho_{22}-\rho_{33})-\Omega_{12}\rho_{31})\\
\frac{\mathrm{d}\rho_{31}}{\mathrm{dt}}&=-\mathrm{i}\omega_{31}\rho_{31}+\mathrm{i}(\Omega_{23}\rho_{21}-\Omega_{12}\rho_{32})
\end{aligned} \tag{6.2.1}$$

Here, $\Omega_{12}=\Omega_{21}=\mu_{12}E_1(r,t)/\hbar$ and $\Omega_{23}=\Omega_{32}=\mu_{23}E_2(r,t)/\hbar$ are the time dependent Rabi frequencies for the transition with electric dipole moments μ_{12} and μ_{23}, respectively. It should be noted that $\omega_{\mathrm{ij}}=\omega_{\mathrm{i}}-\omega_{\mathrm{j}}$ and $\rho_{\mathrm{ij}}=\rho_{\mathrm{ji}}^{*}$. Using an approach based on the density matrix equations and Ehrenfest's theorem, we derive the following expression for the optical dipole force [73, 195]:

$$\vec{F}_t = \mu_{12}\sum_{n=0}^{N-1} u\{[\vec{\nabla}A_1(t-nt_r)]\cos(\omega_1(t-nt_r)+\alpha_1(t-nt_r)^2+\omega_{D1}+\phi_1(z))\}$$
$$+\mu_{23}\sum_{n=0}^{N-1} v\{[\vec{\nabla}A_2(t-nt_r)]\cos(\omega_2(t-nt_r)+\alpha_2(t-nt_r)^2+\omega_{D2}+\phi_2(z))\} \quad (6.2.2)$$

Here $u=(\rho_{21}+\rho_{12})$ and $v=(\rho_{32}+\rho_{23})$.

6.3 Numerical Results and Discussions

We solve Eq. 6.2.1 and Eq. 6.2.2 numerically using a standard fourth-order Runge-Kutta method. We assume that initially all the atoms are in the ground state $|1\rangle$. The Following typical parameters are used for simulation: for chirped-pulse excitation, $\omega_{21}=\omega_1=3.19$ rad/fs, $\omega_{32}=\omega_2=1.65$ rad/fs, and $\alpha_1=\alpha_2=\pm 0.02\,\text{fs}^{-2}$; on the other hand for non-resonant excitation of atoms, $\Delta_1=\omega_{21}-\omega_1=\pm 1.19$ rad/fs, and $\Delta_2=\omega_{32}-\omega_2=\pm 0.65$ rad/fs. The rest of the simulation parameters are as follows: $\Omega_{21}=\Omega_{32}=1.30$ rad/fs, $\mu_{12}=\mu_{23}=1.85\times10^{-29}$ C·m [32], $r=7.07\,\mu m$, $\omega_0=10\,\mu m$, and $v_z=1000$ m/s in the direction of pulse laser fields. The temporal pulse width is taken to be $\tau_p=23.5$ fs. In the present study, the centre of mass is taken to be M=22.99 amu. It can be deduced from Eq. 6.2.2 that the transverse force is maximum at r =7.07 μm and minimum at r =0 μm.

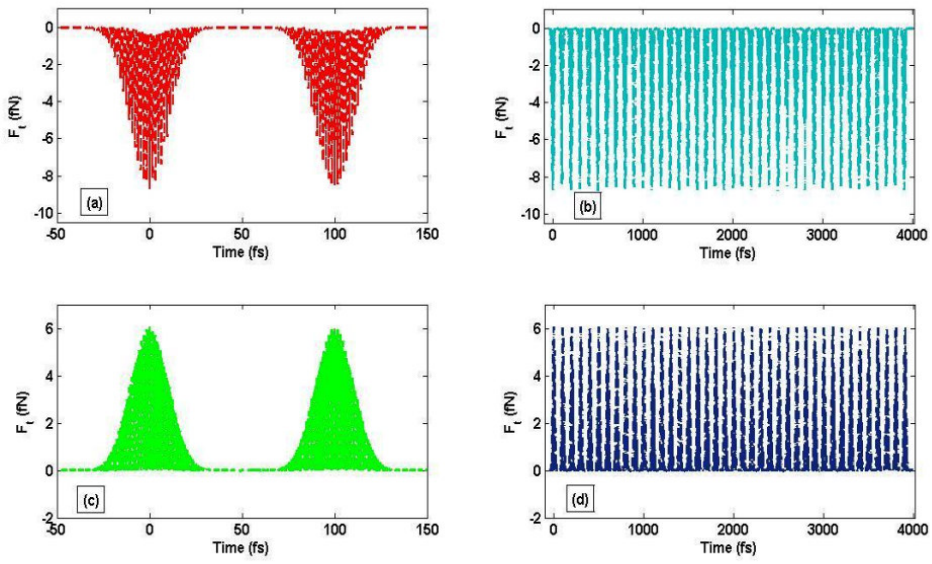

Fig. 6.2 Temporal evolution of optical dipole force under non-resonant excitation: (a) N=2, Δ_1=1.19 rad/fs and Δ_2=0.65 rad/fs; (b) N=40, Δ_1=1.19 rad/fs and Δ_2=0.65 rad/fs; (c) N=2, $\Delta_1=-1.19$ rad/fs and $\Delta_2=-0.65$ rad/fs; and (d) N=40, $\Delta_1=-1.19$ rad/fs and $\Delta_2=-0.65$ rad/fs.

In Fig. 6.2 we depict the temporal evolution of optical dipole force on atoms under non-resonant excitation of atoms. It can be observed from Fig. 6.2(a) and 6.2(b) that the optical dipole force is negative for positive detuning which may lead to the focusing of atoms, while Figs. 6.2(c) and 6.2(d) show that the optical dipole force is positive for negative detuning, and may lead to the defocusing of atoms. In Fig. 6.3 we depict the temporal evolution of the optical dipole force for an increased number of pulses, N=1000, compared to one used in Fig. 6.2.

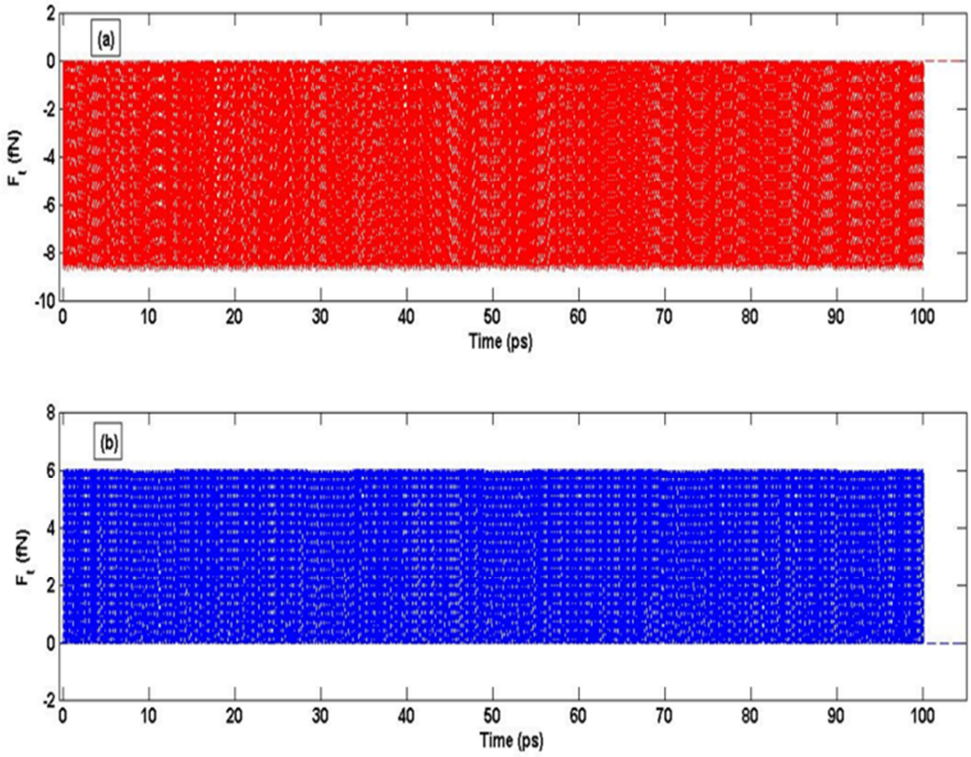

Fig. 6.3 Temporal evolution of optical dipole force under non-resonant excitation: (a) N=1000, $\Delta_1 = 1.19$ rad/fs and $\Delta_2 = 0.65$ rad/fs; (b) N=1000, $\Delta_1 = -1.19$ rad/fs and $\Delta_2 = -0.65$ rad/fs.

One may observe from Figs. 6.2 and 6.3 that the magnitude of the optical dipole force remains identical even with the increased number of pulses. Again, the temporal evolution of the optical dipole force remains similar even if the number of pulses is increased. The optical dipole force is negative for positive detuning and positive for negative detuning throughout the interaction time. It is worthwhile to mention that in the work by Bjorkholm et al. [167] the magnitude of the optical force on neutral atoms, induced by a CW laser field, was around 0.01×10^{-18} N or 0.01 aN. By contrast, in the present study, the time-averaged force is

approximately 3.30 fN for $\Delta_1 = \omega_{21} - \omega_1 = 1.19$ rad/fs, $\Delta_2 = \omega_{32} - \omega_2 = 0.65$ rad/fs and 2.49 fN for $\Delta_1 = \omega_{21} - \omega_1 = -1.19$ rad/fs, and $\Delta_2 = \omega_{32} - \omega_2 = -0.65$ rad/fs with N=1000. Clearly, the force considered in this work is much larger than the one considered by Bjorkholm et al. [167].

In Fig. 6.4 below, we show the trajectory of atoms subjected to the optical dipole force for N=1000.

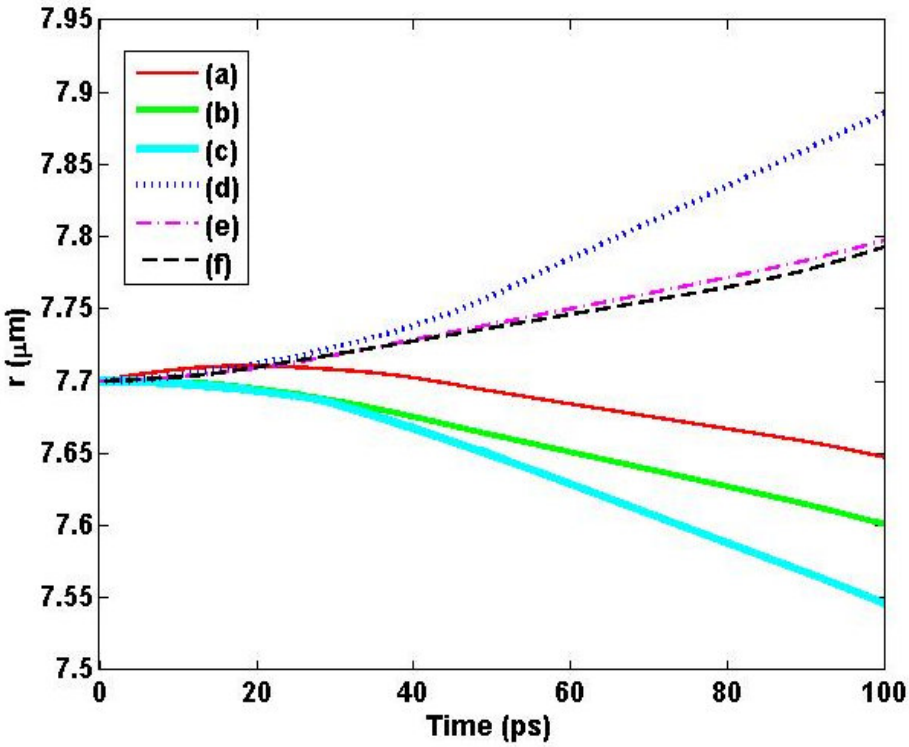

Fig. 6.4 Focusing(a-c) and defocusing (d-f)of atoms due to optical dipole force: (a) $\Delta_1 = 1.19$ rad/fs, $\Delta_2 = 0.65$ rad/fs and v_t=1000 m/s; (b) $\Delta_1 = 1.19$ rad/fs, $\Delta_2 = 0.65$ rad/fs and v_t=100 m/s; (c) $\Delta_1 = 1.19$ rad/fs, $\Delta_2 = 0.65$ rad/fs and v_t=1 m/s; and (d) $\Delta_1 = -1.19$ rad/fs, $\Delta_2 = -0.65$ rad/fs and v_t=1000 m/s (e) $\Delta_1 = -1.19$ rad/fs, $\Delta_2 = -0.65$ rad/fs and v_t=100 m/s (f) $\Delta_1 = -1.19$ rad/fs, $\Delta_2 = -0.65$ rad/fs and v_t=1 m/s.

It can be observed from Fig. 6.4 (a), Fig. 6.4 (b) and Fig. 6.4 (c) that due to the optical dipole force with positive detuning, atoms are being focused. So it appears that the optical dipole force is acting like an ultrafast optical lens for the diverging atomic beam. On the other hand, Fig. 6.4 (d), Fig. 6.4 (e) and Fig. 6.4 (f) show that the atoms are defocused by the optical dipole force with negative detuning. Hence the trains of few-cycle pulse laser fields may be used for effective focusing and defocusing of atoms in an atomic beam. In Fig. 6.5, we study

the temporal evolution of optical dipole force on atoms induced by trains of chirped pulse laser fields.

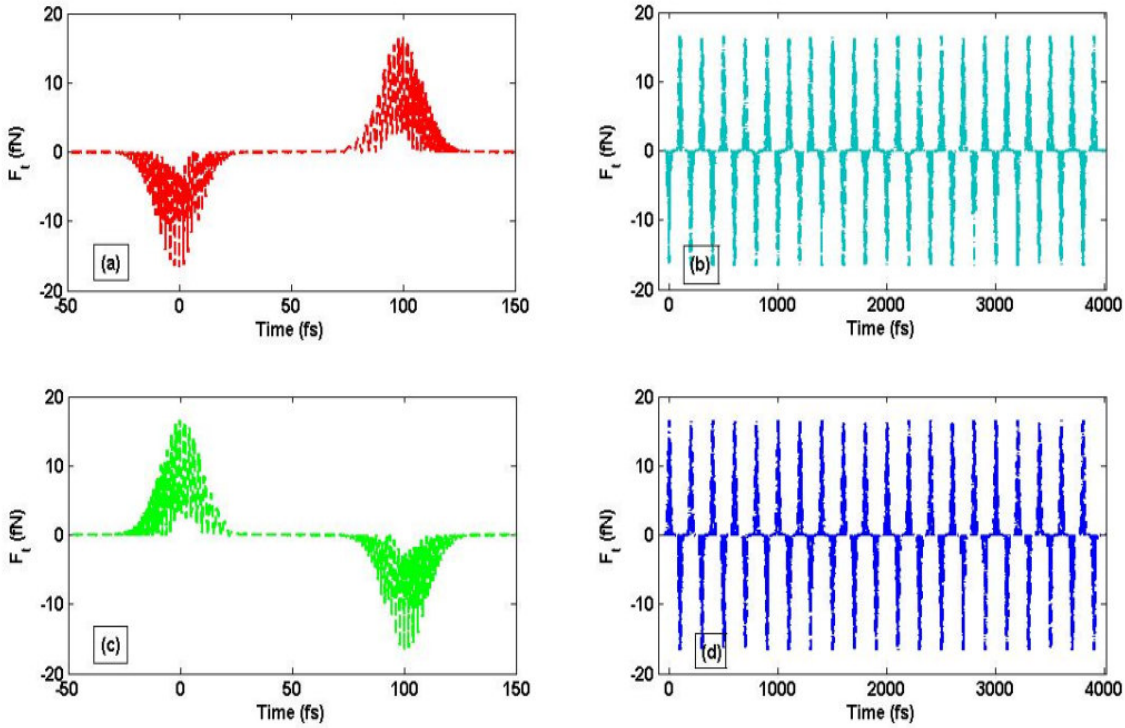

Fig. 6.5 Temporal evolution of optical dipole force under chirped-pulse excitation: (a) N=2, α_1=0.02 fs^{-2} and $\alpha_2 = 0.02$ fs^{-2}; (b) N=40, α_1=0.02 fs^{-2} and $\alpha_2 = 0.02$ fs^{-2}; (c) N=2, $\alpha_1 = -0.02$ fs^{-2} and $\alpha_2 = -0.02$ fs^{-2}; and (d) N=40, $\alpha_1 = -0.02$ fs^{-2} and $\alpha_2 = -0.02$ fs^{-2}.

It can be seen from Fig. 6.5(a) and Fig. 6.5(b) that the optical dipole force on atoms is negative for each odd number of pulses in the pulse trains, while it is positive for each even number of pulses in the pulse trains for up-chirped pulse trains. On the other hand, the opposite of the above occurs in the case of down-chirped pulse trains, as can be seen from Fig. 6.5(c) and Fig. 6.5(d). Hence the atoms in an atomic beam will encounter equal time-dependent positive and negative optical dipole forces from the chirped-few-cycle pulse trains in contrast to the optical dipole force induced by the non-resonant interaction of atoms with the few-cycle pulse trains. So the chirped-few-cycle pulse trains may not be useful for the focusing and defocusing of atoms. However, here it is worth to mention that the chirped-few-cycle pulse trains may be used for some other interesting applications such as ultrafast optical switching and ultrafast coherent population oscillations etc. [133, 29]. Finally, we consider the chirped nanosecond pulse excitation of atoms. The pulse duration (τ_p=2 ns) is assume still to be less than all of the relaxation times. Fig. 6.6 depicts the temporal evolution of

coherent population transfer, optical dipole force and trajectory of atoms under the influence of the optical dipole force. The chosen simulation parameters are realistic: $\Omega_{21} = \Omega_{32}$ =300 rad/ns, and $\alpha_1 = \alpha_2 = \pm$ 10 ns^{-2}; other simulation parameters remain similar to the ones used earlier.

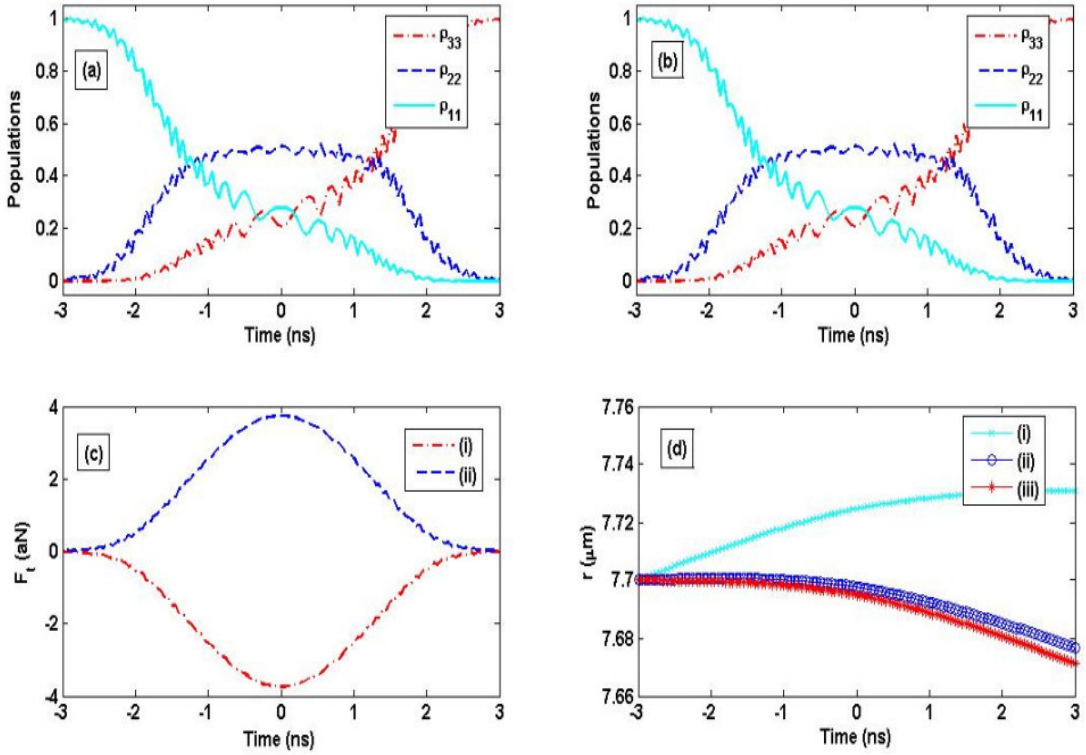

Fig. 6.6 Temporal evolution of (a) Populations with $\alpha_1 = \alpha_2 =$ 10 ns^{-2}; (b)Populations with $\alpha_1 = \alpha_2 =$ -10 ns^{-2}; (c) Optical dipole force with (i) $\alpha_1 = \alpha_2 = 10$ ns^{-2}, and (ii) $\alpha_1 = \alpha_2 = -10$ ns^{-2}; and (d) Trajectory of atoms with $\alpha_1 = \alpha_2 = 10$ ns^{-2} for (i) v_t =10 m/s, (ii) v_t =1 m/s, (iii) v_t =0.1 m/s.

It can be seen from Fig. 6.6(a) and Fig. 6.6(b) that after the interaction, all the atomic populations is in the state $|3\rangle$ and is independent of the sign of the chirping parameters. On the other hand, as is evident from Fig. 6.6(c), the optical dipole force is negative for $\alpha_1 = \alpha_2 = 10$ ns^{-2}, while it is positive for $\alpha_1 = \alpha_2 = -10$ ns^{-2}. Hence, the optical dipole force may be used for focusing and defocusing of atoms with judicious control of the sign of the chirping parameters. Focusing and defocusing atoms is dependent on the transverse velocity of the atoms as well, as could be seen from Fig. 6.6(d). For the chosen parameters, we find that atoms with transverse velocities up to and below 1 m/s are focused due to the optical dipole force. So, these chirped nanosecond pulses may be used for coherent population transfer and

focusing of atoms simultaneously, subject to the appropriate choice of parameters as discussed above. However, trains of few-cycle pulses may be used for focusing the atoms moving with higher transverse velocities compared to chirped nanosecond pulses, as can be observed from Fig. 6.4 and Fig. 6.6 (d).

6.4 Chapter Summary

This chapter discusses the optical dipole force in a ladder like three-level atomic system induced by the trains of few-cycle-pulse laser fields. We have considered the non-resonant as well as the chirped pulse excitation of three-level atoms. The force is calculated by numerically solving the force equation and the density matrix equations self-consistently beyond the rotating wave approximations. By analyzing the centre-of-mass motion, it is shown that under non-resonant excitation, the optical dipole force induced by trains of few-cycle-pulses may be used for focusing and defocusing of atoms in an atomic beam. Moreover, we have demonstrated that the chirped nanosecond pulses may be used for both coherent population transfer and focusing or defocusing of atoms simultaneously, with judicious choice of parameters.

Chapter 7

Conclusions and Future Aspects

7.1 Conclusions

This thesis describes theoretical studies of coherent control and manipulation of atoms using femtosecond pulses. In the context of coherent control, coherent population transfer (CPT) in two-, Λ-like three- and Y-like four-level atoms is investigated. The phenomenon of ultrafast coherent population oscillations (UCPOs), in which the complete population oscillates between the ground and excited states of an atom, is predicted in two-level atoms illuminated by a train of femtosecond pulses. It is found that the quantum state of the atoms and the frequency of UCPOs may be controlled by controlling the number of pulses in the pulse trains and the pulse repetition time. Some possible applications of the observed UCPOs are suggested. In Λ-like three-level atoms, a simple and fairly robust scheme is proposed to achieve efficient and fast CPT by utilizing either a nonlinearly chirped Gaussian shaped few-cycle laser pulse or an unchirped sinc-shaped few-cycle laser pulse. It is reported that compared to the so-called stimulated Raman adiabatic passage (STIRAP) technique, the scheme proposed for complete population transfer with few-cycle Gaussian shaped laser pulses requires less pulse area. An efficient scheme to achieve ultrafast and selective population transfer in Y-like four-level atoms, by utilizing a single nonlinearly chirped femtosecond pulse, is also proposed. It is found that selective CPT may be achieved just by manipulating the frequency offset.

In the later part of the thesis, femtosecond pulse induced optical forces on two- and three-level atoms in an atomic beam are investigated. In the context of two-level atoms, the optical force on a beam of neutral atoms illuminated by a few-cycle-pulsed Gaussian laser field under both resonant and off-resonant condition is studied. The effects of the optical force on the motion of neutral atoms are analyzed. It is suggested that the so-called optical potential may be used for stable trapping of the neutral two-level atoms for large positively detuned interaction. Finally, the optical dipole force on a ladder like three-level atomic system induced by trains of femtosecond pulses is investigated. Both non-resonant and the

chirped pulse excitation of three-level atoms were considered. By analyzing the centre-of-mass motion, it is shown that under non-resonant excitation, the optical dipole force induced by trains of femtosecond pulses may be used for focusing and defocusing of atoms in an atomic beam. Moreover, it is reported that chirped nanosecond pulses may be used for both coherent population transfer and focusing or defocusing of atoms simultaneously.

7.2 Future Aspects

In this thesis the study of coherent control and manipulation of atoms is based on the numerical solution of the appropriate density matrix equations. No study with regard to pulse propagation in the chosen atomic systems (two-, three- and four-level atoms) is carried out in the present thesis. However, to clarify certain assumptions, pulse propagation studies could be quite useful. For example, in the second chapter of this thesis, based on the literature [98, 133], an assumption was made that, when a switching signal enters into the absorbing medium ($w<0$), it may be absorbed by the medium. Also it was assumed that the switching signal will not be absorbed when a switching signal enters into the amplifying medium ($w>0$). These assumptions, though they may not be wrong entirely, could only be verified by investigating the propagation of the switching signal in the medium (absorptive or amplifying). Moreover, few-cycle pulse propagation studies in the systems considered in this thesis might yield much physics and insights, and could easily be a fruitful topic for future research.

Controlling the population transfer into Rydberg states of atoms may be another future aspect of the research reported in this thesis. A Rydberg atom is an atom whose valence electrons are in states with a very large principal quantum number “n”. The spatial excursions of highly excited Rydberg atoms exceed the size of ground-state atoms by orders of magnitudes. Such large excursions of the Rydberg electron imply very long lifetimes, high susceptibilities to external fields and strong interactions between the atoms. They may be used in a variety of potential applications: as elements in fast quantum gates [196, 197], single photon sources [198, 199], and in the generation of mesoscopic entanglement [200].

Bibliography

[1] M. Shapiro and P. Brumer, *Principles of the quantum control of molecular processes*, (Wiley Inter-science, New Jersey, 2003).

[2] P. Kral, I. Thanopulos and M. Shapiro, Rev. Mod. Phys. **79**, 53 (2007).

[3] K. Bergmann, H. Theuer and B. W. Shore, Rev. Mod. Phys. **70**, 1003 (1998).

[4] N. V. Vitanov, T. Halfmann, B. W. Shore, and K. Bergmann, Annu. Rev. Phys. Chem. **52**, 763 (2001).

[5] B. W. Shore, *The Theory of Coherent Atomic Excitation* (Wiley, New York, 1990).

[6] W.-T. Liao, A. Pálffy, C. H. Keitel, Phys. Lett. B **705**, 134 (2011).

[7] P. Lambropoulos, D. Petrosyan, *Fundamentals of quantum optics and quantum information* (Springer, 2007).

[8] D. Yan, C.-L. Cui, M. Zhang, and J.-H. Wu, Phys. Rev. A **84**, 043405 (2011).

[9] H. Maeda, J. H. Gurian, D. V. L. Norum, and T. F. Gallagher, Phys. Rev. Lett. **96**, 073002 (2006).

[10] M. M. Martin, J. T. Hynes, *Femtochemistry and Femtobiology: Ultrafast Events in Molecular Science* (Elsevier, 2004).

[11] M. Shapiro, P. Brumer, *Quantum Control of Molecular Processes* (WILEY-VCH Verlag GmbH & Co, 2012).

[12] M. Oberst, H. Münch, and T. Halfmann, Phys. Rev. Lett. **99**, 173001 (2007).

[13] B. D. Fainberg and V. A. Gorbunov, J. Chem. Phys. **117**, 7222 (2002).

[14] M. Külz, M. Keil, A. Kortyna, B. Schellhaa\S, J. Hauck, and K. Bergmann, Phys. Rev. A **53**, 3324–3334 (1996).

[15] P. Dittmann, F. P. Pesl, J. Martin, G. W. Coulston, G. Z. He, and K. Bergmann, J. Chem. Phys. **97**, 9472 (1992).

[16] Y. Ohta, K. Hoki, and Y. Fujimura, J. Chem. Phys. **116**, 7509 (2002).

[17] C. M. Simon, T. Belhadj, B. Chatel, T. Amand, P. Renucci, A. Lemaitre, O. Krebs, P. A. Dalgarno, R. J. Warburton, X. Marie, and B. Urbaszek, Phys. Rev. Lett. **106**, 166801 (2011).

[18] L. F.Wei, J. R. Johansson, L. X. Cen, S. Ashhab, and F. Nori, Phys. Rev. Lett. **100**, 113601 (2008).

[19] L. S. Goldner, C. Gerz, R. J. C. Spreeuw, S. L. Rolston, C. I. Westbrook, and W. D. Phillips, Phys. Rev. Lett. **72**, 997 (1994).

[20] J. Lawall and M. Prentiss, Phys. Rev. Lett. **72**, 993–996 (1994).

[21] R. Sussmann, R. Neuhauser, and H. Neusser, J. Chem. Phys. **100**, 4784 (1994).

[22] T. A. Collins and S. A. Malinovskaya, Opt. Lett. **37**, 2298 (2012).

[23] D. Møller, L. Bojer Madsen, and K. Mølmer, Phys. Rev. Lett. **100**, 170504 (2008).

[24] J. L. Sørensen, D. Møller, T. Iversen, J. B. Thomsen, F. Jensen, P. Staanum, D. Voigt and M. Drewsen, New J. Phys. **8**, 261 (2006).

[25] T. Beth, G. Leuchs, *Quantum Information Processing* (WILEY-VCH Verlag GmbH & Co, 2005).

[26] M. Saffman and T. G. Walker, Rev. Mod. Phys. **82**, 2313 (2010).

[27] H. Suchowski, Y. Silberberg, and D. B. Uskov, Phys. Rev. A **84**, 013414 (2011).

[28] C. Y. Ye, V. A. Sautenkov, Y. V. Rostovtsev, and M. O. Scully, Opt. Lett. **28**, 2213 (2003).

[29] P. Kumar and A. K. Sarma, Phys. Rev. A **87**, 025401 (2013).

[30] U. Gaubatz, P. Rudecki, S. Schiemann, and K. Bergmann, J. Chem. Phys. **92**, 5363 (1990).

[31] J. Klein, F. Beil, and T. Halfmann, Phys. Rev. Lett. **99**, 113003 (2007).

[32] K. Winkler, F. Lang, G. Thalhammer, P. V. d. Straten, R. Grimm, and J. H. Denschlag, Phys. Rev. Lett. **98**, 043201(2007).

[33] T. Peters, L. P. Yatsenko, and T. Halfmann, Phys. Rev. Lett. **95**, 103601 (2005).

[34] S. Stellmer, B. Pasquiou, R. Grimm, and F. Schreck, Phys. Rev. Lett. **109**, 115302 (2012).

[35] Fu-quan Dou, Li-bin Fu, and J. Liu, Phys. Rev. A **87**, 043631(2013).

[36] M. Sukharev and S. A. Malinovskaya, Phys. Rev. A **86**, 043406 (2012).

[37] A. A. Rangelov and N. V. Vitanov, Phys. Rev. A **85**, 055803 (2012).

[38] L. Wang, X.-L. Song, A.-J. Li, H.-H. Wang, X.-G. Wei, Z.-H. Kang, Y. Jiang, and J.-Y. Gao, Opt. Lett. **33** 2380 (2008).

[39] N. G. Kalugin and Y. V. Rostovtsev, Opt. Lett. **31** 969 (2006).

[40] C. Y. Ye, V. A. Sautenkov, Y. V. Rostovtsev, M. O. Scully, Opt. Lett. **28**, 2213 (2003).

[41] E. A. Shapiro, V. Milner and M. Shapiro, Phys. Rev. A **79**, 023422 (2009).

[41] E. A. Shapiro, V. Milner, C. Menzel-Jones, and M. Shapiro, Phys. Rev. Lett. **99**, 033002 (2007).

[43] E. A. Shapiro, Avi Pe'er, J. Ye, and M. Shapiro, Phys. Rev. Lett. **101**, 023601 (2008).

[44] X. H. Yang, Z. H. Zhang, Z. Wang and X. N. Yan, Eur. Phys. J. D **57**, 253 (2010).

[45] S. Chelkowski and G**.** N. Gibson, Phys. Rev. A **52**, 3417 (1995).

[46] J. C. Davis and W. S. Warren, J. Chem. Phys. **110**, 4229 (1999).

[47] J. S. Melinger, S. R. Gandhi, A. Hariharan, D. Goswami, and W. S. Warren, J. Chem. Phys. **101**, 6439 (1994).

[48] G. P. Djotyan, J. S. Bakos, G. Demeter and Z. Sörlei, J. Opt. Soc. Am. B **17**, 107 (2000).

[49] V. S. Malinovsky and J. L. Krause, Eur. Phys. J. D **14**, 147 (2001).

[50] F. Bloch, Phys. Rev. **70**, 460 (1946).

[51] S. Avrillier, J.-M. Raimond, C. J. Borde, D. Bassi and G. Scoles, Opt. Commun. **30**, 311 (1981).

[52] A. G. Adam, T. E. Gough, N. R. Isenor, and G. Scoles, Phys. Rev. A **32**, 1451 (1985).

[53] E. B. Treacy, Phys. Lett. A **27**, 421 (1968).

[54] D. Grischkowsky and M. M. T. Loy, Phys. Rev. A **12**, 1117 (1975).

[55] T. Lu, X. Miao, and H. Metcalf, Phys. Rev. A **71**, 061405 (2005).

[56] R. Yamazaki, Ken-ichi Kanda, F. Inoue, K. Toyoda, and S. Urabe, Phys. Rev. A **78**, 023808 (2008).

[57] T. Noel, M. R. Dietrich, N. Kurz, G. Shu, J. Wright, and B. B. Blinov, Phys. Rev. A **85**, 023401 (2005).

[58] R. T. Brierley, C. Creatore, P. B. Littlewood, and P. R. Eastham, Phys. Rev. Lett. **109**, 043002 (2012).

[59] Y. Wu, I. M. Piper, M. Ediger, P. Brereton, E. R. Schmidgall, P. R. Eastham, M. Hugues, M. Hopkinson, and R. T. Phillips, Phys. Rev. Lett. **106**, 067401 (2011).

[60] **A.** Maluckov, G. Gligorić, L. Hadžievski, B. A. Malomed, and T. Pfau, Phys. Rev. Lett. **108**, 140402 (2012).

[61] B. W. Shore, *Manipulating quantum structures using laser pulses*, (Cambridge University Press, New York, 2011).

[62] J. M. Sage, A. J. Kerman, and J. Chiaverini, Phys. Rev. A **86**, 013417 (2012).

[63] D. Gallego, S. Hofferberth, T. Schumm, P. Krüger, J. Schmiedmayer, Opt. Lett. **34**, 3463 (2009).

[64] S. Nedev, A. S. Urban, A. A. Lutich, and J. Feldmann, Nano Lett. **11**, 5066 (2011).

[65] D. G. Grier, Nature **424**, 21 (2003).

[66] K. Sasaki, M. Koshioka, H. Misawa, N. Kitamura, and H. Masuhara, Appl. Phys. Lett. **60**, 807 (1992).

[67] K. Svoboda, and S. M. Block, Ann. Rev. Biophys. and Biomol. Struct. **23**, 247 (1994).

[68] M. L. Juan, M. Righini and R. Quidant, Nature Phot. **5**, 349 (2011).

[69] A. N. Grigorenko, N. W. Roberts, M. R. Dickinson and Y. Zhang, Nature Phot. **2**, 365 (2008).

[70] P. Meystre, *Atom Optics* (Springer, Berlin, 2001).

[71] V. S. Letokhov, *Laser Control of Atoms and Molecules* (Oxford University Press, Oxford, 2007).

[72] J. Weiner, *Light-Matter Interaction*, Vol. 1, (John Wiley & Sons, New Jersey).

[73] R. J. Cook, Phys. Rev. A **20**, 224 (1979).

[74] V. E. Lembessis and D. Ellinas, J. Opt. B: Quantum Semiclass. Opt. **7**, 319 (2005).

[75] R. W. Boyd, *Nonlinear Optics*, (Academic Press, Elsevier, 2008).

[76] K. Blum, *Density Matrix Theory and Applications,* (Springer, 2012).

[77] J.-C. Diels and W. Rudolph, *Ultrashort Laser Pulse Phenomena,* (Elsevier, Academic Press, 2006).

[78] M. Wegener, *Extreme Nonlinear Optics*, (Springer, 2005).

[79] Z. Chang, *Fundamentals of attosecond Optics*, (CRC Press, Taylor & Francis Group, 2011).

[80] F. X. Kartner, *Few-Cycle Laser Pulse Generation and Its Applications*, (Springer, 2004).

[81] A. M. Weiner, *Ultrafast Optics,* (John Wiley & Sons, 2011).

[82] G. Cerullo and C. Vozzi, Physics **5**, 138 (2012).

[83] X. Xie, K. D.-Dier, S. Roither, M. S. Schoffler, D. Kartashov, H. Xu, T. Rathje, G. G. Paulus, A. Baltuska, S. Grafe, and M. Kitzler, Phys. Rev. Lett. **109**, 243001 (2012).

[84] E. N. Nerush and I. Y. Kostyukov, Phys. Rev. Lett. **103**, 035001 (2009).

[85] V. Roudnev and B. D. Esry, Phys. Rev. Lett. **99**, 220406 (2007).

[86] D. Mathur, K. Dota, A. K. Dharmadhikari, and J. A. Dharmadhikari, Phys. Rev. Lett. **110**, 083602 (2013).

[87] T. Nakajima, E. Cormier, Opt. Lett. **32**, 2879 (2007).

[88] X. Zhao, J. Chen, P. Fu, X. Liu, Z-C Yan, and B. Wang, Phys. Rev. A **87**, 043411 (2013).

[89] C. Figueira de Morisson Faria, T. Shaaran, and M. T. Nygren, Phys. Rev. A **86**, 053405 (2012).

[90] W. C. Wallace, M. G. Pullen, D. E. Laban, O. Ghafur, H. Xu, A. J. Palmer, G. F. Hanne, K. Bartschat, A. N. Grum-Grzhimailo, H. M. Quiney, I. V. Litvinyuk, R. T. Sang and D. Kielpinski, New J. Phys. **15** 033002 (2013).

[91] T. Brabec and F. Krausz, Rev. Mod. Phys. **72**, 545 (2000).

[92] J. K. Ranka and A. L. Gaeta, Opt. Lett. **23**, 534 (1998).

[93] B. Thomas and F. Krausz, Phys. Rev. Lett. **78**, 17 (1997).

[94] T. Nakajima, and S. Watanabe, Phys. Rev. Lett. **96**, 2 13001, (2006).

[95] T. Tritschler, O. D. Mucke, and M. Wegener, Phys. Rev. A **68**, 033404 (2003).

[96] S. Hughes, Phys. Rev. Lett. **81**, 3363 (1998).

[97] S. Swain, J. Phys. A **6**, 192 (1973).

[98] R. W. Ziolkowski, J. M. Arnold and D. M. Gogny, Phys. Rev. A **52**, 3082–3094 (1995).

[99] C. Hess, S. Funk, M. Bonn, D. N. Denzler, M. Wolf, G. Ert, Appl. Phys. A **71**, 447 (2000).

[100] T. Laarmann, I. Shchatsinin, P. Singh, N. Zhavoronkov, M. Gerhards, C. P. Schulz, and I. V. Hertel, J. Chem. Phys. **127**, 201101 (2007).

[101] H. Lippert, J. Manz, M. Oppel, G. K. Paramonov, W. Radloff, H.-H. Ritzea and V. Sterta, Phys. Chem. Chem. Phys. **6**, 4283 (2004).

[102] S. Zamith, Y. Ni, A. Gürtler, L. D. Noordam, H. G. Muller, and M. J. J. Vrakking, Opt. Lett. **29**, 2303 (2004).

[103] M. F. Kling and M. J. J. Vrakking, Annu. Rev. Phys. Chem. **59**, 463 (2008).

[104] M. Klaiber, Karen Z. Hatsagortsyan, Carsten Müller, and Christoph H. Keitel, Opt. Lett. **33**, 411 (2008).

[105] C. Altucci, R. Esposito, V. Tosa, and R. Velotta, Opt. Lett. **33**, 2943 (2008).

[106] T. Popmintchev, M.-C. Chen, P. Arpin, M. M. Murnane and H. C. Kapteyn, Nature Phot. **4**, 822 (2010).

[108] Z. Zeng, Y. Zheng, Y. Cheng, R. Li and Z. Xu, J. Phys. B: At. Mol. Opt. Phys. **45** 074004 (2012).

[109] S. Sukiasyan, K. L. Ishikawa, and M. Ivanov, Phys. Rev. A **86**, 033423 (2012).

[110] Z. Walters and O. Smirnova, J. Phys. B **43**, 161002 (2010).

[111] F. Dausinger, F. Lichtner, H. Lubatschowski, *Femtosecond Technology for Technical and Medical Applications*, (Springer, 2004).

[112] J. Ye, S. T. Cundiff, *Femtosecond Optical Frequency Comb: Principle, Operation and Applications,* (Springer, 2005).

[113] C. Hnatovsky, V. G. Shvedov, W. Krolikowski, and A. V. Rode, Opt. Lett. **35**, 3417 (2010).

[114] A. G. Okhrimchuk, V. K. Mezentsev, V. V. Dvoyrin, A. S. Kurkov, E. M. Sholokhov, S. K. Turitsyn, A. V. Shestakov, and I. Bennion, Opt. Lett. **34**, 3881 (2009).

[115] R. Osellame, G. Cerullo, R. Ramponi, *Femtosecond Laser Micromachining,* (Springer, 2012).

[116] Y. Jiang, T. Narushima and H. Okamoto, Nature Phys. **6**, 1005 (2010).

[117] U. Eichmann, T. Nubbemeyer, H. Rottke, and W. Sandner, Nature **461**, 1261 (2009).

[118] B. J. Roxworthy and K. C. Toussaint Jr., Sci. Rep. **2**, 660 (2012).

[119] B. L. Brown, A. J. Dicks, and I. A. Walmsley, Phys. Rev. Lett. **96**, 173002 (2006).

[120] M. Nakazawa, K. Kurokawa, H. Kubota, and E. Yamada, Phys. Rev. Lett. **65**, 1881 (1990).

[121] E. Gershnabel and I. Sh. Averbukh, Phys. Rev. Lett. **104**, 153001 (2010).

[122] A. M. Weiner, Rev. Sci. Instrum. **71**, 1929 (2000).

[123] K.-A. B. Soderberg, N. Gemelke and C. Chin, New J. Phys. **11** 055022 (2009).

[124] A. Goepfert, I. Bloch, D. Haubrich, F. Lison, R. Schütze, R. Wynands, and D. Meschede, Phys. Rev. A **56**, 3354 (1997).

[125] X. Miao, E. Wertz, M. G. Cohen, and H. Metcalf, Phys. Rev. A **75**, 011402 (2007).

[126] D. Stack, J. Elgin, P. M. Anisimov, and H. Metcalf, Phys. Rev. A **84**, 013420 (2011).

[127] G. Demeter, G. P. Djotyan, Zs. Sörlei, and J. S. Bakos, Phys. Rev. A **74**, 013401 (2006).

[128] T. Laupretre, S. Kumar, P. Berger, R. Faoro, R. Ghosh, F. Bretenaker, and F. Goldfarb, Phys. Rev. A **85**, 051805 (2012).

[129] A. Eilam, I. Azuri, A. V. Sharypov, A. D. Wilson-Gordon, and H. Friedmann, Opt. Lett. **35**, 772 (2010).

[130] C. S. Yelleswarapu, S. Laoui, R. Philip, and D. V. G. L. N. Rao, Opt. Exp. **16**, 3844 (2008)

[131] M. S. Bigelow, N. N. Lepeshkin, and R. W. Boyd, Phys. Rev. Lett. **90**, 113903 (2003).

[132] M. Scalora and C. M. Bowden, Phys. Rev. A **51**, 4048 (1995).

[133] M. E. Crenshaw, M. Scalora and C. M. Bowden, Phys. Rev. Lett. **68**, 911 (1992).

[134] K. Xia, S. Gong, C. Liu, X. Song and Y. Niu, Opt. Exp. **13**, 5913 (2005).

[135] C. M. Bowden, H. M. Gibbs, and S. L. McCall, *Optical Bistability* (Plenum, New York, 1984).

[136] C. M. Bowden, A. Postan and R. Inguva, J. Opt. Soc. Am. B **8**, 1081 (1991).

[137] X. H. Song, S. Q. Gong, W. F. Yang, and Z. Z. Xu, Phys. Rev. A **70**, 1 (2004).

[138] V. P. Kalosha and J. Herrmann, Phys. Rev. Lett. **83**, 544-547 (1999).

[139] L. Allen and J. H. Eberly, Optical Resonance and Two-Level Atoms (Wiley, New York 1975)

[140] C. Serrat and J. Biegert, Opt. Exp. **16**, 19667 (2008).

[141] F. Trager, Handbook of Lasers and Optics (Springer, Berlin 2007).

[142] M. Krug, T. Bayer, M. Wollenhaupt, C. Sarpe-Tudoran, T. Baumert, S. S. Ivanov and N. V. Vitanov, New J. Phys. **11**, 105051 (2009).

[143] I. R. Sola, V. S. Malinovsky, B. Y. Chang, J. Santamaria, and K. Bergmann, Phys. Rev. A **59**, 4494 (1999).

[144] A. Kuhn, G.W. Coulston, G.Z. He, S. Schiemann, K. Bergmann, and W.S. Warren, J. Chem. Phys. **45**, 5297 (1992).

[145] A. Kuhn, S. Steuerwald, and K. Bergmann, Eur. Phys. J. D **1**, 57 (1998).

[146] B.W. Shore, K. Bergmann, A. Kuhn, S. Schiemann, J. Oreg, and J.H. Eberly, Phys. Rev. A **45**, 5297 (1992).

[147] B. Broers, H. B. van Linden van den Heuvell, and L. D. Noordam, Phys. Rev. Lett. **69**, 2062 (1992).

[148] P. Balling, D. J. Maas, and L. D. Noordam, Phys. Rev. A **50**, 4276 (1994).

[149] V. S. Malinovsky and D. J. Tannor, Phys. Rev. A **56**, 4929 (1997).

[150] Y. B. Band, S. Kallush, and R. Baer, Chem. Phys. Lett. **392**, 23 (2004).

[151] N. Cui, Y. Xiang, Y. Niu and S. Gong, New J. Phys. **12**, 013009 (2010).

[152] J. L. Carini, J. A. Pechkis, C. E. Rogers, III, P. L. Gould, S. Kallush, and R. Kosloff, Phys. Rev. A **85**, 013424 (2012).

[153] J. J. Carrera and S.-I. Chu, Phys. Rev. A **75**, 033807 (2007).

[154] O. Nahmias, O. Bismuth, O. Shoshana and S. Ruhman, *Ultrafast phenomena XV*, **88,** 312 (Springer, Berlin, 2007).

[155] G. M. Genkin, Phys. Rev. A **58**, 758 (1998).

[156] L. Rutherford, I.C. Lane and J. F. MacCann, J. Phys. B: At. Mol. Opt. Phys. **43**, 185504 (2010)

[157] I. Fan, T. L. Chen, Y. S. Liu, Y. H. Lien, J. T. Shy and Y. W. Liu, Phys. Rev. A **84**, 042504 (2011).

[158] B. Klöter, C. Weber, D. Haubrich, D. Meschede, and H. Metcalf, Phys. Rev. A **77**, 033402 (2008).

[159] J. I. Kim, D. Haubrich, and D.Meschede, Opt. Exp. **17**, 21216 (2009).

[160] Y. B. Band and O. Magnes, Phys. Rev. A **50**, 584 (1994).

[161] X. Yang and S. Zhu, Phys. Rev. A **78**, 023818 (2008).

[161] X. Yang, Z. Zhang, X. Yan, and C. Li, Phys. Rev. A **81**, 035801 (2010).

[163] G. P. Djotyan, J. S. Bakos, Zs. Sörlei, and J. Szigeti, Phys. Rev. A **70**, 063406 (2004).

[164] Z. Zhang, X. Yang, and X. Yan, J. Opt. Soc. Am. B **30**, 1017 (2013).

[165] A. Ashkin, Phys. Rev. Lett. **25**, 1321 (1970)

[166] A. Ashkin, Phys. Rev. Lett. **40**, 729 (1978)

[167] J. E. Bjorkholm, R. R. Freeman, A. Ashkin and D. B. Pearson, Phys. Rev. Lett. **41**, 1361 (1978)

[168] H. J. Metcalf and P. Van der Straten, *Laser Cooling and Trapping* (Springer, 1999).

[169] A. D. Cronin, J. Schmiedmayer and D. E. Pritchard, Rev. Mod. Phys. **81**, 1051 (2009).

[170] M. H. Anderson, J. R. Ensher, M. R. Mathews, C. E. Wieman and E. A. Cornell, Science **269**, 198 (1995).

[171] J. I. Cirac and P. Zoller, Phys. Today **57**, 38 (2004).

[172] R. J. Cook, Phys. Rev. A, **21**, 268 (1980).

[173] J. Dalibard and C. Cohen-Tannoudji, J. Opt. Soc. Am. B **2**, 1707 (1985).

[174] N. P. Bigelow and M. G. Prentiss, Opt. Lett. **15**, 1479 (1991).

[175] P. C. Chaumet and M. N.-Vesperinas, Opt. Lett. **25**, 1065 (2000).

[176] H. -R. Noh and W. Jhe, J. Opt. Soc. Am. B **27**, 1712 (2010).

[177] X. Cai, J. Zheng, and Q. Lin, Phys. Rev. A **87**, 043401 (2013).

[178] T. Tritschler, O. D. Mucke, and M. Wegener, Phys. Rev. A **68**, 033404 (2003).

[179] M.W. Walser, C.H. Keitel, A Scrinzi and T. Brabec, Phys. Rev. Lett., **85**, 5082 (2000).

[180] S Hughes, Phys. Rev. A **62**, 055401 (2000).

[181] G. Grynberg, A. Aspect and C. Fabre, *Introduction to Quantum Optics* (Cambridge, 2010).

[182] T. Tritschler, O. D. Mu¨cke, M. Wegener, U. Morgner, and F.X.Kartner, Phys. Rev. Lett. **90**, 217404 (2003).

[183] A. Aspect, E. Arimondo, R. Kaiser, N. Vansteenkiste, and C. C.-Tannoudji, Phys. Rev. Lett. **61**, 826 (1988).

[184] V. G. Minogin, M. A. Olshany, and S. U. Shulga, J. Opt. Soc. Am. B **6**, 11 (1989).

[185] J. Javanainen, Phys. Rev. Lett. **64**, 519 (1990).

[186] P. R. Hemmer, M. S. Shahriar, M. Prentiss, D. P. Katz, K. Berggren, J. Mervis, and N. P. Bigelow, Phys. Rev. Lett. **68**, 3148 (1992).

[187] W. Rooijakkers, W. Hogervorst, and W. Vassen, Phys. Rev. A **56**, 3083 (1997).

[188] P. V. Panat and S. V. Lawande, Phys. Rev. A **61**, 063406 (2000).

[189] T. Vanderbruggen, and M. W. Mitchell, Phys. Rev. A **87**, 033410 (2013).

[190] P. F. Barker and M. N. Shneider, Phys. Rev. A **66**, 065402 (2002).

[191] D. M. Villeneuve, S.A. Aseyev, P. Dietrich, M. Spanner, M.Yu. Ivanov, and P. B. Corkum Phys. Rev. Lett. **85**, 542, (2000).

[192] O. Steuernagel, Phys. Rev. A **79**, 013421 (2009).

[193] G. M. Gallatin and P. L. Gould, J. Opt. Soc. Am. B **8**, 502 (1991).

[194] B. S. Zhao, H. S. Chung, K. Cho, S. H. Lee, S. Hwang, J. Yu, Y. H. Ahn, J.Y. Sohn, D. S. Kim, W. K. Kang, and D. S. Chung, Phys. Rev. Lett. **85**, 2705 (2000).

[195] P. Kumar and A. K. Sarma, Phys. Rev. A **84**, 043402 (2011).

[196] P. T. Greenland, S. A. Lynch, A. F. G. van der Meer, B. N. Murdin, C. R. Pidgeon, B. Redlich, N. Q. Vinh and G. Aeppli, Nat. **465**, 1057 (2010).

[197] D. Jaksch, J. I. Cirac, P. Zoller, S. L. Rolston, R. Cote, and M. D. Lukin, Phys. Rev. Lett. **85**, 2208 (2000).

[198] T. Cubel, B. K. Teo, V. S. Malinovsky, J. R. Guest, A. Reinhard, B. Knuffman, P. R. Berman, and G. Raithel, Phys. Rev A **72**, 023405 (2005).

[199] M. Saffman and T. G. Walker, Phys. Rev. A **66**, 065403 (2002).

[200] M. D. Lukin, M. Fleischhauer, R. Cote, L. M. Duan, D. Jaksch, J. I. Cirac, and P. Zoller, Phys. Rev. Lett. **87**, 037901 (2001).

Publications

A. Thesis Publications: Peer Reviewed Journals

1. **Parvendra Kumar** and Amarendra K. Sarma, "Frequency modulated few-cycle optical pulse-train induced controllable ultrafast coherent population oscillations in two-level atomic systems," *Physical Review A* **87** 025401 (2013)**.**
2. **Parvendra Kumar** and Amarendra K. Sarma, "Optical dipole force on ladder-like three-level atomic systems induced by few-cycle-pulse laser fields," *Physical Review A* **86,** 053414, (2012).
3. **Parvendra Kumar** and Amarendra K. Sarma, "Gaussian and sinc-shaped few-cycle pulse driven ultrafast coherent population transfer in Λ- like atomic systems," *Physical Review A* **85**, 043417 (2012). (Also selected in virtual journal of ultrafast science).
4. **Parvendra Kumar** and Amarendra K. Sarma, "Optical force on two-level atoms by few-cycle-pulse Gaussian laser fields beyond the rotating-wave approximation," *Physical Review A* **84**, 043402 (2011). (Also selected in virtual journal of ultrafast science).
5. **Parvendra Kumar** and Amarendra K. Sarma, "Ultrafast and selective coherent population transfer in four-level atoms by a single frequency chirped few-cycle pulse," Physical Review A **88**, 033823 (2013).
6. Pawan Kumar**, Parvendra Kumar** and Amarendra K. Sarma, "Simultaneous control of optical dipole force and coherence creation by super-Gaussian pulses in lambda-like atomic systems," [Manuscript is submitted to Physical Review A].

B. Thesis Publications: Conferences(International/National)

1. **Parvendra Kumar** and Amarendra K. Sarma, "A numerical study of optical dipole force on three-level atoms by chirped few-cycle-pulse laser fields", Frontiers in Optics/Laser science XXVIII meeting, Rochester, USA, Oct. 14, 2012.

2. **Parvendra Kumar** and Amarendra K. Sarma, "Coherent population transfer in Λ- like three state atomic systems with few-cycle femtosecond pulses", National conference on advances in physics, department of physics, IIT Roorkee, India, Feb. 25-26, 2012.

3. **Parvendra Kumar** and Amarendra K. Sarma, "Time dependent optical force on two-level atoms by few cycle pulsed Gaussian laser field beyond the rotating wave approximation", 3rd International conference on Current developments in atomic, molecular, optical and nano physics, New Delhi, Dec. 14-16, 2011.

C. Related Publications: Peer Reviewed Journals

1. Amarendra K. Sarma and Parvendra Kumar, "Modulation Instability of ultrashort pulses in quadratic nonlinear media beyond the slowly varying envelope approximation," *Applied Physics B* **106**, 289 (2012).

D. Related Publications: Conferences(International/National)

1. Amarendra K. Sarma and **Parvendra Kumar**, "Modulation instability of few-cycle pulses in quadratic nonlinear Media", 3rd International conference on Current developments in atomic, molecular, optical and nano physics, New Delhi, Dec. 14-16, 2011.

2. Parvendra Kumar and Amarendra K. Sarma, "Extreme nonlinear optics: Effect of carrier envelope offset phase on the dynamics of two-level atomic systems", *AIP Conf. Proc.* Vol. 1391, pp. 677-679 Optics: phenomena, materials, devices and characterization: Optics 2011: International Conference on Light.

Vita

The author, Mr. Parvendra Kumar was born on 11 Feb. 1986 in Uttar Pradesh, India. He did his B.Sc. with Physics and Mathematics as the main subjects from Mahatma Jyotiba Phule Rohilkhand University, Bareilly, India in 2005 and M.Sc. in Physics from Gurukula Kangri Vishwavidyalaya, Haridwar, India in 2007. In 2008, he joined plasma devices laboratory, Central Electronics Engineering Research Institute, Pilani, India as a project assistant. He joined Indian Institute of Technology Guwahati as a PhD student in 2009. He was awarded Junior Research Fellowship in 2009 and Senior Research Fellowship in 2011 by Ministry of Human Resource Development, Government of India.